Molecular Semiconductors in Organic Photovoltaic Cells

Alexander W. Hains, Ziqi Liang, Michael A. Woodhouse, and Brian A. Gregg*

National Renewable Energy Laboratory, 1617 Cole Boulevard, Golden, Colorado 80401

Received September 4, 2009

Contents

* To whom correspondence should be addressed. E-mail: brian.gregg@nrel.gov.

1. Introduction

We begin with a general description of the chemical, physical, and electrical properties of organic semiconductors, OSCs, a class of materials that includes molecular semiconductors, MSCs, the focus of the rest of this Review, as well as π-conjugated polymers. The term excitonic semiconductor, XSC, is a mechanistic description that refers to materials in which electrostatically bound excitons are formed upon light absorption; this seems to include all OSCs at room temperature and most inorganic semiconductors at low temperature. Excitons formed in quantum dots are distinct, however, because they are spatially, rather than electrostatically, confined. We review the mechanisms of photoconversion, the testing and analysis of organic photovoltaic, OPV, cells, and conclude with an extensive review of the recent literature of small molecule OPV. The number of papers published in the fields of MSCs and OPV has been growing exponentially in the past decade, and we could cover only a fraction of them here. Some common abbreviations employed in this Review are included in section 10.

The development of renewable energy is essential for the sustainability of our ecosystem. The toxic and climate-changing byproducts of our current energy sources are doing serious damage to the planet. We cannot continue with "business as usual"; the photoconversion of sunlight directly into electricity and/or fuels seems to be the only viable long-term strategy for a sustainable energy future.[1−4] Organic semiconductors show great promise for photoconversion through their synthetic variability, their low-temperature processing similar to that applied to plastics, and the possibility of producing lightweight, flexible, easily manufactured, and inexpensive solar cells.[5−13] Organic semiconductors may eventually replace inorganic semiconductors, ISCs, in photovoltaic cells, as OSCs have been slowly replacing them in other applications that require a combination of low cost, large area, and flexibility, but without requiring rapid switching speeds. Examples are photocopiers, laser printers, light-emitting diodes, and white light panels for room lighting.[14,15]

To realize the potential of OSCs requires first understanding the fundamental chemical, electrical, and photoconversion properties.[6,16−21] Although research into organic photovoltaics, OPV, is more than 50 years old,[22−31] it was a neglected backwater for much of this time. Interest in the field has slowly been rekindled by a growing appreciation for the

10.1021/cr9002984
Published on Web 02/25/2010

Alexander W. Hains earned a B.A. from Saint Olaf College in 2001, majoring in Chemistry and Spanish. After graduation he went to the University of Massachusetts, Amherst, and received an M.S. in 2003. He then attended Northwestern University in pursuit of a Ph.D. in Chemistry, which he was awarded in 2009. After graduate school, he accepted his current position as a postdoctoral researcher at the National Renewable Energy Laboratory (NREL). His research at Northwestern and NREL has largely focused on interfaces in organic photovoltaics and their influence on device physics and performance.

Michael A. Woodhouse developed the methodology to rapidly produce novel semiconductors from liquid precursors using inkjet printing for his doctoral dissertation. The multielement photocatalysts were then tested for their ability to produce hydrogen by water splitting using visible wavelength light as the sole energy input in a custom-made laser-scanning analysis system. Combinatorial studies were then undertaken for materials optimization. He is currently developing new materials and architectures, as well as analyzing the commercial markets for organic-based solar cells at the National Renewable Energy Laboratory in Golden, CO, under Dr. Brian Gregg.

Ziqi Liang obtained his Ph.D. in Polymer Science from the Department of Materials Science and Engineering at The Pennsylvania State University in May 2006, and then took a postdoctoral research associate position at the University of Cambridge. Since June 2008, he has been a postdoctoral researcher in the Chemical and Materials Science Center at the National Renewable Energy Laboratory (NREL) working with Dr. Brian A. Gregg. His research areas/interests span π-conjugated polymers, molecular organic semiconductors, and inorganic nanostructures for optoelectronic devices and broadly toward alternative energy applications.

Brian A. Gregg obtained a Ph.D. in physical chemistry from the University of Texas at Austin in 1988. After a two year postdoctoral appointment in the field of enzyme electrodes, he joined the National Renewable Energy Laboratory (then known as the Solar Energy Research Institute) where he is now a Principal Scientist. His research interests include the design and synthesis of materials for solar energy conversion and storage, unified models of photoconversion, organic semiconductors, exciton dynamics, photoelectrochemistry, and photoelectrocatalysis.

necessity of inexpensive renewable energy and by the commercial interest surrounding organic light-emitting diodes, OLEDs.[6,14,32−39] There is also growing interest in organic electronic elements and circuits,[40−48] and even lasers.[49]

It is often noted that OLEDs function as OPV cells in reverse, converting electrical current into light, and indeed there is useful overlap in materials and cell design between the two fields. There are also fundamental differences. For example, OPV requires efficient exciton dissociation into free charge carriers, while OLEDs require efficient recombination of free carriers to form excitons.[34,35,37] Light scattering, and thus crystallinity in the OSC films, can be detrimental for OLEDs but may be beneficial for OPV. Moreover, to be successful, OPV must be much less expensive and produced in far larger areas than OLEDs. Still, it is encouraging that commercial OLEDs can survive being driven at high current density for >10 000 h,[39] suggesting that stability in OPV cells is not an issue that will prevent commercialization.

There are currently two major classes of organic semiconductors: the MSCs covered in this Review and the π-conjugated polymers such as poly(thiophenes) and poly(phenylene vinylenes) covered in separate reviews in this issue. They have many features in common, such as their excitonic nature, and we will occasionally point out the similarities between them and some differences. The major use of MSCs at present is in nonsemiconducting applications such as pigments and dyes.[15,50] Perylene dianhydride derivatives and phthalocyanines are manufactured on a large scale for use in automobile paints, carpet, and fabric dyes, and similar applications.[50] These two families of MSCs, in particular, are inexpensive and chemically stable. One of the first applications in which OSCs displaced inorganics was in electrophotography. The original photoactive element in photocopiers was selenium, but these were soon replaced

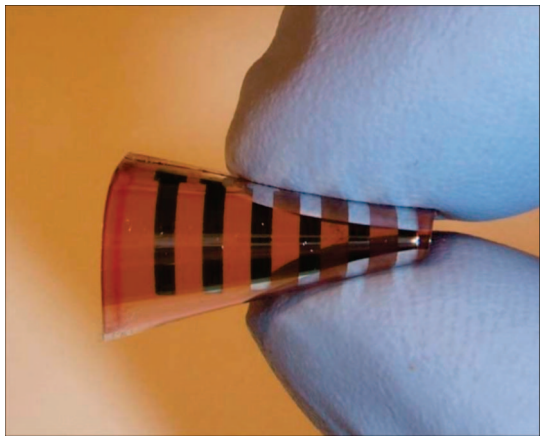

Figure 1. Photograph of polymer-based OPV device on a flexible plastic substrate. Reprinted with permission from ref 9. Copyright 2009 Materials Research Society.

by perylene diimides and other MSCs.[15,51] Today, some photocopiers and laser printers employ MSCs such as perylene bis(phenethylimide), PPEI, or titanyl phthalocyanine, TiOPc, as the photoactive element. One reason for choosing these particular compounds from the many known perylene diimides and phthalocyanines is that they form highly photoactive polycrystalline phases in which much of the oscillator strength resides in a low energy charge transfer absorption band,[52,53] as discussed below. This attribute apparently contributes to their enhanced charge generation efficiency.[11,51,54]

Although flexibility is not necessary in all PV applications, its primary importance in OPV may be 2-fold: first, it enables the use of high-speed roll-to-roll manufacturing processes for the inexpensive production of OPV modules. Second, it minimizes balance-of-systems costs by employing lightweight substrates that are easily installed on many surfaces. Companies are now beginning to produce polymer-based OPV modules in this fashion (Figure 1).[55] Although module efficiencies are still low, ongoing improvements in materials and cell design should be readily incorporated into the manufacturing process.

We begin this Review by describing some of the relevant chemical, physical, and electrical properties of OSCs and making some comparisons to silicon, the prototypical inorganic semiconductor. We treat first (poly)crystalline materials to illustrate the fundamental properties before considering the more complex, but popular, disordered materials.

2. Physical Characteristics of OSCs

2.1. Low Dielectric Constant

As compared to ISCs such as Si and CdTe, OSCs have a much lower static dielectric constant, ε. As a second row element in the periodic table, the carbon atom's valence electrons are more tightly bound to the nucleus than those of silicon, its neighbor in the third row. The dielectric constant of crystalline carbon (diamond) is $\varepsilon = 5.7$,[56] while in crystalline silicon $\varepsilon = 11.9$.[56] In most MSCs, $\varepsilon = 3.5-5.5$.[6,16,36,37,39] Because separating photogenerated electrons from holes is essential for photoconversion, the low ε is a hindrance. There is an electrochemical analogy: the ionic electrolyte added to a solvent to screen electric fields only works for solvents with a dielectric constant above about $\varepsilon = 8$.[57] Below that, the electrolyte ions are so strongly bound to each other by electrostatic attraction that they cannot dissociate. Likewise, the low ε of OSCs ensures that electrostatic attractions between electrons and holes, or between incipient charge carriers and their counterions, exert a profound and multifaceted influence on their electrical properties.

Even in silicon electrostatic effects play a role, although minor at room temperature. Figure 2 shows some results from the classic 1949 study of doping in silicon by Pearson and Bardeen[58] along with results from a recent study of n-type doping in polycrystalline perylene diimides.[59−61] The results are qualitatively similar. The free charge density in both cases is thermally activated, but the activation energy is an order of magnitude higher in the organic case. Thus, the majority of charge carriers in the MSC remain bound near their dopant counterions, and only a few contribute to the dark current. The activation energies decrease with increasing dopant density (Figure 2b), an effect attributed to the increase in ε of the MSC film caused by the addition of the highly polarizable dopants. These issues are addressed further in section 4.2.

The influence of a localized positive charge on the electron potential energy for $\varepsilon = 4$ is shown in Figure 3 at equilibrium and also under an applied electric field, F. This is a simple model for n-type doping and also for exciton formation. Apparently there can be no shallow (that is, mostly ionized) dopants in XSCs because the binding energy between the incipient carrier and its countercharge is $\gg kT$, the thermal energy. According to Poole and Frenkel,[62,63] this binding energy should decrease with $F^{1/2}$, resulting in an increase in free carrier density in doped OSCs with $\exp(F^{1/2})$.

Seen from a different perspective, the Coulomb field from a single unshielded charged defect or dopant in a film with $\varepsilon = 4$ will shift the energy levels of all molecules within a radius of ~10 nm by an amount ranging from 26 meV (kT at room temperature) at the 10 nm radius up to ~500 meV for close neighbors (Figure 3). One charged defect can alter the energy levels of ~10 000 neighboring molecules in an OSC, thus having a far more widespread influence than a single charge in a high-dielectric ISC. Also, the charged defect density in most OSCs is surprisingly high (section 4.4).

The changes in dielectric properties that occur at interfaces between different materials in OPV cells may influence their photoconversion behavior. For example, Zakihidov and Yoshino have calculated that a decrease in dielectric constant at an OSC interface can cause a barrier to carrier transport as the band gap of the OSC widens at the junction.[64] Likewise, a decrease in refractive index at an interface can cause a barrier to exciton transport.

2.2. Exciton Generation

It was realized in the original studies of OSCs that their photovoltaic behavior was in some ways fundamentally different from that of ISCs.[29,31,65] Photocurrents and photovoltages were achieved in the absence of any obvious junction, either p−n or Schottky, and the photocurrent action spectra indicated a process controlled by light absorbed close to the surface rather than in the bulk. This was later attributed correctly to the photoinduced creation of excitons,[31] electrically neutral quasi-particles consisting of a bound electron−hole pair,[28,66,67] and their subsequent diffusion to, and dissociation at, the illuminated electrode interface.[29,51,68,69] Exciton forma-

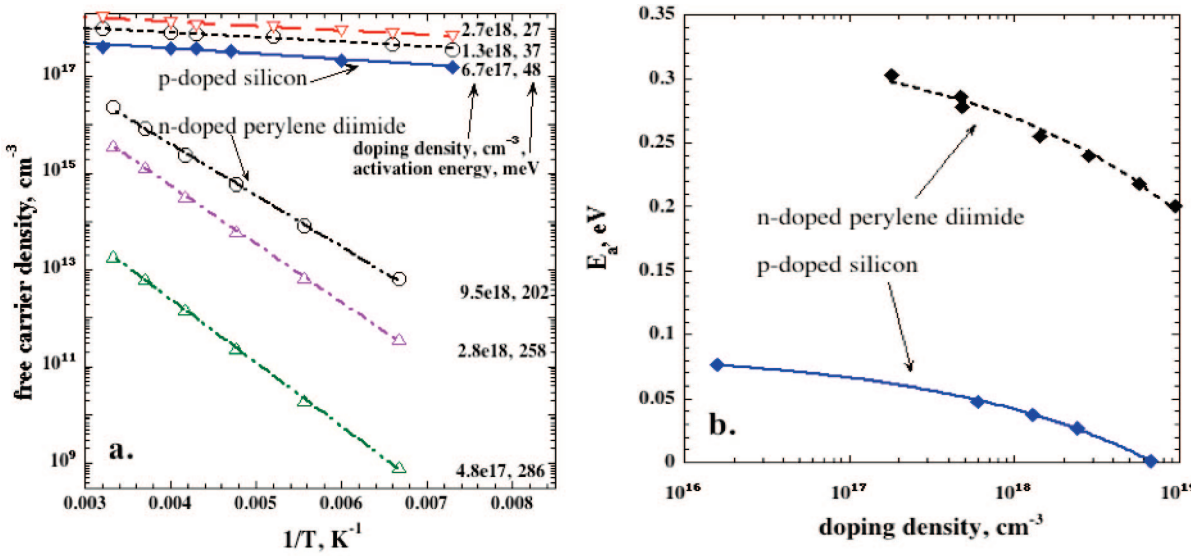

Figure 2. Qualitatively similar behavior in p-doped silicon and n-doped perylene diimide. (a) Free carrier density versus reciprocal temperature for three doping densities. (b) Free carrier activation energies decrease with the cube root of the doping density. Perylene diimide data assume a constant electron mobility of 10^{-3} cm^2/(V s). Silicon data are replotted and used with permission from ref 58. Copyright 1949 American Physical Society. Perylene diimide data are replotted and used with permission from ref 59. Copyright 2005 American Chemical Society.

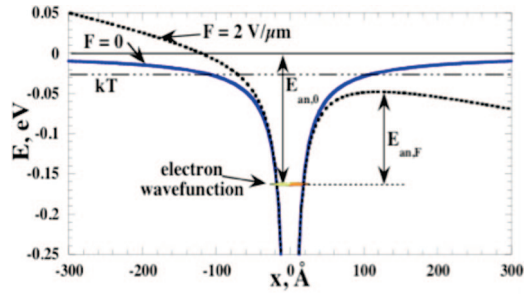

Figure 3. Model of electrostatic attractions in OSCs showing the Coulomb potential around a positive charge localized at $x = 0$ in a dielectric constant of $\varepsilon = 4$. The size of the electron wave function determines how deeply it sits in the potential well. The effect on the barrier height, E_{an}, of applying a field is also shown.

tion results from (1) the low dielectric constant, which causes a broad Coulomb potential well to form around a charge, and (2) the localized carrier wave functions that are small enough to "fit" inside the Coulomb well (Figure 3).[16,70] The exciton binding energy is often in the range of 0.1−0.5 eV. Weakly bound excitons are also formed in ISCs at low temperature,[58,71,72] one of the many similarities between OSCs at room temperature and ISCs at cryogenic temperatures.[60,73] The generation of electrically neutral excitons upon light absorption in OSCs instead of electrically charged free carriers as in ISCs plays a fundamental role in the photoconversion process and mechanistically differentiates OPV from inorganic PV (section 3).[16]

2.3. Electronic Coupling and Lattice Forces

In molecular solids, the strong bonds are those between covalently bound atoms in the molecular framework; the intermolecular forces are much weaker. The electronic coupling between molecules in a solid is far weaker than the coupling between atoms in covalent ISCs such as Si. This results in relatively narrow conduction and valence bands, more localized charge carriers, and lower carrier mobilities in MSCs.[29,72−74] Thus, the bandwidths may vary from ∼250 meV for a strongly coupled MSC[29,75,76] (still just 1/10 that of a typical ISC)[72] to ∼10−20 meV in weakly coupled or disordered materials. Despite its occasional limitations, we employ a semiconductor physics description here for continuity and simplicity. This description is semiquantitatively valid for the "big picture" in OSCs, but it becomes more appropriate at a detailed level as the electronic coupling (bandwidth) of the OSC increases. We refer to the charge carriers as electrons and holes, although in many (low bandwidth) cases a more precise description would be as negative and positive polarons.[17,29,74] Thus, the lattice polarizes around a charge leading to greater localization and slower charge motion (heavier carriers). This exemplifies the strong electron−phonon (lattice vibration) coupling that is common in OSCs.[17,29,77] Such polarization effects are most pronounced in π-conjugated polymers but occur also in MSCs. Partly because of the more localized carriers in OSCs relative to ISCs, the terms HOMO and LUMO (highest occupied and lowest unoccupied molecular orbitals, respectively) are often employed in place of valence band and conduction band, respectively. Neither terminology seems entirely adequate, and the reality may lie between the two.

The intermolecular forces between MSC molecules in a solid are highly directional and spatially complex. The wave functions of the HOMO and LUMO have a distinct spatial and nodal structure, something like a molecular fingerprint (Figure 4). Many planar aromatic MSCs form cofacial π-stacks in which the degree of in-phase electronic overlap between adjacent molecules determines the strength of the intermolecular electronic coupling.[17,29,52,75] The bandwidths (and thus colors) of some MSCs vary substantially as the molecules in the crystal lattice shift just slightly relative to their neighbors, causing the wave functions of the adjacent molecules to move in and out of phase with each other (Figure 5). This "crystallochromy" has been studied most thoroughly among the commercially important perylene diimide pigments.[53,78] Kazmaier and Hoffmann[52] first estimated the band structure in a π-stack of perylene diimides through extended Hückel calculations in the tight-binding approximation (Figure 5). Their results clearly show the

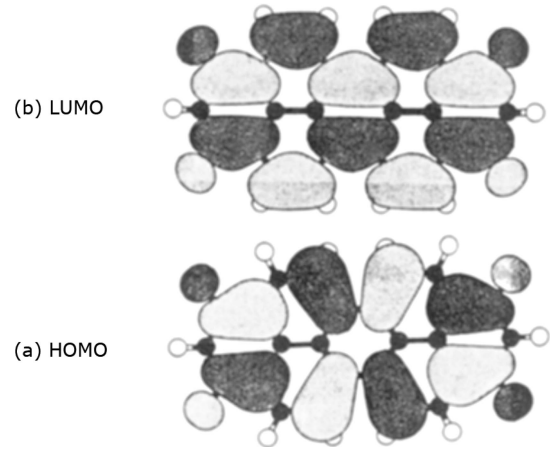

Figure 4. (a) HOMO and (b) LUMO orbitals of a perylene diimide (for chemical structure, see Figure 6b or 24). Shading indicates regions of different phase of the wave function. Reprinted with permission from ref 52. Copyright 1994 American Chemical Society.

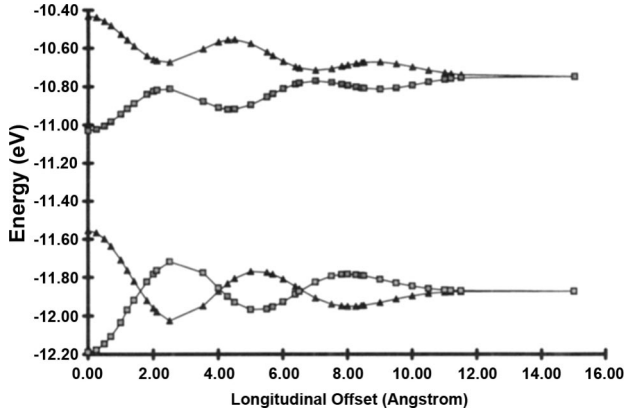

Figure 5. Variation of the valence and conduction bandwidths of perylene diimide as a function of the longitudinal offset between adjacent molecules. Results from tight-binding extended Hückel calculations from ref 52. Copyright 1994 American Chemical Society.

oscillations in conduction and valence band widths expected as the molecules slip longitudinally past one another or, equivalently, as the tilt angle of the π-stack increases. The optimal semiconductor properties for OPV applications, the widest bands and smallest band gap, occur only within a narrow range of lattice parameters. The same organic semiconductor in two slightly different polymorphs can have vastly different optoelectronic properties,[15,34,75,79] as illustrated in Figure 6 (and also Figure 17).

A recent experimental demonstration of this effect[75] was found in the reversible phase transition of rub-aligned films of a liquid crystalline perylene diimide, PPMEEM (structure inset in Figure 6b). This material, like some other perylene diimides,[80,81] can exist in two crystalline phases: a metastable red-colored phase and the stable black phase. The transition between the two, which does not perturb the macroscopic crystallinity, involves a shift of the longitudinal offset between adjacent molecules by ~1.6 Å.[82] Micrographs of a film with the polarizer aligned parallel and perpendicular to the rubbing direction (Figure 6a and b), together with polarized absorption spectra, show that the spatially averaged optical transition dipole moment rotates ~90° during this phase change. The optical band gap, E_{opt}, decreases by ~360 meV from the red to the black phase, suggesting that the energies and widths of the conduction and valence bands shift by a similar amount.[75]

Density functional theory calculations (Figure 6C and D), as well as previous work,[15,34,52,83,84] suggest that the optical transition in the red phase is intramolecular and thus polarized in the molecular plane, equivalent to a Frenkel exciton. The transition in the black phase is primarily an intermolecular charge transfer, CT, transition, or CT exciton,[67] polarized out of plane in the $\pi-\pi$ stacking direction.[75] As mentioned, it is apparently the CT phases of perylene diimides and phthalocyanines that are the most active in electrophotographic devices.[15] Reports are just beginning to appear of these phases employed in OPV cells.[11]

As another example of band energy variations in OSCs, the change in bandwidth of discotic molecular cores as a function of the angle of rotation between neighboring molecules was calculated by Feng et al. (Figure 7).[76] The oscillatory variations with angle are similar to those seen in Figure 5 with longitudinal offset. The large variation in optical and electrical properties with small changes in crystal packing makes understanding and controlling the electronic properties of crystalline MSCs a challenge. Yet it also suggests that when we master these properties, we should be able to achieve substantially higher efficiencies in OPV cells.

2.4. Crystalline Films for OPV

The optical and electrical properties of MSCs are highly anisotropic, much more so than those of most ISCs. Therefore, an optimal OPV cell would presumably employ MSC crystals oriented along the most photovoltaically efficient axis.[85−87] This goal remains elusive. In inorganic PV, the highest efficiency cells employ the cleanest and most crystalline semiconductors. Cells made from less expensive polycrystalline materials have lower efficiencies, and those made from amorphous materials are lower still.[88] It was also in this order, from crystalline to amorphous, that the field evolved.[72,88,89] The OPV field, however, may be evolving in the opposite direction. Most cells now employ amorphous or nanocrystalline OSC films, partly because it is relatively easy to deposit amorphous pinhole-free OSC films that adhere well to substrates and to other films. It is much more difficult to deposit or grow pinhole-free, strongly adherent polycrystalline films. Yet it seems reasonable to expect the same efficiency trend in OPV as in inorganic PV; that is, clean and crystalline should be better. There are an increasing number of studies regarding the growth and characterization of more crystalline MSC films.[35,86,90−92] The methods employed range from epitaxial growth from the vapor phase[35,92−94] to thermal or solvent vapor annealing of amorphous films[11,81,95] to melt or solution deposition methods.[85,86,96,97]

Methods for producing aligned crystalline MSC films via substrate templating have been reviewed by Forrest[35] and by Witte and Wöll.[90] In recent work, Lunt et al. demonstrated quasi-epitaxial growth of a bilayer consisting of 3,4,9,10-perylenetetracarboxylic dianhydride, PTCDA, and copper phthalocyanine, CuPc, on a single crystal KBr substrate.[93] Interestingly, PTCDA provides a template for crystalline growth of CuPc, but the converse is not true. The Armstrong group has employed both controlled thermal sublimation and solvent vapor annealing to produce polycrystalline MSC films for photoelectrochemical cells[98,99] and for OPV.[11,34,54] One study compared the as-evaporated TiOPc film to its long

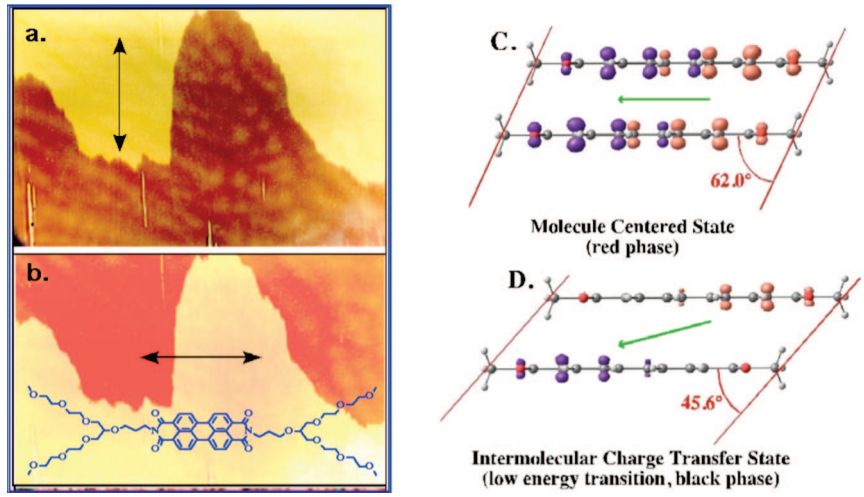

Figure 6. (a,b) Polarized micrographs of a rub-aligned film of PPMEEM (structure in inset). (a) Polarizer aligned along the rubbing axis and (b) aligned perpendicular. The black phase, bottom of micrograph is growing into and displacing the red phase, top. (C,D) Density functional theory calculations of the optical transition in a model dimer of perylene diimide having the molecular offsets of (C) the red phase and (D) the black phase. The optical transition of the red phase is primarily intramolecular, while that of the black phase is intermolecular charge transfer. Reprinted with permission from ref 75. Copyright 2008 American Chemical Society.

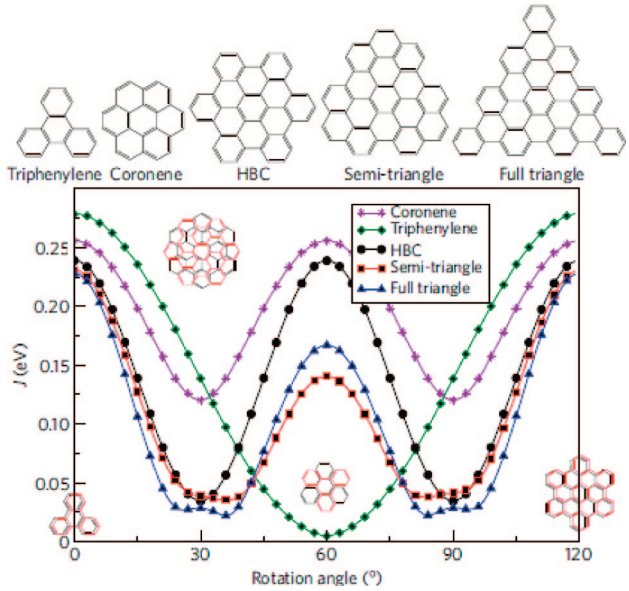

Figure 7. Calculated absolute values of the transfer integral J as a function of the azimuthal rotation angle for several symmetric polyaromatic hydrocarbon cores. The bandwidth equals $J/2$. Reprinted with permission from ref 76. Copyright 2009 Nature Publishing Group.

wavelength (CT) phase in a TiOPc/C_{60} OPV cell. The long wavelength phase (λ_{max} = 850 nm) produced almost twice the photocurrent as the original phase.[11] Liquid crystal, LC, derivatives of MSCs were proposed as a means of growing oriented crystalline films for improved OPV properties.[61,76,100−110] These materials often have substantially higher carrier mobilities than other types of OSCs.[76,111−114] However, the electrically insulating side chains that induce the liquid crystal phase practically eliminate the conductivity in one dimension (smectic-like phases) or two dimensions (discotic phases). Thus, the orientation of the MSC phase becomes crucial to OPV performance. Unfortunately, many of the LC semiconductors tend to align with their conducting axis parallel to the substrate and seem quite resistant to reorienting in the perpendicular (homeotropic) direction needed for PV cells.[82,104,105]

Amorphous and nanocrystalline MSC films lose the potential advantage of the relatively strong electronic coupling between molecules in a crystal lattice, but they often have the advantage of superior film-forming properties. The approximately isotropic electrical properties of amorphous films are expected to be substantially poorer than the properties of crystalline films along some axes. The density of both charged and uncharged defects is usually much higher in disordered films than in crystalline materials (section 4.4),[6,29,115−117] and this can result in shorter exciton diffusion lengths and decreased carrier mobilities.[76,77,116,118] Nevertheless, Perez et al. recently reported that the open-circuit photovoltage, V_{oc}, in a series of OPV cells with different donors was consistently higher in devices made from amorphous MSC films than in those made from nanocrystalline films.[119] This was attributed to more rapid charge generation in the dark, and therefore higher recombination currents, in the nanocrystalline materials.

2.5. Interfacial Energies and Surface Adhesion

Most OPV cells have at least three interfaces: the electrode/D, D/A, and A/electrode interfaces, where D and A are the donor and acceptor semiconductors, respectively. Many cells have additional interfaces. The stability of these interfaces over time is a crucial issue for OPV cells. At interfaces between two MSCs, or between an MSC and another material, the relative strengths of the interfacial and intermolecular forces determine the stability of the interface. When intermolecular forces are stronger, apparently the usual case, a disordered interface is inherently unstable, and MSC crystallization and interface dewetting or delamination can occur. Of course, the interface may be kinetically stable. Given the spatially complex nature of the attractive forces between MSCs (section 2.3), it is not surprising that the molecules often stick to each other more tightly than they stick to "foreign" molecules. Even the quintesssential MSC donor and acceptor materials, phthalocyanine and perylene diimide, spontaneously phase separate from each other and lose interfacial contact when annealed.[120,121] This suggests that, given the opportunity, many films of MSCs may disadhere from interfaces. Interfacial films (see section 7.3)

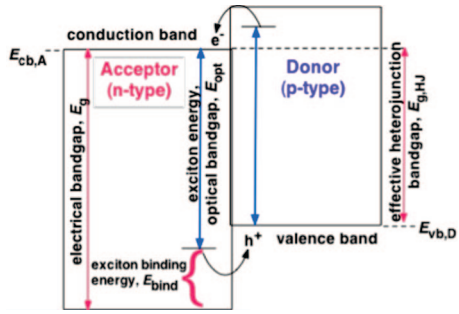

Figure 8. Band diagram of a bilayer heterojunction, HJ, showing the relevant energies.

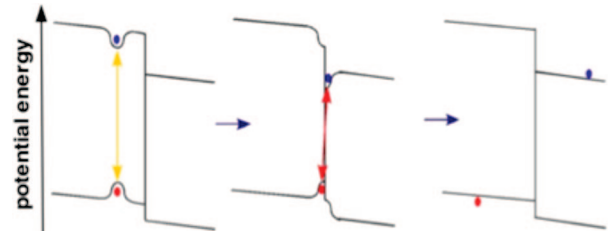

Figure 9. A schematic band diagram showing the formation of an exciton by light absorption (left), its dissociation into a bound charge pair at the HJ interface (middle), and escape from the interface to form free carriers (right, polaronic effects not shown). The bound charge pair may also undergo geminate recombination.

are often employed between the electrode and the MSC film, partly to improve adhesion.

Good adhesion between two MSC films requires some force to overcome their natural tendency to phase separate. The force most relevant to OPV may derive from charge transfer across the heterojunction interface. If the electrochemical potentials (Fermi level, E_f, or work function) of the two MSCs are substantially different, electron transfer should occur across the interface and promote adhesion.[122] The desired positioning of the Fermi levels may be achieved via doping, either on purpose or by defects (section 4). Another way to create relatively stable interfaces is to employ polymeric OSCs, and it may be partly for this reason that many of the most efficient OPV cells are currently polymer based. A polymer adsorbed on a surface can only desorb if a substantial number of its segments desorb simultaneously, which is improbable and thus slow. Polymer interfaces are often kinetically stable.

Despite being a problem in some OPV cells, the tendency of OSCs to self-associate is put to good use in the various types of bulk-heterojunction OPV cells[123,124] (section 7.2) in which a more or less controlled phase separation generates the desired nanostructuring between donor and acceptor phases. Whether the phase separation process can be halted once the optimal morphology is achieved is not yet known and may depend on the individual system.

3. Photoconversion Processes in XSCs

3.1. Band Diagrams and Interfacial Recombination

A simplified band diagram of a bilayer OPV cell is shown in Figure 8 where the exciton energy is equated with the optical band gap, E_{opt}. The exciton binding energy, E_{bind}, is the difference between the electrical band gap, E_g, sometimes called the transport gap,[39,125] and E_{opt}. The band diagram contains a useful subset of the information needed to understand OPV cells, but it is far from complete. It does not treat the Coulomb attractions between individual charges, it contains no information about kinetics, and it does not include triplet states, charge transfer states, and other peculiarities of OSCs. OPV is far more complex mechanistically than inorganic PV.

An exciton must arrive at the heterojunction, HJ, interface (Figure 8) to dissociate productively into a free electron and hole. If it dissociates in the bulk MSC, the carriers often recombine.[68,126] Most current OPV cells employ a type-2 heterojunction between the n-type (or acceptor) SC and the p-type (or donor) SC such as shown in Figure 8. The band offset at the HJ between the two semiconductors must necessarily be greater than the exciton binding energy for the exciton to dissociate. The kinetic factors controlling exciton dissociation are not well understood. Even after dissociation, the electron and hole may remain electrostatically bound to each other across the interface (Figure 9). This bound state, which may not be formed in all cases, has variously been called a charge transfer exciton, a bound radical pair, a geminate charge pair, and a bound polaron pair.[21,67,125,127,128] Geminate recombination can occur from this state and is a major factor limiting efficiency in some systems.[21,125,127,128] If the carriers become free from the interface, they can then either contribute to the photocurrent by traversing the film and being collected at the electrode, or recombine in a second-order process if they eventually return to the HJ interface. Recombination in the bulk is often not a concern[73,115] because there are few free electrons in the donor film and few free holes in the acceptor film (section 4.3). Some photogenerated carriers will, however, leak over the HJ barrier under illumination, especially near open circuit.

3.2. Forces and Fluxes

Many of the important processes in OPV cells, charge carrier generation, separation, and recombination, occur at the heterojunction interface, whereas in inorganic PV cells these processes occur throughout the bulk. This causes a fundamental mechanistic difference between PV in XSCs and that in (room temperature) ISCs. The difference lies mainly in the influence of the chemical potential gradient.[16,73,129] There are only two important forces driving the PV effect: the gradient of the electrical potential, ∇U, and the gradient of the chemical potential, $\nabla\mu$. Together they make up the gradient of the electrochemical potential or quasi-Fermi level, ∇E_f.[88] The current density of electrons through a device can be written most simply in terms of ∇E_f:

$$J_n(x) = n(x)\mu_n\{\nabla U(x) + \nabla\mu(x)\} = n(x)\mu_n\nabla E_{fn}(x) \quad (1)$$

where $n(x)$ is the electron density and μ_n is the electron mobility. This equation shows that ∇U and $\nabla\mu$ are equivalent forces. Yet $\nabla\mu$ often plays an insignificant role in inorganic PV cells because photogeneration, separation, and recombination occur mainly in the bulk SC, and because the high carrier mobility tends to minimize concentration gradients. Furthermore, most inorganic PV cells are minority carrier devices, whereas OPV cells are majority carrier devices. Thus, for inorganic PV, but not for excitonic PV, the maximum photovoltage is usually limited by the equilibrium built-in potential drop across the cell, V_{bi}.[88] This value is set by the maximum difference between Fermi energies of the individual cell components.

Chemical potential gradients are far more important in OPV cells because carrier generation and recombination occur at the HJ interface and thus generate substantial concentration gradients.[16,73] The best example of the importance of $\nabla\mu$ to excitonic photoconversion is the dye-sensitized solar cell, DSSC.[19,130−132] Here, the presence of ∼0.5 M electrolyte ions surrounding the nanostructured TiO_2 network effectively screens the electric field, thus $\nabla U \approx 0$ throughout the device (except within ∼1 nm of the electrodes).[19,131] Changing the work function (Fermi level) of the electrodes over 1.5 V is reported to have no influence on the open-circuit photovoltage, V_{oc}, suggesting that V_{oc} is independent of V_{bi}.[131,133] Thus, photoconversion in DSSCs seems to be driven almost entirely by $\nabla\mu$.[19,131,134−137] Despite eliminating the electric field as a driving force, or perhaps because of it, DSSCs are still the most efficient type of excitonic solar cell.

OPV cells must contend with both ∇U and $\nabla\mu$ because there is (usually[138]) no mobile electrolyte to neutralize the fields and because the photoinduced interfacial concentration gradients ensure that $\nabla\mu$ cannot be neglected.

3.3. Photovoltage

The origin of V_{oc} in OPV cells has been the subject of much discussion,[37,60,73,119,125,127,139,140] as it was earlier for DSSCs.[16,19,73,131,133,135,136,141−147] Some examples are discussed in later sections. In section 5.2, we discuss V_{oc} in the context of the generalized Shockley equation and a circuit model. Here, we briefly mention some historical results and present a simple quasi-thermodynamic model of V_{oc}.[16,88,148] It was discovered early on that V_{oc} of 100−400 meV can be photogenerated in electrically symmetrical OPV cells,[31,65,100] that is, cells in which a single MSC is sandwiched between two identical electrodes. The hidden asymmetry necessary to separate the charge carriers in this case derives from two factors: (1) illumination of only one side of the optically thick film, and (2) the interfacial exciton dissociation process that preferentially injects one carrier type into the electrode.[16,31,65,100] Cells with an electron-selective thin film on one electrode and a hole-selective film on the other produced $V_{oc} = 1.0$ V despite having $V_{bi} \approx 0$.[149] Cells designed to probe the relative importance of V_{bi} (∇U) and interfacial exciton dissociation ($\nabla\mu$) show that the latter can overwhelm the former, producing a PV effect of opposite polarity from that expected from V_{bi} alone.[150,151] These results show that V_{oc} is not, in general, governed wholly by the work function difference between the two electrodes or between two cell components. In specific cases, ∇U can be the controlling factor, but, in general, the influence of both ∇U and $\nabla\mu$ must be considered.

The quasi-Fermi level concept provides a simple understanding of photovoltage in PV cells.[72,88,89,148,152] It has the virtue of containing no device-specific assumptions, although we describe it here using the example of a donor/acceptor bilayer MSC cell shown in Figure 8. The one-dimensional quasi-Fermi levels of electrons in A and holes in D are expressed as[72]

$$E_{fn,A}(x) = E_{cb,A} - kT\ln(n_A(x)/N_{c,A}) \quad (2)$$

$$E_{fp,D}(x) = E_{vb,D} + kT\ln(p_D(x)/N_{v,D}) \quad (3)$$

where $n_A(x)$ and $p_D(x)$ are the electron and hole concentrations in A and D, respectively, and $N_{c,A}$ and $N_{v,D}$ are the corresponding densities of states. Assuming perfect contacts, V_{oc} measures the difference between $E_{fn,A}$ at one contact and $E_{fp,D}$ at the other.[73,88,148] Thus,

$$qV_{oc} \le E_{fp,D} - E_{fn,A} \quad (4)$$

where q is the electronic charge and the equality holds for cells with perfect contacts. The relevant band edge energies are $E_{cb,A}$ and $E_{vb,D}$ (Figure 8). To achieve $qV_{oc} = E_{vb,D} - E_{cb,A} = E_{g,HJ}$ (sometimes considered to be the maximum possible V_{oc}) would require a photogenerated carrier density equal to the density of states, that is, $\sim 10^{21}$ cm^{-3}.[6,115,117] This is unlikely to occur even in an ideal cell except under high intensity laser illumination. At more realistic, but still high, values $n \approx p \approx 10^{19}$ cm^{-3}, each quasi-Fermi level would be $\sim kT$ ln(100) inside the band edges. In this example, the achievable maximum photovoltage at room temperature would be

$$qV_{oc} \approx E_{vb,D} - E_{cb,A} - 2kT\ln(100) = E_{g,HJ} - 0.24\ \text{eV} \quad (5)$$

In many OPV cells, the Coulomb attraction of an incipient electron−hole pair at the HJ interface must be overcome before free carriers are formed (section 3.1). Although this is not necessarily a limitation for all OPV cells, a consensus seems to be emerging that most existing OPV cells lose ∼0.4−0.9 eV overcoming this attraction.[21,39,125,127,153] This decreases the achievable V_{oc} by a similar amount. It also alters the relationship between the band gap and the cell efficiency. Shockley and Quiesser calculated an optimal band gap for a single homojunction PV cell (OPV cells are heterojunctions) by maximizing the product of the short-circuit current density, J_{sc}, the open-circuit photovoltage, V_{oc}, and the fill factor, FF, as a function of band gap.[154] The value they obtained, $E_g \approx 1.4$ eV, is sometimes regarded as a target for synthesis of new OSCs with improved efficiency. However, the Shockley−Quiesser model does not include overcoming an interfacial Coulomb attraction. If it did, the optimal band gap would probably be greater than 1.4 eV.

3.4. Carrier Mobilities and Transport

Mobilities are measured by a variety of techniques that may be sorted by the conductivity range over which they are applicable. At the lowest conductivities, space charge limited, SCL, currents occur and provide a measure of the mobility;[29,155−159] SCL currents can be observed only when the bulk free carrier density is much less than the carrier density injected by the electrodes. In practice, this often requires a free carrier density less than $\sim 10^{14}$ cm^{-3}.[160] Therefore, SCL currents are not expected in most π-conjugated polymers because the free carrier density is too high (section 4.3). Poole−Frenkel-like currents, which often do occur, are easily mistaken for SCL currents, but their origin is fundamentally different.[160,161] SCL currents are, however, observed in clean MSCs.[29,158,162]

At low to moderate conductivity, mobilities can be measured by the time-of-flight technique,[163−167] while for higher conductivity, CELIV, charge extraction at linearly increasing voltage, is recommended.[168−170] Hall effect measurement is the preferred technique for measuring mobilities (simultaneously with carrier densities) in ISCs,[58,71,72,171] but it is often too insensitive for OSCs. Mobilities can also be measured in a field-effect transistor, FET, configuration.[41,42,44,47,48] Most techniques measure the bulk mobility

perpendicular to the substrate plane and thus are relevant to OPV cell behavior, but FETs measure the mobility parallel to the substrate in a few monolayers nearest the gate electrode and thus are not directly comparable to the other techniques. Conductivities can also be measured, and mobilities estimated, by contactless techniques such as time-resolved microwave conductivity, TRMC.[111−114,172,173] A similar technique, teraherz spectroscopy, can measure mobilities directly.[174,175] Because of the high frequencies employed in these two techniques, the charge carriers oscillate over a very short path length (∼1 Å). Thus, these mobilities are not comparable to bulk mobilities, in which the effective path length equals the cell thickness, and the values obtained are often 1−2 orders of magnitude higher than bulk mobilities.

Carrier transport in MSC films has recently been reviewed by Shirota and Kageyama.[176] There are sophisticated theoretical models for transport in crystals of MSCs.[17,29,77] Theoretical models of transport in thin films of disordered OSCs are often derived from Bässler's Gaussian disorder model, GDM.[17,155,164,177−181] The GDM was originally developed to describe transport in insulating polymers containing electroactive small molecules, such as the hole transport layers of electrophotography.[163,177,182]

The GDM postulates that each electroactive site has an energy that is uncorrelated to its neighbors due to its discrete local solvation, orientation, and dipolar effects. Furthermore, it predicts Poole−Frenkel, PF, behavior of the carrier mobility [μ proportional to $\exp(F^{1/2})$] only at high fields ($F > 3 \times 10^5$ V/cm). Experimentally, however, the energy levels in disordered OSCs usually appear to be correlated, and PF mobilities are often observed at arbitrarily low fields.[17,164,178,180,181] Several versions of correlated disorder models based on the GDM have been proposed with different explanations for the origin of the correlations and the PF mobilities.[164,165,178,180,181,183] However, none of these models take account of the charge density in the OSC films (section 4). Thus, an alternative explanation has been proposed:[160] the long-range electrostatic fluctuations generated by the charges may cause both the energetic correlations between neighboring sites and the PF behavior of the mobility (see, for example, section 4.2 and Figures 3 and 13). The charge density in many OSCs, especially π-conjugated polymers, seems high enough to support this interpretation (section 4).[115,160] One recent model that does treat the effect of charges on carrier transport is the doped Gaussian disorder model.[179] The essential behavior is apparently also captured by the simpler Poole−Frenkel model[62,63] and its more recent extensions.[59,129,160,183]

3.5. Exciton Diffusion Length, L_{ex}, and Nanostructured Interfaces

The most common method of measuring L_{ex} in OSCs is by measuring the change in fluorescence intensity with film thickness or wavelength for films contacted by a quencher on one surface.[95,116,155,184−190] Data are fit to a diffusion-reaction model with appropriate boundary conditions, and approximations are often made to simplify the fitting. The measured values of L_{ex} in OSCs are often quite short, 5−30 nm,[8,34−36,190−192] substantially less than the optical absorption length, $1/\alpha$ (α is the absorption coefficient). When $L_{ex} < 1/\alpha$, only a fraction of absorbed photons can be successfully harvested in a planar bilayer configuration (such as in Figure 8) because many of the excitons will not survive to reach the HJ interface. To harvest more excitons in this case, some form of interfacial nanostructuring is often employed, such as a planar multilayer cell with layer thicknesses on the order of L_{ex} (section 7.5) or a bulk heterojunction, BHJ[193] (section 7.2). Unfortunately, because carrier recombination occurs primarily at the HJ interface, increasing the interfacial area via nanostructuring may increase the rate of (nongeminate) recombination.

The exciton diffusion length may not always be the major limitation for OPV cells that it is believed to be. First, because most models to which experimental data are fit assume an infinite quenching rate of excitons, L_{ex} measurements made with a less than perfect quencher will underestimate its true value. Measurements of L_{ex} have been fraught with uncertainty for 50 years. A survey of previously published L_{ex} measurements led Kenkre et al. to conclude that the majority were, in fact, limited by the quenching rate rather than by the diffusion length.[184,185] In an OPV cell, these very different limitations would lead to the same observed behavior, but would require different strategies to overcome. The quenching rate must be known, ideally from independent experiments, before an accurate value of L_{ex} can be obtained.[95]

Furthermore, L_{ex} has been measured mostly in amorphous, defect-rich OSC films that have a high density of potential quenching sites. Charged defects, for example, are known to quench excitons.[29,115,172] Decreasing the charged defect density in poly(3-hexylthiophene) has been shown to double L_{ex}.[116,118] Studies of cleaner, more crystalline MSCs show improved values of L_{ex}.[173,184,185,191,194−196] In some cases, L_{ex} approaches or is greater than $1/\alpha$.[69,95,197] If the OPV field is indeed evolving toward more crystalline, less defective materials, the simple bilayer cell may eventually become more efficient than cells with nanostructured interfaces, a reversal of the current state of affairs.

4. Defects and Doping

4.1. Lattice Forces and Defect Density

Even the most perfect crystal has defects. The free energy of crystal formation involves a trade-off between minimizing enthalpy by stacking molecules in an optimal geometry and maximizing entropy by creating defects, such as misplaced molecules or lattice vacancies. The thermodynamic minimum equilibrium defect density is expected to increase exponentially as the energetic cost of creating a defect decreases.[72,115] When lattice forces are weak, as they are in most MSCs, the defect density will be large. Single crystal anthracene at room temperature has $\sim 10^{14}$ cm^{-3} lattice vacancies (one vacancy per $\sim 10^7$ molecules), along with other types of defects.[29,115] Some of the morphological defects may create electronic states in the band gap, a fraction of which will be charged.[115,160] States created outside the band gap generally have little influence on the electrical properties. Of course, no films yet employed in OPV begin to approach the purity and crystallinity of anthracene crystals; thus the defect density is expected to be substantial in all OPV materials. More attention seems to have been paid to uncharged defects in OSCs and their influence on carrier mobility than to charged defects and their influence on mobility, carrier density, exciton diffusion length, band bending, chemical stability, etc. We briefly discussed in section 3.5 the effect of uncharged defects (modeled as Gaussian disorder) on carrier mobility. Here, we discuss the influence of charged defects.

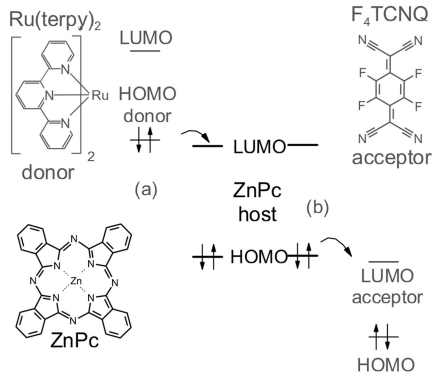

Figure 10. Energetic requirements for (a) n-type and (b) p-type doping of the same organic host material ZnPc. $Ru(terpy)_2$ is formally in the Ru^0 oxidation state. Reprinted with permission from ref 215. Copyright 2005 American Physical Society.

4.2. Doping by Design

Charged defects, whether purposely added as dopants or not, often have a controlling influence on the properties of inorganic semiconductors.[72,89,171] Their influence on OSCs is attracting ever more attention.[115−118,160,179,198] Doping studies of MSCs go back at least to Meier's work in the 1960s.[25] Molecular semiconductors have been doped with alkali metals,[199−202] gases (mostly O_2),[203] halogens,[202,204] Lewis acids,[205] organometallic complexes,[32,206] and molecular dopants.[15,23−25,70,200,202,204,207−210] Doping typically increases the conductivity and improves the photovoltaic or photoelectrochemical activity by decreasing resistance limitations. More recently, the groups of Leo[37,207,208,211,212] and Kahn[122,213,214] have performed extensive studies of doping via coevaporation of the MSC and a dopant. Besides shifting the Fermi levels as expected for a doping process, doping also diminishes the interfacial resistance of contacts.[213] These groups studied thermally evaporated amorphous or highly disordered films. Gregg et al. studied n-type doping in solution-cast, highly crystalline thin films.[59,61,70,129] Key results from these studies, such as the superlinear increase in conductivity with increasing dopant concentration and the corresponding decrease in activation energy (Figure 2), are observed both in crystalline[59,61,70,129] and in quasi-amorphous materials.[37,207,208] Apparently, these phenomena are not caused by disorder. Some differences in interpretation remain, however. Gregg et al. consider that most free carriers remain bound in the Coulomb well surrounding the dopant ion and only a thermally activated fraction of them are free, while others base their model on the assumption of shallow dopants that are completely ionized.[37,207,208] This assumption seems unlikely, however, since it does not even occur in doped silicon,[58] which has a much higher dielectric constant (Figure 2). As a general rule, it would seem that shallow dopants cannot occur in low dielectric media (section 2.1).[60]

Harada et al. doped zinc phthalocyanine, ZnPc, both n-type and p-type.[215] Their work illustrates the energetic requirements for doping (Figure 10). The n-type dopant was the reduced form of ruthenium terpyridine $[Ru(terpy)_2]^0$, while the p-type dopant was 2,3,5,6-tetrafluoro-7,7,8,8-tetracyanoquinodimethane, F_4TCNQ. Efficient doping is observed in this case because the HOMO of the n-type dopant is negative of the LUMO of ZnPc, while the LUMO of the p-type dopant is positive of the HOMO of ZnPc (Figure 10, however, see also section 4.4). The investigated devices, with both p−n and p−i−n junctions, showed a high built-in potential $V_{bi} = 0.8$ V. Effects of illumination were not reported.

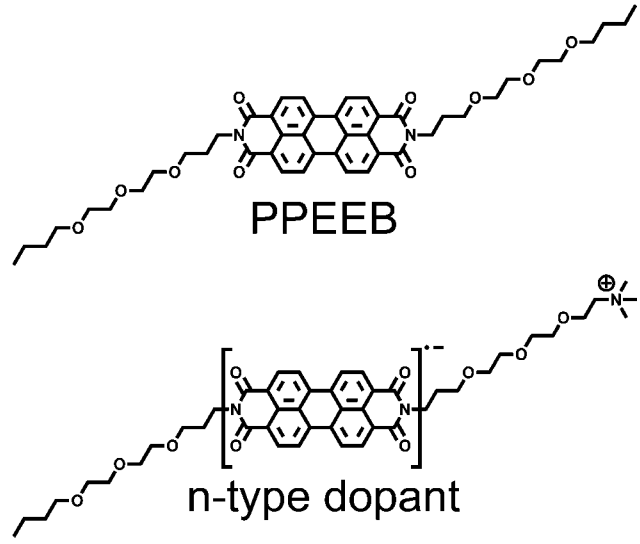

Figure 11. The chemical structure of the host semiconductor, PPEEB, a liquid crystal perylene diimide, which is in the solid state at room temperature, and its associated n-type dopant, a reduced derivative of PPEEB with a covalently attached counterion on the side chain. There are no mobile ions in these doped films.

Both Gao and Kahn[214] and Gregg and Cormier[61] pointed out that while the somewhat mobile dopants employed in most studies could increase the conductivity, they could not form stable p−n junctions. Both ∇U and $\nabla \mu$ in a p−n junction force the two dopant types together. If mobile dopants are employed to dope both sides of a p−n junction (or OLED), they will eventually drift and diffuse together to form a salt, at which point the device becomes indistinguishable from an electrically undoped device in which the same salt was added as an electrolyte.

To overcome the problem of diffusing dopants, and to study doping in clean, crystalline MSC films, Gregg et al. designed an anionic dopant with a covalently attached countercharge that would fit without disruption in the lattice of a liquid crystal perylene diimide (Figure 11).[59,61,70,80,216] As mentioned, the conductivity increases superlinearly with dopant concentration, n_d (Figure 12, top). Extrapolating from doping studies of Si and Ge at low temperature,[58,71] this was interpreted as an increase in dielectric constant with increasing concentration of the highly polarizable dopant molecules. The increase in ε causes a decrease in binding energy between the electron and the cation, thus freeing an increasing fraction of the carriers at higher doping levels. The activation energy for the current decreases with $n_d^{-1/3}$, consistent with this interpretation (Figures 2b and 12, bottom). It also decreases with applied field, as expected for carriers bound in Coulomb wells (Figures 3 and 12, bottom).[62,63] All data from these studies were self-consistently described by a Poole−Frenkel-like model that accounts only for the electrostatic attraction between opposite charges in a low dielectric medium.[59−61,70,129,216,217] Given the potential complexity of the current−voltage−temperature behavior, the fact that it can be semiquantitatively modeled by a simple Coulomb's Law treatment strongly suggests that electrostatic interactions are the dominant force controlling the behavior of this doped MSC.

As mentioned, the majority of dopant electrons (or holes in other systems) remain bound near a counterion (Figure 3). These un-ionized dopants create a dipolar electric field that perturbs the conduction and valence band edges (section 2.1). Above minimal doping levels ($\sim 10^{16}$ cm^{-3}),[160] the

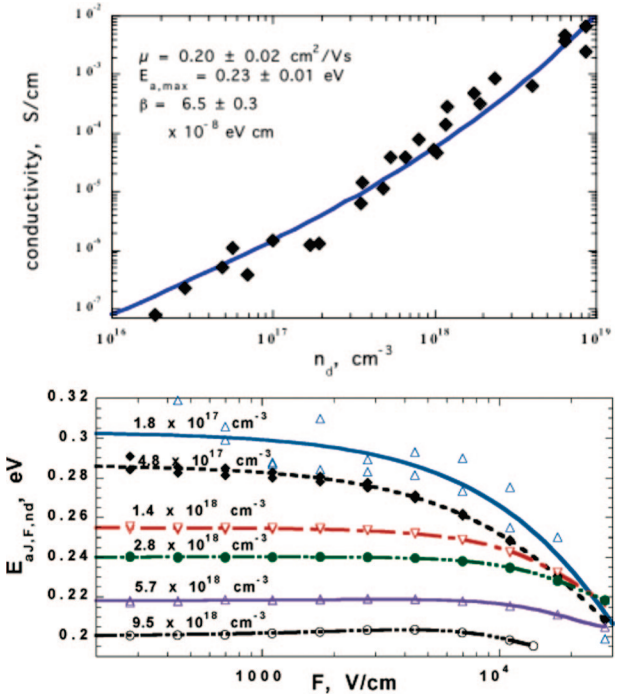

Figure 12. Top: Conductivity of PPEEB films ($F = 0.9$ V/μm) versus dopant concentration. Bottom: Activation energy for the current, $E_{aJ,F,nd}$, as a function of field, F, and doping density, n_d. Reprinted with permission from ref 59. Copyright 2005 American Chemical Society.

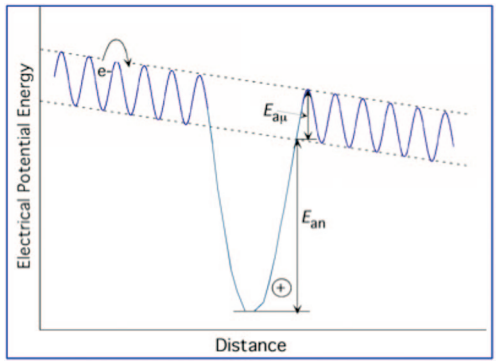

Figure 13. Model of the conduction band energy of an n-doped MSC under an applied field showing an ionized dopant and the energetic fluctuations generated by the dipolar field from un-ionized dopants.

fluctuations in the band edges should lead to Poole−Frenkel behavior of the mobility. A simple model for doping and carrier mobility (Figure 13) shows both the free carrier density and the carrier mobility being thermally activated with activation energies, E_{an} and $E_{a\mu}$, respectively, that decrease with applied field as $\sim F^{1/2}$.[60,62,63,129] Obviously such a simple model overlooks many details, but it seems to capture some essential aspects of doped OSC behavior.[60,73,129] The same electrostatic treatment may also apply to less well-defined OSC systems that are doped by their defects (section 4.5), although additional complications may occur in these cases.

Most studies of doping and transport in OSCs have been performed on disordered films. Being more complex than crystalline films, more variables can be invoked to explain their behavior. Energetic disorder, especially, has been invoked to explain diverse phenomena. Yet electrostatic interactions also exert a powerful effect on OSCs, despite sometimes being overlooked in favor of more complicated explanations.

A key part of any successful OPV cell design is to minimize the energy-wasting recombination of photogenerated electrons and holes, which occurs primarily at the HJ interface (section 3.1). Imposing an electric field across the interface by doping one side n-type and the other p-type would be expected to improve the photoconversion efficiency by sweeping carriers away from the interface before they can recombine. Figure 14 shows numerical simulations comparing a purposely doped OPV device to an "undoped" device (that is, one with a typical background defect doping of 10^{14} cm^{-3}).[16,73,115] The total potential drop across the cell is the same in both cases. The field drops uniformly across the undoped cell but is concentrated near the heterojunction interface in the doped cell (Figure 14A). Upon illumination, the interfacial recombination rate drops markedly in the doped case, resulting in a 23-fold increase in simulated photoconversion efficiency (Figure 14B).

4.3. Free Carrier Density in Undoped OSCs

If an OSC with a band gap of 2 eV were truly intrinsic (defect free), it would have a free carrier density of $\sim 10^5$ cm^{-3}.[72,115,160] Together with typical OSC carrier mobilities, $\mu \approx 10^{-5}-10^{-2}$ cm^2/(V s), this would lead to almost immeasurably small conductivities of $\sigma \approx 10^{-19}-10^{-16}$ S/cm. Typically observed, however, are conductivities of $10^{-12}-10^{-7}$ S/cm[6,61,70,117] in MSC films and $10^{-8}-10^{-5}$ S/cm[118,157,161,169,170,218] in π-conjugated polymer films. Being vastly higher than expected for intrinsic semiconductors, these data suggest that the conductivity of most OSC films is dominated by their dopant-like charged defect density, N_{def}. Other semiconductor properties such as charge carrier mobilties and exciton diffusion lengths are also expected to be strongly influenced by N_{def}.[29,70,118] We are not aware of any direct measures of N_{def}, but the free carrier density produced from the defects is easily estimated.

The product of the free electron and free hole densities, $n_f p_f$, in a doped semiconductor equals that in the intrinsic material:[72,88]

$$n_f p_f = n_i p_i = n_i^2 \tag{7}$$

With $n_i \approx 10^5$ cm^{-3} for a band gap of 2 eV,[72,160] and a measured free carrier density $>10^{14}$ cm^{-3}, it is safe to assume that most OSCs have only a single type of free carrier at equilibrium. The free holes have annihilated any free electrons, or vice versa. The countercharges to the free carriers may be deeply trapped carriers, perhaps better called anions or cations.

Assuming an n-type material, the dark conductivity is

$$\sigma(T,F) = q n_f(\mathrm{T,\ F}) \mu_n(\mathrm{T,\ F}) \tag{8}$$

Once the electron mobility, μ_n, is known, the zero-field conductivity provides a measure of the equilibrium value of n_f. The free carrier density in MSCs is commonly in the range of $10^{11}-10^{15}$ cm^{-3},[6,61,70] although higher values have been reported,[117] while that in π-conjugated polymers is $10^{15}-10^{17}$ cm^{-3}.[118,157,161,169,170,218] Every carrier at equilibrium must have a counterion to maintain electroneutrality. The total charge density in OSCs must be at least as great as the free carrier density, but it can be much higher because many charges may not produce free carriers.

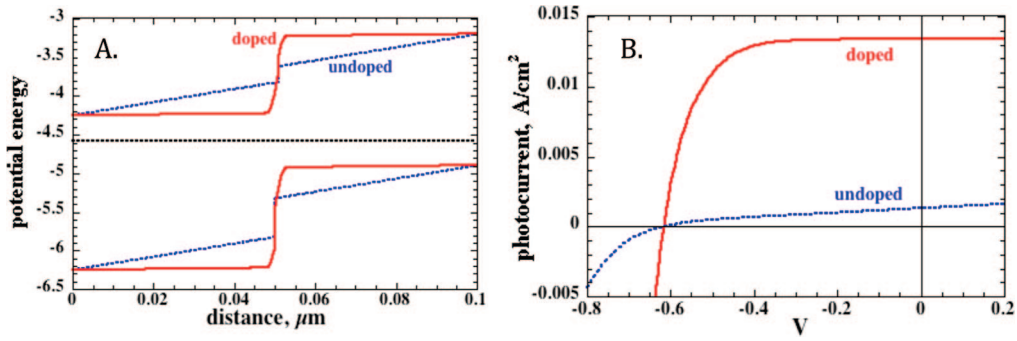

Figure 14. Numerical simulations of (A) the band diagrams and (B) the photocurrent−voltage curves of two bilayer OPV cells identical except for doping level. Reprinted with permission from ref 115. Copyright 2009 Royal Society of Chemistry.

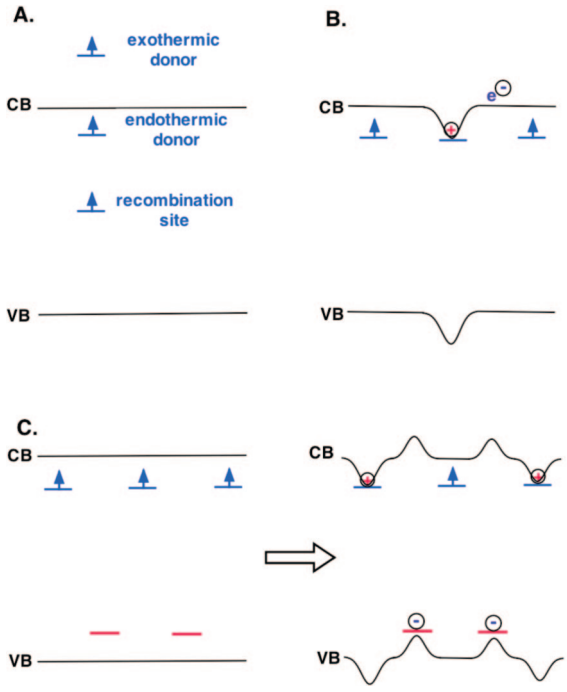

Figure 15. (A) The behavior of a donor state depends on its energy level relative to the semiconductor band edges. (B) Endothermic dopants lying ∼5−10 *kT* below the band edge may be mostly uncharged resulting in fewer electrostatic perturbations per free carrier than exothermic dopants (compare Figure 13). (C) The effect of compensating dopants (acceptor states in this case) shown before and after equilibration. Compensation reduces the free carrier density but increases the total charge density.

4.4. Defect Energy Levels

The influence of a dopant-like defect will depend on its energy level relative to the energy levels of the host semiconductor. Three ranges may be distinguished, as illustrated for a donor (n-type) defect in Figure 15A. This state is assumed to be either neutral (filled) or positively charged (empty). When the energy level of the donor state is above the conduction band edge, the electron will be transferred irreversibly to the semiconductor; thus the donor will always remain charged. However, the electron will still remain attracted to the donor cation with a typical activation energy of 100−250 meV;[59,60,116] thus only 1% or less of these charged defects may produce a free carrier at room temperature. This is the typical case of purposely added dopants as described above and was the basis for the model shown in Figure 13.

At the other extreme, if the donor state lies deep in the band gap, the activation energy for free carrier production will be so high that few carriers will be produced. The state will often be uncharged (that is, lie below the Fermi level) and may act primarily as a trap and recombination center for photoexcited holes rather than as a dopant.

The intermediate case of endothermic donors (Figure 15) is still poorly understood, but it must bridge the behavior of the two extremes. That is, if the energy level of the donor state lies exactly at the conduction band edge most of the donors will be ionized (but most carriers will remain bound), while if the state lies many *kT* below the band edge most of the donors will remain uncharged. Some electrons from the endothermic donors will still be thermally emitted into the conduction band leaving a positive ion behind. The activation energy for this process may often be dominated by the Coulomb attraction between the charges, as it was in the exothermic donor case. A PF-like increase in free carrier density with applied field would then also be expected. At the same donor concentration, the total charge density in the endothermic case should be lower than in the exothermic case. Yet because the activation energies may be similar, it seems possible that endothermic dopants at the right potential could be more effective than exothermic dopants because they would provide the same free carrier density but with less electrostatic perturbation (compare Figure 15B to Figure 13).

The physical/chemical origin of dopant-like defects is not well understood. For whatever reason, the majority of defects in films of perylene diimides, for example, tend to be donors and thus act as n-type dopants. On the other hand, the majority of defects in films of phthalocyanines tend to be acceptors, rendering them p-type. Phthalocyanines are also often p-doped by oxygen. It seems likely that in many materials both donor and acceptor defects will coexist, in which case they will compensate each other. Which one dominates may depend on subtle factors. If the material acts n-type, the donor states will have transferred electrons to the acceptor states thereby eliminating any holes (Figure 15C, see also eq 7). The effect of such compensating dopants is to decrease the free carrier density but increase the total charge density and thus the density of electrostatic perturbations.

The understanding of dopant-like defects in OSCs is still in its infancy. We are unaware of any experimental measures of the donor and acceptor density or of the total charge density in these materials. Despite our lack of knowledge, however, the defects may sometimes control the observed optoelectronic properties.

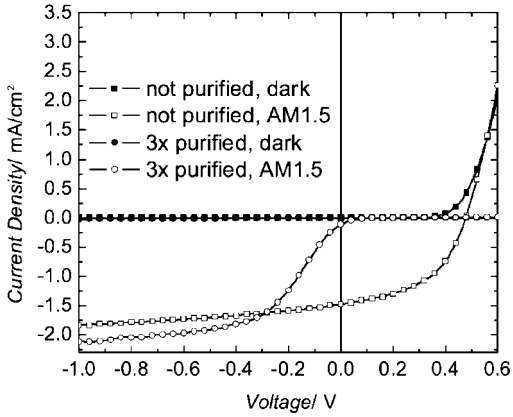

Figure 16. Current density−voltage for identical device structures, ITO/CuPc (34 nm)/PPEI (34 nm)/Ag (100 nm), with purified (circles) and impure (squares) PPEI in the dark (filled symbols) and under 88 ± 4 mW/cm^2 illumination (open symbols). Reprinted with permission from ref 117. Copyright 2008 Wiley-VCH Verlag GmbH & Co. KGaA.

4.5. Defect Doping

In many not purposely doped MSC films, and probably in most π-conjugated polymer films, dopant-like defects play a major role.[115−118,160] In some cases, it seems that the most defect-rich materials yield the best OPV devices, possibly because doping by defects is better than no doping at all.[117,219]

An ironic demonstration of defect doping was recently reported by Peumans et al.[117] They prepared bilayer OPV cells by thermally evaporating films of a rather impure perylene diimide and a phthalocyanine. Both of these materials seemed to be strongly doped by their defects, and the cells exhibited typical bilayer OPV characteristics with an efficiency of 0.4% (Figure 16). Contrary to most expectations, after rigorous purification of the perylene diimide, the efficiency dropped 200-fold. One explanation was that the defects in the original materials made the cell act as a doped p−n junction cell, similar to the doped cell in Figure 14. Purifiying the perylene diimide, however, eliminated many of its dopant-like defects, causing the field to drop more uniformly across the device. Because the field was no longer concentrated across the heterojunction where it is most effective, many photogenerated carriers could not escape the Coulomb attraction of their geminate partner and recombined. Thus, charged defects are not always deleterious.

In an investigation of unintentional doping, strong dipoles (terminal cyano groups) were introduced into an otherwise nonpolar perylene diimide (PPE_4CN, Figure 17).[70] This material self-organizes into films with crystalline domains on the 5−10 μm scale, similar to films of the same molecule without cyano groups (PPEEB). The first effect of the cyano groups was an increase in the zero-field conductivity by 4−7 orders of magnitude. Because the mobility decreased slightly, the increase in conductivity was caused by a large increase in free carrier density. This was explained by assuming that the dipole preferentially stabilizes (traps) one carrier type, freeing carriers of the opposite type. This is somewhat analogous to inducing carriers in an FET by the field from the gate electrode. The second effect was unexpected: in the originally formed red phase, the conductivity was $\sim 10^2$ times higher under air than under N_2, suggesting p-type conductivity. This is unusual for a perylene diimide. Yet as the film underwent the red-to-black phase transition (Figure 6 shows a similar system), the conductivity

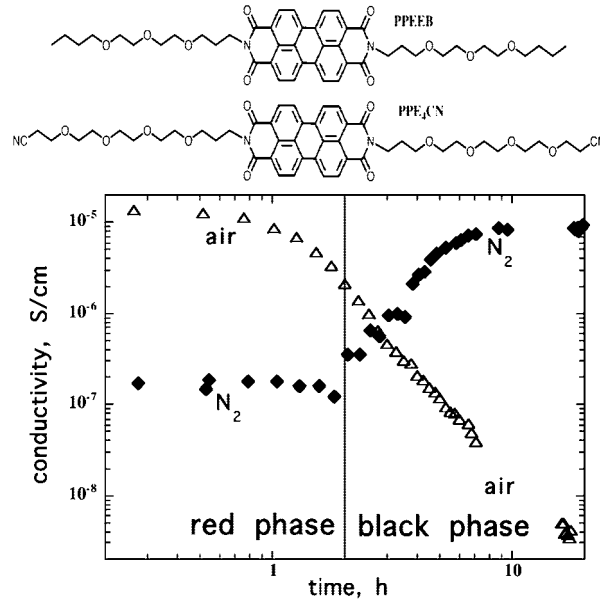

Figure 17. Top: A nonpolar liquid crystal perylene diimide derivative, PPEEB, and a similar compound with cyano groups, PPE_4CN. Bottom: The conductivity of an undoped, polycrystalline PPE_4CN film as it spontaneously converts from the red phase to the black phase under air or N_2. Reprinted with permission from ref 70. Copyright 2004 American Chemical Society.

under N_2 increased by $\sim 10^2$, while the conductivity under air fell by $\sim 10^4$, consistent with n-type conductivity (Figure 17). In this transition, the molecules in the crystal lattice move just ~1.6 Å relative to their neighbors.[75,82] Thus, a film of chemically very pure, crystalline MSC containing no dopants acts moderately p-doped in one crystal polymorph and moderately n-doped ($n_f \approx 10^{15}$ cm^{-3}) in a slightly different polymorph. The "dopants" in this case are uncharged cyano groups that induce the formation of about one free carrier per 10^6 dipoles.[70] Again, small changes in crystal packing can cause large changes in electrical properties.

5. Device Characterization

5.1. Efficiency Measurements

Accurate efficiency measurements are crucial to evaluating new materials systems or processing technologies. The testing conditions for reported efficiencies are not always comparable; because the spectral output of the light source, the spectral sensitivity of the reference detector, the active area of the device, etc., may vary substantially. To account for these differences, a standardized and consistently applied set of measurement techniques and equipment is important for accurate comparison of device performance. In the U.S., the Cell Performance Laboratory at the National Renewable Energy Laboratory, NREL, certifies solar cell efficiency measurements and provides reference-cell calibrations. There are similar test facilities in Germany and Japan. Several certified efficiencies have been reported for polymer-based bulk-heterojunction devices,[220] but until very recently, to our knowledge, only one MSC cell was certified: a single-junction ITO/PEDOT:PSS/CuPc/C_{60}/BCP/Al (BCP is 2,9-dimethyl-4,7-diphenyl-1,10-phenanthroline; see section 7.3) device with a 1.03% power conversion efficiency.[221] Far higher efficiencies of 5−6% were claimed, but only recently was a MSC-based tandem

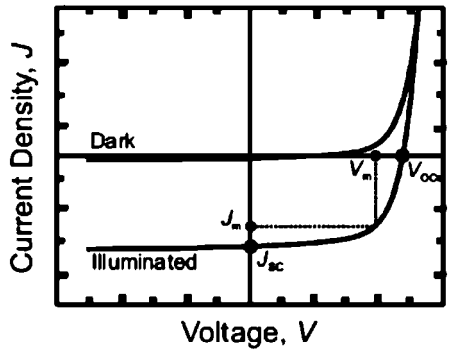

Figure 18. Current−voltage curves for an MSC solar cell. The maximum power point is at J_mV_m; J_{sc} and V_{oc} are labeled; $FF = J_mV_m/J_{sc}V_{oc}$.

(section 7.6) OPV device topping 6% power conversion efficiency certified.[222]

The power conversion efficiency, η_p, is defined as the ratio of the maximum power delivered by the device, P_{max}, to incident power, P_{in}, from the light source. $P_{max} = J_mV_m$, where J_m and V_m are the current and voltage at the maximum power point, respectively (Figure 18).

$$\eta_p = J_mV_m/P_{in} = J_{sc}V_{oc}FF/P_{in} \quad (9)$$

where J_{sc} is the short-circuit photocurrent density, V_{oc} is the open-circuit voltage, and FF is the fill factor. The latter is an indication of the diode quality and is mainly influenced by charge carrier transport and recombination (or series and shunt resistances, see below). Optimized OPV devices may have values of FF in the range 0.5−0.7.[223]

In measuring the efficiency of an organic solar cell, a number of factors must be considered. One is a comparison of the test light source to the solar spectrum. The spectral irradiance of the sun as measured beyond the earth's atmosphere is defined as air mass 0, AM0, and approximates that of a 5780 K blackbody spectrum.[224] At the earth's surface, certain wavelengths are absorbed by water vapor and other atmospheric components, and the degree of absorption is dependent upon the optical path length through the earth's atmosphere. This path length is determined in turn by the angle of the sun relative to the point of measurement. Air mass 1.5, AM1.5, designates that photons pass through 1.5× the mass of the atmosphere directly overhead, translating to the sun having an angle of 48.19° from the zenith (Figure 19a). The AM1.5G173 global reference solar spectrum shown in Figure 19b has been adopted as the most accurate representation of the average annual spectral output measured at sea level with a south-facing (in the northern hemisphere) surface that is tilted 37° to best approximate the average latitude of the U.S.[225−227] This geometry is illustrated pictorially in Figure 19a.[226] Testing solar cells using the AM1.5G spectrum at 25 °C and a total irradiance of 100 mW/cm^2 represents standard reporting conditions.

As represented in Figure 19b, J_{sc} should be equal to the flux obtained by integrating the external quantum efficiency, EQE, of the device over the spectrum of the excitation source. However, the spectral irradiance of an artificial light source will never exactly match the AM1.5G173 reference spectrum nor will the spectral response of the reference and test cells ever correlate perfectly. To account for these errors, the spectral mismatch factor, M, is included in the calculation

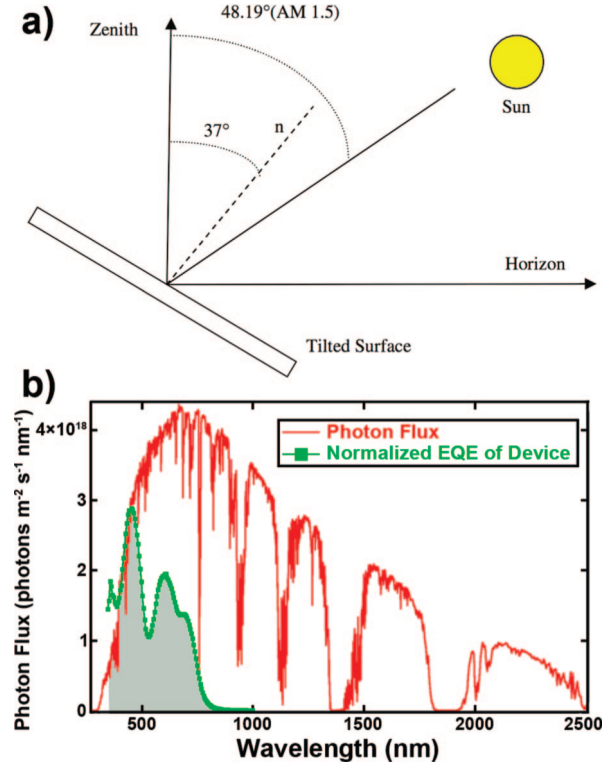

Figure 19. (a) Illustration of the geometry used to derive the standard AM1.5 spectrum. (b) Overlay of the AM1.5G solar flux spectrum with a normalized EQE of a CuPc/C_{60} device measured at short-circuit. Integration of the shaded area represents the hypothetical J_{sc} of the device. Part a is reprinted with permission from ref 226. Copyright 2008 Elsevier.

of efficiency. The somewhat complex details of how this is done are described elsewhere.[221]

One simple method to improve cell efficiency measurements for OPV devices is to use glass filters (most commonly the Schott KG5 filter) in front of the Si reference photodiode to eliminate the near IR response. This greatly improves M (brings it closer to 1) relative to an unfiltered Si photodiode or a thermal detector that can give ∼35% error in estimating OPV efficiency.[221] When measuring the EQE with chopped light, the response time of the cell is important. For example, the dye-sensitized solar cell, DSSC, has a very slow response, resulting in an apparent decrease in quantum efficiency with increasing chopping frequency.[228,229] The response time of most solid-state OPV devices, however, appears to be fast enough that frequencies around 150 Hz can be employed.[221]

In addition to the spectral mismatch factor, another potential source of error in measuring η_p is in defining the active area of the device, A, especially as A gets smaller. To reduce the probability of electrical shorts, test OPV devices are usually quite small. A typical OPV test cell fabricated on patterned indium tin oxide, ITO, substrates with evaporated metal back contacts is shown in Figure 20. The area of the device is defined by the overlap between the evaporated metal and the underlying ITO. However, the shadow masks used for the evaporations can yield different areas than what is assumed because of shadowing effects during deposition.[221] Also, collection of charges photogenerated outside the active area via waveguiding or lateral charge transport to the electrodes may also contribute to the photocurrent, falsely inflating the measured value of J_{sc}.[230,231] The best way to mitigate both problems is to illuminate the cell through a mask of known aperture that is smaller than

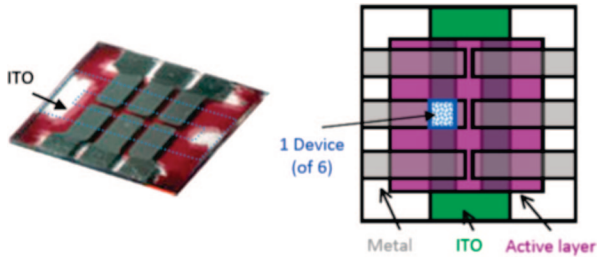

Figure 20. Left: Photograph of an OPV cell fabricated on a patterned ITO substrate with an evaporated metal back contact. Right: Diagram of the array showing the active area (0.1 cm^2) for one of the six devices. Courtesy of Matthew Reese, NREL.

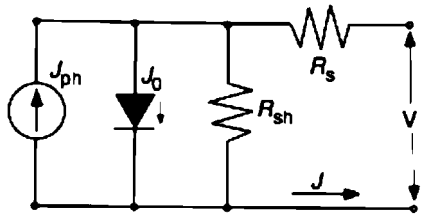

Figure 21. Basic circuit model for a solar cell showing the photocurrent and reverse saturation current densities, J_{ph} and J_0, respectively, and the series and shunt resistances, R_s and R_{sh}, respectively. Other resistors, capacitors, and diodes can be added to model more complex behavior.

the device area. The area of the aperture then determines A. In general, it is difficult to accurately measure η_p in devices of $A < 0.1$ cm^2. Some of the highest efficiencies have been reported for unmasked cells with $A < 0.01$ cm^2.

5.2. Equivalent Circuit Model

The generalized Shockley equation describes the current density through a solar cell modeled as an equivalent circuit (Figure 21) consisting of a photocurrent source, a diode, a series resistance, R_s, and parallel, or shunt, resistance, R_{sh}:

$$J = \frac{R_{sh}}{R_s + R_{sh}}\left\{J_0\left[\exp\left(\frac{q(V - JR_s)}{nkT}\right) - 1\right] + \frac{V}{R_{sh}}\right\} - J_{ph}(V) \quad (10)$$

where V is the voltage, n is the diode quality factor, J_0 is the dark saturation (recombination) current, and $J_{ph}(V)$ is the voltage-dependent photocurrent.[88,119] In cells with low leakage currents, $R_{sh} \gg R_s$, and the equation simplifies to:

$$J = J_0\left[\exp\left(\frac{q(V - JR_s)}{nkT}\right) - 1\right] - J_{ph}(V) \quad (11)$$

When R_s is negligible, eq 11 can be rearranged at open circuit to yield[56,119]

$$V_{oc} = \frac{nkT}{q}\ln\left(\frac{J_{sc}}{J_0}\right) \quad (12)$$

Values of n are typically around 2 for most OPV devices (ideally, $n = 1$), which indicates that J_0 may be recombination controlled.[119,232] Ideally J_{sc} increases linearly with light intensity, I, V_{oc} increases with $\ln(I)$, and the FF is independent of I. Thus, maximum power ideally increases as $\ln(I)$. In an ideal cell, $R_s = 0$ and $R_{sh} = \infty$. Power losses are minimized as the values in actual cells approach the ideal values. The effects of changing R_s and R_{sh} on solar cell performance are shown in Figure 22. A high value of R_s does not affect V_{oc} but reduces J_{sc} and FF. High R_s may result from low charge carrier mobilities and barriers to charge extraction at the electrodes.[221,233] For large area devices, resistance losses within the electrodes may also contribute significantly. A low value of R_{sh} does not affect J_{sc} but reduces V_{oc} and FF. Thin spots in the cell caused by the evaporated metal contact penetrating into the organic film are one source of shunting. A flat spot or kink near V_{oc} is sometimes observed in the $J-V$ curve, which greatly reduces FF.[234,235] The cause of this behavior is still a matter of investigation, but it may involve a field-dependent separation of geminate carriers (section 3.1) or the buildup of space charge.[39,119,234,236−239]

6. Constituent Materials of OPV Devices

The materials requirements for the most basic architecture of small molecule OPV devices include a transparent substrate, a transparent electrode, a light-absorbing organic active layer, and a counter-electrode. Additional interfacial layers, IFLs, on either side of the active layer are often used, and several examples are given in section 7.3. Completed devices also frequently employ some encapsulation method for protection against ambient oxygen and moisture. Figure 23 displays a generic representation of an OPV device for which common materials of the essential layers are discussed in this section, and the interfacial layers are discussed in section 7.3.

6.1. Substrate

The most frequently employed OPV substrate in the scientific literature is glass for a variety of reasons. It is cheap, it provides a good barrier against oxygen and water diffusion into the device, and it is commercially available precoated with the common anode material tin-doped indium oxide, ITO. Furthermore, because the substrate is not the subject of research in most OPV studies, typically alternative substrates are not used because they could introduce new variables during device fabrication. However, it is routinely cited that a major advantage of OPV devices over inorganic PVs, such as crystalline Si, is compatibility with flexible substrates, such as plastic. A number of studies have demonstrated fully flexible devices, and at least one company, Konarka Technologies, is already producing large quantities of plastic OPV material, called Power Plastic, via roll-to-roll methods for imminent use in commercial products.[55,246] The use of flexible substrates, for example, poly(ethylene terephthalate), PET, polycarbonate, or polyethersulfone, PES, is often illustrated with polymer-based, rather than small molecule-based, OPVs (see Figure 1) to emphasize the unique advantages associated with polymeric materials such as the low-temperature large-area solution processing and roll-to-roll deposition techniques. For vapor-deposited small molecule OPVs, however, deposition on glass or plastic substrates is equally feasible, and although few studies have been conducted on plastic to date,[244,245,247,248] in fact small molecule OPV devices have similar potential for production on flexible substrates as polymer OPVs. Prior work by Forrest et al. with flexible vacuum-deposited organic light-emitting diodes, OLEDs, further demonstrates this.[249] The ability to fabricate vacuum-deposited OPVs on plastic

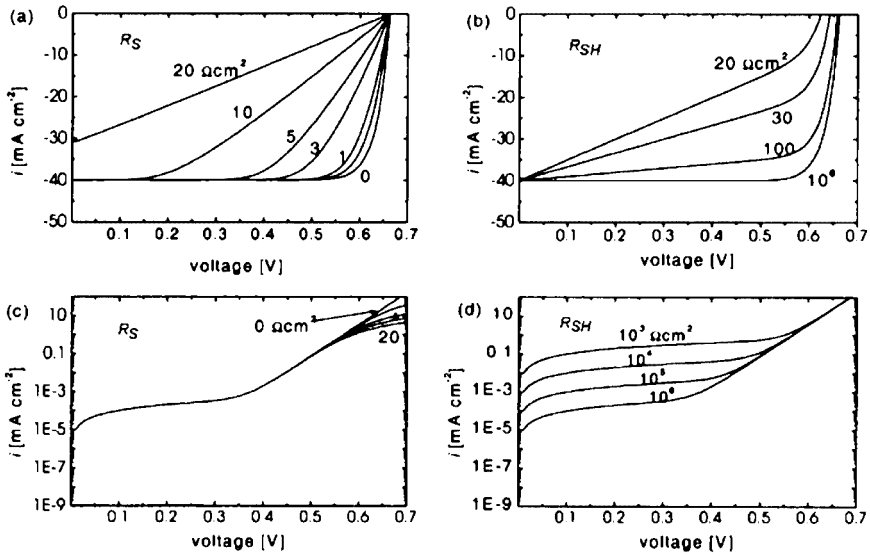

Figure 22. The influence of series resistance, R_s, and parallel (shunt) resistance, R_{sh}, on the $J-V$ characteristics of a hypothetical solar cell. (a) Under illumination, R_s varied as shown. (b) Under illumination, R_{sh} varied as shown. (c) Dark, R_s varied as shown. (d) Dark, R_{sh} varied as shown. Reprinted with permission from ref 240. Copyright 2001 Imperial College Press.

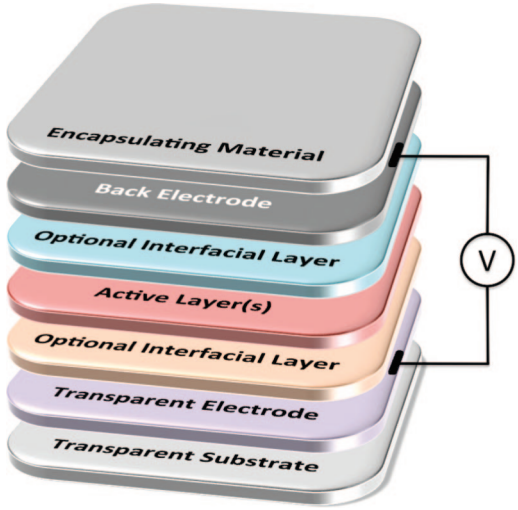

Figure 23. Depiction of general organic photovoltaic device architecture with electrical contacts. If the bottom transparent substrate is not glass, then a transparent encapsulating material on the bottom (not shown) may also be required to prevent oxygen and water ingress.

substrates also implies that tandem cells (see section 7.6) based on small molecules can be prepared on flexible substrates.

In addition to flexibility, other substrate property considerations include the transparency, the thermal stability of the substrate versus the highest fabrication processing temperature employed, and the substrate oxygen and water permeabilities.[250,251]

6.2. Transparent Electrode

On top of the substrate is deposited a transparent electrode. The most common material used for this purpose is the transparent conducting oxide, TCO, tin-doped indium oxide, ITO. ITO is readily available commercially as a film on glass or plastic in a wide variety of thicknesses, conductivities, and surface roughnesses. The transparency of ITO, a semiconductor with a wide band gap, E_g, of 3.2−4.0 eV,[252−254] is typically >85% through the visible region of the spectrum, which allows efficient light-harvesting by the active layer of the OPV device. The conductivity of ITO on glass ranges from ∼3000−6000 S/cm and is lower on plastic (<1500 S/cm).[255] The ITO work function lies in the broad 3.7−5.1 eV range, often considered to be ∼4.7 eV, and it is greatly dependent on the surface pretreatment method used for cleaning, as well as on the In/O and In/Sn atomic ratios and on the surface carbon content.[256−260] Procedures such as solvent cleaning lower the observed ITO work function (shift it closer to vacuum) by leaving a high concentration of surface C contamination, and UV ozone or oxygen plasma cleaning methods tend to raise the work function (shift it away from vacuum) by effectively removing carbonaceous contamination and possibly also by affecting the oxygen vacancy concentration at the ITO surface.[256,258−261] While the inconsistency in ITO work function is a persistent variable differentiating OPV studies performed at various research institutions worldwide, it can also be advantageous such that ITO work function tuning to match energy levels with adjacent organic materials can be achieved via simple surface treatment variations.

Despite the standard use of ITO as a transparent electrode in OPVs, there are several potential areas for improvement. For example, Forrest and others have observed that the resistivity of ITO is too high and adversely affects OPV performance, especially at larger active areas, implying that a TCO with a higher conductivity would be beneficial.[223,262] Another factor that precludes ITO from being an ideal OPV anode is that ITO exhibits n-type conductivity, but it is most often used as a hole-collecting anode in OPVs. A p-type TCO would be preferable for this role, but few p-type TCOs exist, none of which currently surpass ITO performance.[263−269]

Finally, the significant cost of ITO stemming from its high indium content (∼93 at.% of metal, ∼77 wt % of ITO) has reserved ITO use for only the most demanding applications. Current indium prices are ∼$650−$700/kg and could go up if thin film solar industries using the metal significantly increase demand.[270,271] The high cost has spurred researchers to seek alternative TCOs that contain less indium. Various indium-free TCOs have been used in OPVs, including fluorine-doped tin oxide, FTO, aluminum-doped zinc oxide, AZO, and TiO_2. FTO is commonly used in DSSCs, but its

increased surface roughness versus ITO likely contributes to a poor interface with small molecule and polymer-based OPVs resulting in high series resistance (R_s) values, and therefore ITO is typically chosen as the transparent anode for these types of devices despite the greater cost.[272,273] In an effort to utilize economical ITO alternatives in small molecule OPV devices, Bernède et al. have shown that coating different TCOs with a thin layer of metal leads to performance of copper phthalocyanine, CuPc/C_{60} bilayer devices comparable to standard devices, which include a commonly used layer of poly(3,4-ethylenedioxythiophene): poly(styrene sulfonate), PEDOT:PSS (see section 7.3), on ITO.[274,275] Moreover, by coating the various TCOs investigated with only ~0.5 nm of Au, devices incorporating ITO, FTO, or AZO as the transparent electrode were all reported to exhibit approximately equal performance metrics, opening up the possibility of an indium-free anode. Inclusion of the thin metal overlayer also yields devices of equal performance regardless of the underlying TCO cleaning procedure, which is well-known to typically have a strong influence upon surface properties and optoelectronic device performance.[238,276] The metal employed affects the anode work function, which could be beneficial, but it also could be detrimental if the work function of ITO is more closely aligned to the proximate organic layer HOMO energy.

One clever way to retain the well-known work function and surface properties of ITO while significantly reducing the indium content in the anode is through the use of a bilayer TCO. Liu et al. have employed a highly conductive (~12 000 S/cm) TCO film, indium-doped cadmium oxide, CIO, coated with a thin layer of ITO as an OPV anode.[277,278] The bilayer CIO/ITO film offers higher conductivity at the cost of slightly reduced transmission (<5% difference), and the replacement of a ~150 nm film of commercial ITO with a bilayer CIO/ITO film (170 nm/40 nm) reduces the indium content in the TCO from 77% to 18% by weight, thereby greatly reducing materials cost. The bilayer TCO was demonstrated in poly[2-methoxy-5-(3′,7′-dimethyloctyloxy)-1,4-phenylene vinylene]: [6,6]-phenyl-C_{61}-butyric acid methyl ester, MDMO-PPV: PCBM, OPVs to achieve comparable η_p values to devices made on commercial ITO, and these results should translate well to small molecule-based devices.

Apart from TCOs, carbon nanotubes, CNTs, have been investigated for use as OPV anodes.[279−281] They were first employed successfully as a transparent electrode material in bulk-heterojunction, BHJ, OPV devices by Rowell et al. in 2006.[281] In that work, devices on PET/CNT substrates achieved efficiencies of 2.5%, just slightly lower than the 3.0% recorded for devices on glass/ITO. The performance difference between the architectures was observed in the fill factor, *FF*, which was lower in the CNT devices because of the higher sheet resistance (~200 Ω/□) demonstrated in these anodes compared to ITO (15 Ω/□). More recently, a tandem device using multiwalled carbon nanotubes, MWCNTs, as an interlayer anode incorporated both blended poly(3-hexylthiophene):[6,6]-phenyl-C_{61}-butyric acid methyl ester, P3HT:PCBM, and bilayer CuPc/C_{60} active layer systems.[280] In this case, the high sheet resistance of the nanotube electrode/organic interface was blamed for a low observed J_{sc} value. Both works stressed that many film and device parameters were unoptimized in these initial studies, and there is significant room for improvement in CNT use as an ITO electrode replacement for OPVs.

Conductive polymers represent a final materials category utilized to date as an ITO alternative in OPV devices. The ubiquitous PEDOT:PSS[282−284] has been used for this purpose, but PEDOT:PSS films exhibit relatively high sheet resistance as compared to ITO. Therefore, the conductivity of PEDOT:PSS must be enhanced when it is used for a charge-collecting electrode material rather than an ITO-modifying IFL. This is often achieved by "doping" the PEDOT:PSS with a high-boiling point alcohol such as sorbitol, mannitol, or glycerol.[262,285,286] Kushto, Kim, and Kafafi have used highly conductive PEDOT:PSS films as anodes in OPV devices consisting of *N*,*N*′-(α-naphthyl)-*N*,*N*-diphenyl-1,1′-biphenyl-4,4′-diamine (α-NPD) and buckminsterfullerene to achieve 1% power conversion efficiency, comparable to ITO-based devices constructed in parallel.[245] Again, however, the high sheet resistance of even the "doped" PEDOT:PSS electrode film (~450 Ω/□) yields reduced *FF* values as compared to lower sheet resistance ITO devices (~30 Ω/□), signifying that even greater PEDOT:PSS conductivity is needed, especially at active areas larger than the 0.04 cm^2 devices used in the aforementioned study.

6.3. Active Layer

Many MSCs have been known and studied for decades. Of these, only a small fraction has been used with success in OPV devices because of the various electrical, optical, and stability requirements demanded of the chosen materials. The MSC charge carrier mobility, exciton diffusion length, thin film morphology including both crystallinity and packing structure, frontier energy level alignment, band gap, and absorption coefficient all greatly influence OPV device performance. Other MSC characteristics such as ambient stability, thermal durability, and interfacial robustness can also affect device performance and become increasingly important when considered over the device lifetime rather than in terms of an immediate efficiency measurement. Herein, some of the donor and acceptor materials most commonly used in the OPV device active layer are described, many of their structures are shown in Figure 24, and the corresponding OPV devices are discussed.

6.3.1. Porphyrins

Porphyrins were studied early on as photoactive materials for organic solar cells partly because the porphyrin structure is a synthetically tractable analogue of chlorophyll, which is the molecule used in nature to collect photons and generate energy via photosynthesis.[287] Porphyrins have extensively conjugated π systems, are amenable to fast electron transfer to an acceptor, absorb light well in the blue and moderately in the green regions of the visible spectrum with high molar absorption coefficients, and have tunable redox properties via synthetic modification of the periphery or via metal insertion into the cavity.[288,289] These attributes make porphyrins attractive semiconductors for use in the active layer of OPV devices.

Although most frequently employed as an electron donor, porphyrins have fulfilled a variety of roles in OPV cells as described below through examples from the literature. They have found use as both donor and acceptor, depending on the electron-donating or -accepting characteristics of the bound substituents, the metal center, and the frontier orbital energies of the other active layer species.[100,110,290−298] Porphyrins have also been coupled to the common acceptor,

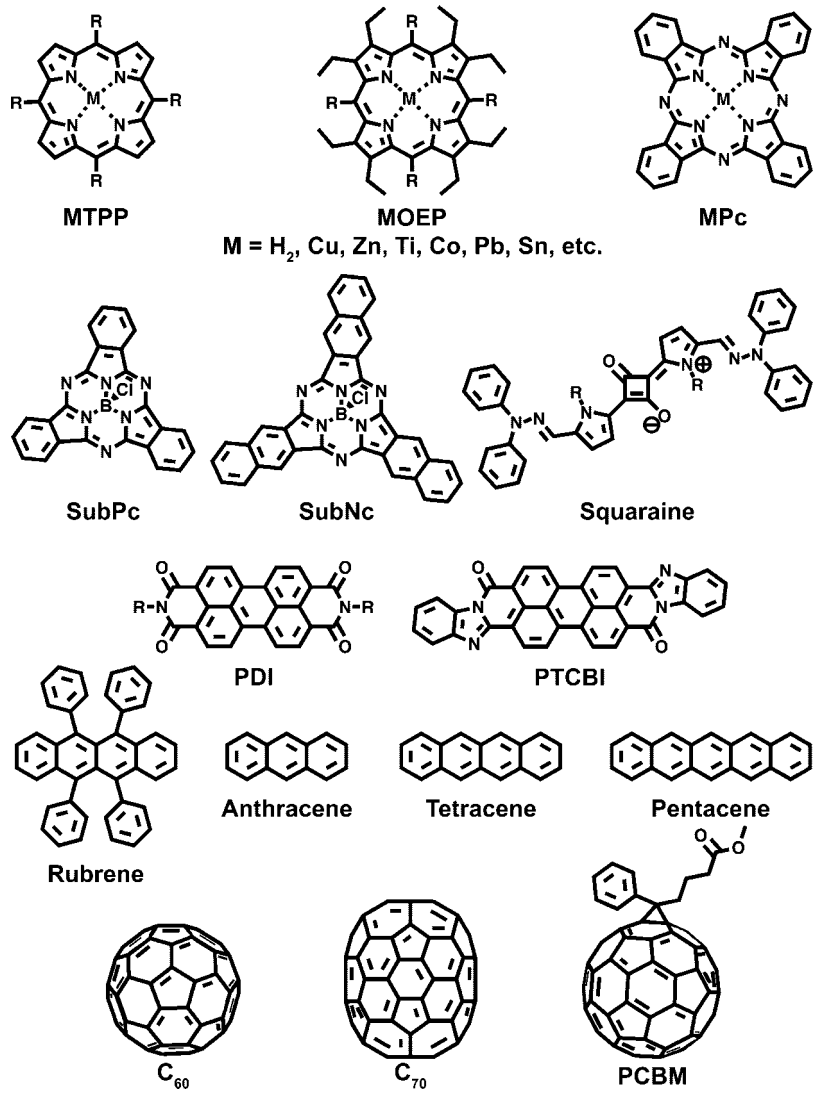

Figure 24. Chemical structures and abbreviations of common active layer materials in small molecule OPV devices. MTPP = metallotetraphenylporphyrin, where R is usually a phenyl derivative. MOEP = metallooctaethylporphyrin. MPc = metallophthalocyanine. SubPc = chloro[subphthalocyanine]boron(III). SubNc = chloro[subnaphthalocyanine]boron(III). PDI = perylene diimide. PTCBI = 3,4,9,10-perylenetetracarboxylic bis-benzimidazole. Rubrene = 5,6,11,12-tetraphenyltetracene. PCBM = [6,6]-phenyl-C_{61}-butyric acid methyl ester.

C_{60}, in molecular dyads, supramolecular structures with D and A species held in close physical and electrical contact by covalent bonds (see also section 6.3.6).[287,299] Also, porphyrins have been employed as an extra light-absorbing species added to the active layer of complete devices.[300−302]

A variety of acceptor or donor molecules and polymers have been coupled with porphyrins in the standard bilayer device configuration; however, the short exciton diffusion length (<10 nm) of porphyrins tends to limit device η_p.[294] An early study paired a wide array of metal-free porphyrin donors with several different perylene acceptors in bilayer devices, and white light power conversion efficiencies exceeding 0.03% were never observed.[298] Detailed device fabrication processes and film thicknesses were not presented, making a thorough analysis of these cells difficult, but the short exciton diffusion in porphyrins coupled with the layer thickness required to absorb most incident light is likely at the root of the low efficiencies. In another report of porphyrins in bilayer OPV devices, porphyrin derivatives comprised both the active layer donor and the acceptor.[295] Zinc tetra(4-hydroxyphenyl) porphyrin, ZnTHOPP, was electropolymerized onto an ITO substrate and used as a donor polymer. The quaternized pyridyl groups modifying tetra(methyl pyridinium) porphyrin, H_2TMPyP, induce electron-accepting behavior and designate this spin-coated porphyrin derivative as an acceptor. Devices of this bilayer design, however, also exhibit low incident photon to current efficiency, IPCE, values.

Bilayer OPV devices have also been fabricated from porphyrins in conjunction with poly(3-hexylthiophene), P3HT,[290] a polymer commonly used in polymer:fullerene BHJ OPV devices that have achieved efficiencies exceeding 4%.[303−306] In the case of the porphyrin/P3HT bilayer, the P3HT acts as the electron donor, and the porphyrin, H_2TMPyP, fulfills the role of electron acceptor. The P3HT chains deposited on the H_2TMPyP exhibit a high degree of organization and therefore have long exciton diffusion lengths. As compared to many other small molecule/P3HT bilayer devices, the H_2TMPyP/P3HT devices yield relatively high IPCE values (~20%) across both the porphyrin and the P3HT optical absorption regions, demonstrating that photons absorbed in either active layer material contribute to the observed photocurrent. Despite this, both layers are significantly thicker (H_2TMPyP/P3HT, 25 nm/75 nm) than the

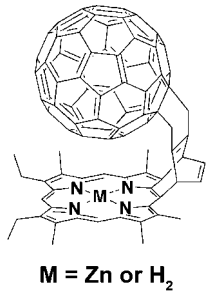

Figure 25. Structure of first reported porphyrin−fullerene dyads.[309]

determined exciton root-mean-square displacement in either material (H_2TMPy, 14 nm; P3HT, 18 nm), which implies that a device architecture employing a shorter required exciton diffusion length, such as a bulk heterojunction, would likely succeed in boosting efficiency (see section 7.2).

Sun et al. compared the performance of porphyrins in bilayer and bulk−heterojunction devices. In this work, spin-coated liquid crystalline porphyrin derivatives were elected as donors for each device configuration. Vapor-deposited C_{60} was chosen as the acceptor in bilayer devices, while [6,6]-phenyl C_{61}-butyric acid methyl ester, PCBM, was selected as the acceptor in BHJ devices.[110] For both architectures, photovoltaic performance metrics were recorded for devices having undergone active layer annealing to enhance porphryin alignment and for those omitting the annealing process. The annealing step yields vastly improved J_{sc} and η_p values in both device configurations because the thermally induced liquid crystalline porphyrin alignment allows for optimum hole transport through the films. The BHJ architecture demonstrates greatly increased J_{sc} and η_p values as compared to the bilayer arrangement because of the shorter distance excitons need to travel to reach an interfacial charge transfer site. The highest device efficiency found in this study is 0.775% for an annealed BHJ porphyrin:PCBM active layer.

To prepare a BHJ layer comprised entirely of small molecules, Vilmercati et al. codeposited porphyrin and fullerene molecules by powder sublimation.[307] Identical deposition rates for Zn-tetraphenylporphyrin, ZnTPP, and C_{70} were achieved during the codeposition, and the resultant films are ∼110 nm thick. This process yields ordered films in which the macrocycle and fullerene align to form a supramolecular multilayer structure that promotes chromophore interaction and induces donor−acceptor, D−A, behavior. While no actual OPV devices were fabricated in this work, the findings that the excited charge transfer from the porphyrin to the C_{70} proceeds at a time scale faster than 1−2 fs and that the molecules are ordered in the film on a mesoscopic scale bode well for the separation of photogenerated excitons and the subsequent collection of charges at electrodes in working porphyrin−fullerene OPV devices.

In studies complementary to those utilizing distinct porphyrin and fullerene molecules in close contact within an active layer, the photochemistry and intramolecular charge transfer of porphyrin−C_{60} dyad molecules have been extensively studied[308] (see section 6.3.6) since Liddell et al. reported the first linkage in 1994, shown in Figure 25.[309] The research groups of Imahori, Fukuzumi, and Yamazaki have constructed silane-based self-assembled monolayers (SAMs) of porphyrin−C_{60} dyad molecules on ITO and compared them to porphyrin monolayers not containing the fullerene. Perhaps unsurprisingly, greatly enhanced photocurrent generation occurs in the case of the D−A pair, which underscores the importance of a proper D−A heterojunction for charge separation.[299,310,311]

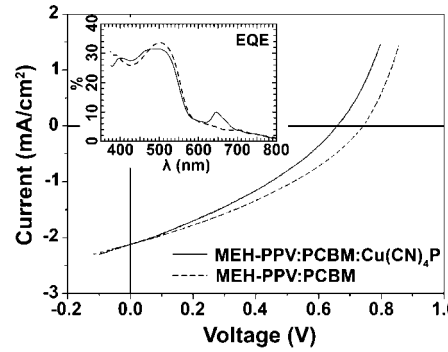

Figure 26. *J*−*V* plot and EQE (inset) for BHJ OPV devices with active layer compositions MEH-PPV:PCBM:$Cu(Cn)_4P$ (1:8:1) and MEH-PPV:PCBM (2:8) in which the porphyrin acts as a photosensitizer. Modified and reprinted with permission from ref 302. Copyright 2007 American Chemical Society.

Another way in which porphyrins have been incorporated into OPVs is as a photosensitizer, or a light-absorber to efficiently harvest photons that would not be absorbed by the other active layer components.[300−302] Dastoor and Reimers fabricated poly[2-methoxy-5-(2′-ethylhexyloxy)-1,4-phenylene vinylene]:[6,6]-phenyl-C_{61}-butyric acid methyl ester, MEH-PPV:PCBM, BHJ OPV devices that included the porphyrin [2,3,12,13-tetracyano-5,10,15,20-tetrakis(3,5-di-*tert*-butylphenyl)porphyrinato]copper(II), $Cu(CN)_4P$, blended into the active layer.[302] Remarkably, the active layer morphology is largely unchanged upon porphyrin integration, and as shown in Figure 26, the ternary BHJ devices exhibit J_{sc} values comparable to the binary blend devices even though the fraction of the light-absorbing polymer is halved in the ternary blend. EQE measurements presented in the inset of Figure 26 confirm that the porphyrin contributes to the photocurrent by absorbing light in the 600−700 nm range where minimal light absorption existed prior to porphyrin incorporation into the active layer.

One drawback to the parent porphryin structure is that charge carrier mobilities for porphyrin derivatives are relatively low. Literature values for hole mobilities in porphyrins vary tremendously from 10^{-16} to 10^{-1} $cm^2/(V\ s)$,[111,167,312−318] and most of the reported values are below 10^{-8} $cm^2/(V\ s)$, a mobility that is too low for efficient charge transport in real OPV devices. The discrepancy in the values derives from many factors, including whether the original data were taken from time-of-flight, TOF,[316,318] current−voltage,[297,317] field-effect,[312−315] or microwave conductivity[111] measurements, as well as the material purity and its exposure to ambient atmosphere. The highest porphyrin mobilities arise because of microcrystal or molecular wire formation, including a report of a double wire "ladder-like" structure with bipyridyl groups acting as "rungs" to increase porphyrin planarity and conjugation.[313,319] These highly organized porphyrin structures demonstrate the potential of porphyrin molecules in transporting charges over a long distance, a feat that is necessary for efficient use as an active layer material in OPV devices.

6.3.2. Phthalocyanines

Phthalocyanines are planar and highly aromatic 18-π-electron macrocycles that are structurally related to porphy-

rins (Figure 24). Phthalocyanines comprise four isoindole units connected by 1,3-aza linkages. They represent a subclass of azaporphyrins (porphyrins in which the C atom in the methine bridges is replaced by a N atom, forming azamethine bridges) in which each of the four azaporphyrin pyrrole units is converted to an isoindole group by the presence of a fused benzene ring.[320,321] Phthalocyanine, Pc, derivatives typically exhibit excellent thermal and chemical stability,[321] and, like all MSCs, they offer flexibility in their optical and electronic properties through synthetic modifications, including the addition of functional groups to the molecule perimeter. The structural similarity between Pc and porphyrin molecules offers both classes of molecule an additional method for tuning optoelectronic properties and stacking in the solid state: replacement of the two protons in the molecule cavity with a metal ion. Although over 70 metallic and nonmetallic ions will fit into the phthalocyanine cavity,[322] and many of these MPc complexes have been used in solar cells, Cu and Zn have been the most common choices to date for use in Pc-based OPV devices.

In addition to the shared benefits between porphyrins and phthalocyanines of highly tunable properties due to synthetic variations and metal ion incorporation, the latter structures offer various advantages over the former as potential active layer materials in OPVs. One advantage is an absorption over a wider spectral range,[323] which allows phthalocyanines to absorb more photons, thereby increasing photocurrent generation. Another advantage of Pc compounds as compared to porphyrins is a generally longer exciton diffusion length, L_{ex}.[324] One reason for this is that porphyrin structures typically incorporate substituents that prevent their close stacking. To the contrary, Pc molecules are often used without substituent groups, enabling close stacking that permits a strong electronic coupling partly responsible for the lengthened L_{ex}. Literature values of L_{ex} for CuPc range from 8−68 nm,[324−329] with a fair degree of uncertainty (up to ±20 nm for the highest value) bestowed in part by the fact that neat Pc films do not fluoresce, making accurate L_{ex} measurements somewhat more difficult to achieve.[328] Terao et al. measured L_{ex} values for various metallophthalocyanine, MPc, complexes and observed a perfect correlation between L_{ex} in MPc films and J_{sc} in corresponding MPc/C_{60} OPV devices. Their observations indicate that for these metrics, CuPc > ZnPc > H_2Pc > NiPc > CoPc > FePc,[328] which could contribute to why Cu and Zn are the most popular choices of metals in MPc-based OPV devices.

A third advantage of Pc compounds to porphyrins is their higher hole mobilities.[316] The hole mobility, μ_p, of CuPc is sufficiently high for employment as a donor material for OPV devices, and it is typically found to be superior to that of porphyrins. In Pc films, the value of μ_p perpendicular to the device substrate, that is, the direction of charge transport in OPV devices, has been found to be 2×10^{-5}−5×10^{-4} $cm^2/(V\ s)$.[330,331] However, various literature measurements of the μ_p of CuPc obtained from TOF experiments, which require micrometer-thick films, or from field-effect methods, which measure charge transport in the plane of the film and would not provide representative mobility values for an anisotopic material in an OPV, range widely from 10^{-7}−10^{-2} $cm^2/(V\ s)$.[328,332−335] This wide range of mobilities reflects upon the importance of the measurement technique as well as the purity of the material employed, the exposure to oxygen, and other factors. To underscore the importance of semiconductor purity, Salzman et al. determined that by purifying CuPc to remove the small amount of metal-free Pc, H_2Pc, contaminant present, the electrical properties of the deposited material were affected such that the mobility increased by 3 orders of magnitude, from 4.2×10^{-7} $cm^2/(V\ s)$ for the unpurified CuPc to 1.8×10^{-4} $cm^2/(V\ s)$ after purification.[330] In another investigation of CuPc mobility, Sullivan et al. examined the effect of structural templating on CuPc films using a thin 3,4,9,10-perylenetetracarboxylic dianhydride, PTCDA, layer on ITO in an effort to increase the CuPc μ_p normal to the substrate and therefore increase J_{sc} in CuPc/C_{60} bilayer OPV devices.[94] Typically, the more conductive α-polymorph of CuPc is formed from deposition on a noninteracting substrate, such as ITO, held at room temperature.[336] CuPc self-organizes nearly perpendicular to the substrate in a herringbone packing motif and exhibits anisotropic charge transport properties in which transport parallel to the substrate surface, which occurs via a hopping mechanism, is facilitated by the orientation of the $\pi-\pi$ orbital overlap and is significantly larger than transport vertically through the film (Figure 27).[94] The PTCDA layer, however, lies flat on the ITO surface and acts as a template for CuPc growth. The thin PTCDA layer disrupts the long-range orientation of the CuPc stacking axis perpendicular to the substrate, an effect that has also been observed for films of H_2Pc on PTCDA,[337] and promotes CuPc growth approximately parallel to the templated substrate. J_{sc} increases from 2.56 to 2.93 $cm^2/(V\ s)$ in CuPc/C_{60} devices incorporating the PTCDA structural template because of the higher μ_p through the film in the vertical direction. The V_{oc}, however, decreases by 0.1−0.2 V because the PTCDA energy level alignment creates a barrier to hole collection at the ITO,[94] presenting a research opportunity to find a structural template material with more appropriate energy level alignment.

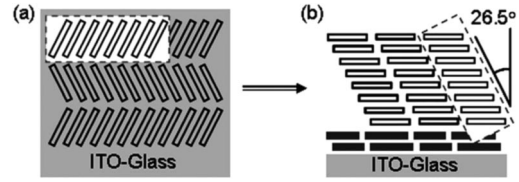

Figure 27. (a) α-CuPc film on ITO substrate and (b) templated CuPc film with PTCDA-covered ITO substrate. The intrastack geometry, denoted by the dashed rectangle, remains the same but is rotated by ~90° relative to the substrate. Reprinted with permission from ref 94. Copyright 2007 American Institute of Physics.

The first notable use of CuPc in a working OPV device was the seminal work of Tang in 1986 that described what at the time was a novel bilayer OPV architecture, incorporating a planar interface of D and A materials.[338] CuPc (30 nm) and PTCBI (50 nm) (Figure 24) were vacuum-evaporated on an ITO-coated glass substrate, and the device was completed with Ag electrode deposition. A paradigm shift ensued from the demonstrated importance of a D/A heterojunction in separating charges and the corresponding jump in device η_p to ~1% under 75 mW/cm^2 simulated AM2 illumination. The current−voltage plot of this original bilayer device is reproduced in Figure 28, with the device architecture shown in the inset. Following this contribution, the Pc/perylene duo was the subject of much research,[35,81,120,121,247,339−350] and it remains a common, well-studied D/A pair in present OPV literature.[93,117,128,193,351−354] It is also often used as a standard baseline system for experiments that require working OPV devices, but focus on an aspect of the OPV device unrelated to the active layer materials system.[259,355,356]

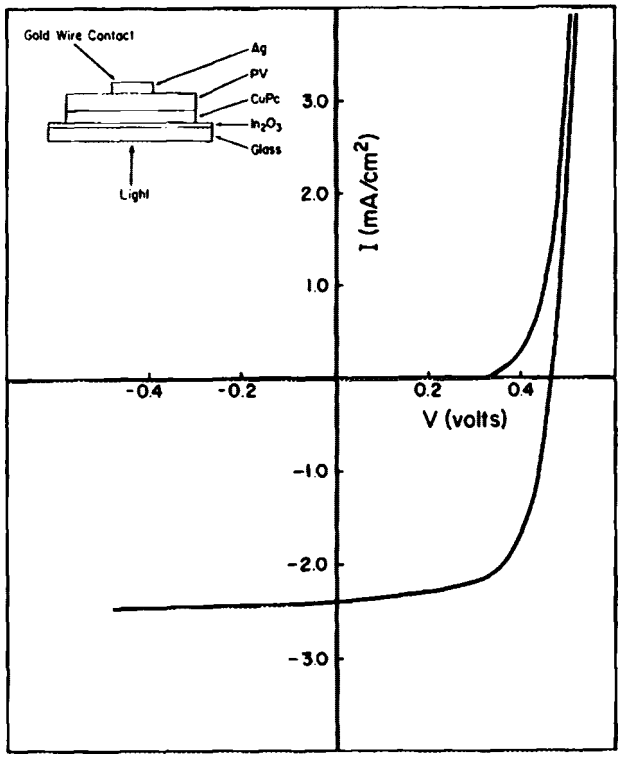

Figure 28. Light and dark current−voltage characteristics for Tang's original bilayer OPV, constructed from CuPc and PTCBI (designated PV in the inset). Inset shows device architecture. Reprinted with permission from ref 338. Copyright 1986 American Institute of Physics.

In addition to perylene diimide acceptors, phthalocyanines are frequently paired with fullerenes in the OPV active layer. The CuPc/C_{60} D/A combination is among the most common for small molecule OPV active layers at present, and devices deriving from this materials system exhibit very high η_p.[223,357−359] For this reason, CuPc/C_{60} has become the archetypical small molecule OPV active layer system, used in a large number of studies having to do with all aspects of OPV device operation. Several specific examples of CuPc/C_{60} devices are discussed in detail below.

In 2001, Peumans and Forrest achieved a η_p of 3.6% for small (active area $\approx 8 \times 10^{-3}$ cm^2) bilayer devices of the architecture ITO/CuPc/C_{60}/BCP/Al at 1.5 suns intensity (1 sun = 100 mW/cm^2) simulated AM1.5G illumination,[357,360] which is a 50% increase in performance over a similar cell by the same group the previous year using PTCBI as the acceptor ($\eta_p = 2.4\%$).[353] Xue et al. reproduced this η_p at 1 sun light intensity, but also investigated the effects of increased light intensity on the CuPc/C_{60} system. An increase in η_p to 4.2% at incident power density, P_0, of ≥440 mW/cm^2 (∼4 suns) was observed. This increase is attributed to an increase in ln(J_{sc}) and V_{oc} with P_0, while *FF* remains approximately constant because of low cell series resistance, R_s, which likely originates in large part from the small contribution of ITO electrode resistance associated with the small device size of 7.5×10^{-3} cm^2 (Figure 29).[223]

By further altering the device architecture, even greater efficiencies were achieved for the CuPc/C_{60} system. Using a three-layer active region consisting of a 1:1 blend film by weight of CuPc:C_{60} between pure films of the blend components, Xue et al. achieved $\eta_p = 5.0\%$ at 120 mW/cm^2 under AM1.5G illumination.[358] Stacking two of these cells together in a tandem cell results in a ∼15% increase in

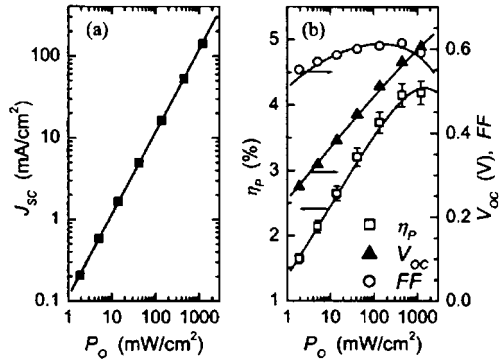

Figure 29. Symbols represent experimental data for the (a) short-circuit current density (J_{sc}) and (b) power conversion efficiency (η_p), open-circuit voltage (V_{oc}), and fill factor (*FF*) as a function of the incident optical power density (P_0) for an ITO/CuPc/C_{60}/BCP/Ag device. Reprinted with permission from ref 223. Copyright 2004 American Institute of Physics.

device performance and a η_p of 5.7% at 1 sun AM1.5G simulated solar illumination, which is the highest reported efficiency for this materials system.[359] Both of these works will be discussed in more detail in section 7 because the advances in efficiency are brought about not by a chemical change to the active materials, but rather through innovative and novel device configurations that lead to enhanced solar cell metrics.

One shortcoming of many MSCs is a narrow absorption band that often does not effectively absorb low-energy photons. This is an important and often difficult issue to address, because while ∼50% of photons in the solar spectrum have energies corresponding to 600 nm < λ < 1000 nm, designing a molecule with a low band gap capable of absorbing these photons often results in a simultaneous reduction of $E_{g,HJ}$, which serves to lower the V_{oc} and negates much or all of the benefit to J_{sc} from the additional absorbance. Nonetheless, several reports have recently come out revealing efforts to increase the active layer absorption into the infrared. One route researchers have explored to achieve this goal is to use nonplanar Pc molecules such as PbPc[361] or SnPc[362−365] because these semiconductors demonstrate significant absorption in the 600−900 nm range, with a cutoff of $\lambda \approx 1000$ nm, as illustrated in Figure 30. The Pb atom lies 1.28 Å[366] or 0.91 Å[367] out of the macrocycle plane in triclinic and monoclinic forms, respectively, and Sn projects 1.13 Å[368,369] out of the Pc plane. The origin of this nonplanarity is a structural manifestation of the inert pair effect in which the divalent Pb and Sn atoms reside in a distorted metal ion coordination environment.[370,371] The resulting polycrystalline Pc films on ITO have exceptionally large intermolecular spacing that results in weaker molecular orbital overlap as compared to CuPc. This likely contributes to the lower observed μ_p, yielding a higher series resistance that reduces *FF*, but also is responsible for an increased low-energy absorption that can potentially increase J_{sc}.[365]

Another donor employed to collect a greater percentage of infrared photons is chloroaluminum phthalocyanine, ClAlPc, which exhibits an absorption peak in the near-IR around 755 nm.[372] In this case, it is the out-of-plane Cl atom bonded to the central Al atom with square-pyramidal geometry that strongly influences the molecular packing, inducing an interleaved slip-stack arrangement. In turn, this packing governs the absorption of the film by extensively red-shifting the Q-band maximum,[98,373,374] leading to the significant observed bathochromic shift in absorption as

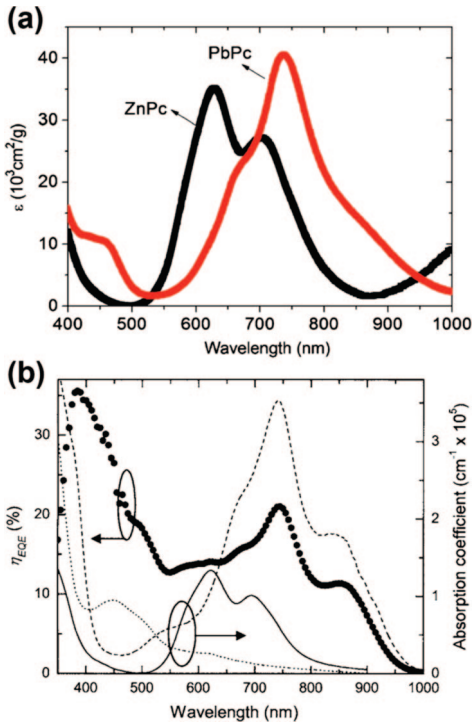

Figure 30. The near IR absorption of nonplanar PbPc and SnPc are demonstrated by plots of (a) the extinction coefficients of ZnPc and PbPc as a function of wavelength and (b) the absorption coefficients of CuPc (—), SnPc (- - -), and C_{60} (• • •). Also shown in (b) is the EQE of a multilayer OPV device with architecture ITO/CuPc/SnPc/C_{60}/BCP/Ag. Part a reprinted with permission from ref 361. Copyright 2007 American Institute of Physics. Part b reprinted with permission from ref 365. Copyright 2005 American Institute of Physics.

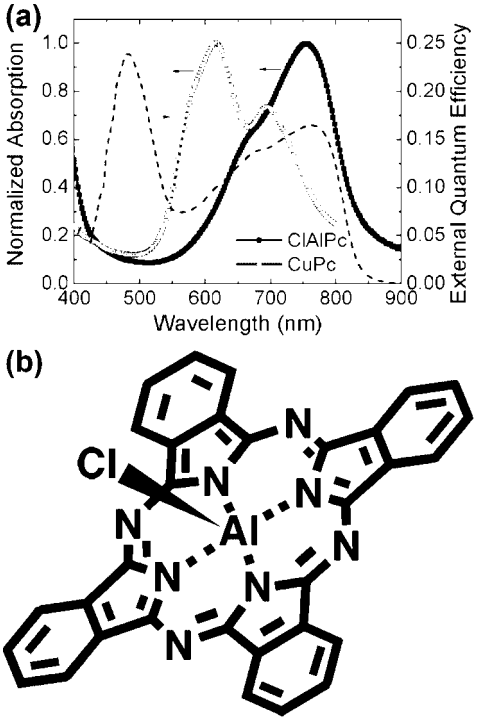

Figure 31. (a) Normalized absorption spectra for ClAlPc and CuPc demonstrating long-wavelength absorption of the former. Also shown is EQE for a device of architecture ITO/ClAlPc/C_{60}/BCP/Ag with an optimized ClAlPc growth rate of 0.5 Å/s. (b) Molecular structure of CuAlPc showing out-of-plane Cl atom. Part a reprinted with permission from ref 372. Copyright 2007 American Institute of Physics.

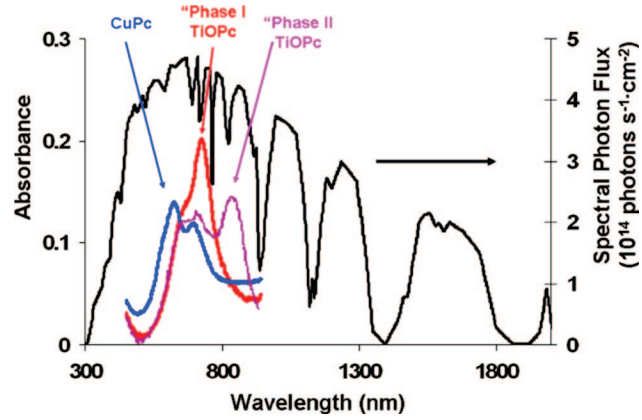

Figure 32. Absorbance spectra for films of CuPc and two phases of TiOPc as compared to the AM1.5G solar spectrum. Reprinted with permission from ref 54. Copyright 2008 American Chemical Society.

compared to the CuPc wavelength of maximum absorption, λ_{max}, of 630 nm, as shown in Figure 31. The ClAlPc/C_{60} device is therefore able to harvest lower energy photons that would pass directly through a CuPc/C_{60} device. As an additional benefit to this material, ultraviolet photoelectron spectroscopy, UPS, measurements indicate that the HOMO energy of ClAlPc is shifted to 5.4 eV, ~0.1 eV farther from vacuum than that of CuPc, which will in theory yield devices that exhibit an increased V_{oc} by ~0.1 V. Device analysis indicates that optimized ClAlPc/C_{60} devices exhibit no increase in J_{sc} from the additional IR absorbance, but achieve comparable current density as well as the small predicted enhancement in V_{oc} as compared to CuPc/C_{60} control devices, resulting in an overall improvement in η_p from 1.8% to 2.1%.[372]

As was the case with ClAlPc, using oxo-titanium phthalocyanine, TiOPc, as a donor material was also successful in leading to both a higher absorbance at long wavelengths and an increased V_{oc} in bilayer TiOPc/C_{60} OPV devices as compared to CuPc.[54] The nonplanar TiOPc is known to exist in several crystalline polymorphs, and the differences in the overlap of transition dipoles in adjacent Pc cores as well as in the charge-transfer character in the optical transition itself result in an extension of the Q-band absorbance into the infrared.[54] Previous studies of TiOPc films have determined that vapor deposition results in the formation of at least two distinct phases, each having a somewhat different value of λ_{max} as shown in Figure 32, which therefore broadens the overall near-IR absorption of the film.[98] Because thermal-annealing and solvent-annealing the film changes the mixed-phase morphology to become richer in the phase that absorbs light at the longest wavelengths (Phase II), a very broad absorption spectrum can be obtained in this way.[11] Brumbach et al. also conducted UPS measurements and predicted an enhancement in V_{oc} for TiOPc/C_{60} devices, stemming from the ~0.2 eV deeper HOMO energy of TiOPc as compared to CuPc.[54] Device fabrication and analysis correlated well with this measurement; TiOPc/C_{60} and CuPc/C_{60} cells exhibit V_{oc} values of 600 ± 20 and 450 ± 10 mV, respectively. Although a low TiOPc HOMO energy leads to a high V_{oc} in TiOPc/C_{60} devices, a corresponding low LUMO energy reduces the driving force for exciton separation at the heterojunction. A greater probability of exciton recombination ensues, which gives rise to reduced photocurrent. Likely a consequence of this, CuPc-based devices exhibit slightly higher J_{sc} values despite TiOPc absorption having a some-

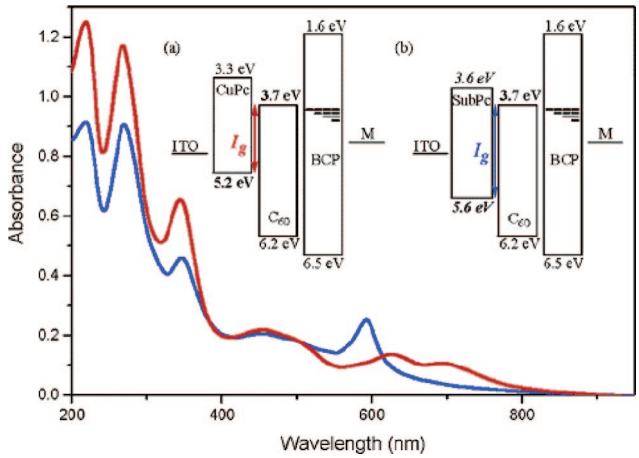

Figure 33. Absorbance spectra on quartz substrates of CuPc (20 nm)/C_{60} (40 nm)/BCP (10 nm) (red line) and SubPc (13 nm)/C_{60} (32.5 nm)/BCP (10 nm) (blue line). Inset: Energy level diagram for CuPc- and SubPc-based OPV devices. Reprinted with permission from ref 380. Copyright 2006 American Chemical Society.

what better overlap with the solar spectrum. This effect, coupled with a slightly lower *FF* in TiOPc devices, counters the effect of the V_{oc}, and comparable η_p for devices with either active layer are observed.

Changes to the V_{oc} of a CuPc/C_{60} active layer were recently correlated to changes in the $D_{HOMO}-A_{LUMO}$ gap, $E_{g,HJ}$, induced by ambient exposure.[375] UPS measurements were employed to monitor the energy level gap responsible for the theoretical maximum V_{oc} when films were prepared in vacuum and in air. Interestingly, $E_{g,HJ}$ increases from 0.64 to 0.81 eV with short ambient exposure,[375] providing a possible explanation why increased V_{oc} with short ambient exposure has been previously observed.[376,377] However, a concomitant deleterious effect of ambient exposure on J_{sc} is also observed due to p-type doping of the fullerene.[376−379] These p-type dopants from O_2-exposure introduce efficient electron trap states near the C_{60} LUMO energy, which function to reduce carrier density and degrade electron mobility in the C_{60}, and as a result the devices exhibit lower J_{sc}.[375,377−379]

6.3.3. Other Electron-Donating Materials

Several donor molecules in addition to porphyrins and phthalocyanines have been used with varying success in OPVs, and there is much ongoing research in pursuit of new molecules with the appropriate energy levels, absorption, and charge transport characteristics. One molecule recently employed in a bilayer OPV with C_{60} as an acceptor is chloro[subphthalocyanine]boron(III), SubPc.[380−382] SubPc is a pyramid-shaped, 14-π-electron aromatic macrocycle with a tetrahedral boron core surrounded by three coupled diiminoisoindole units (see Figure 24 for structure). It can pack in a variety of ways, depending on deposition conditions,[383,384] and its nonplanar geometry contrasts with classical Pc rings and imparts several interesting physical properties, such as high solubility and a low tendency to aggregate.[385] The SubPc was shown to have a deeper HOMO energy than CuPc by ~0.4 eV (inset of Figure 33), and therefore it should exhibit an increase in the V_{oc} of bilayer devices with C_{60} as compared to CuPc/C_{60} devices because of the corresponding increase in $E_{g,HJ}$.[380] At the same time, the SubPc has very good light-absorption (Figure 33) and a high extinction coefficient of 5×10^4 M^{-1} cm^{-1}, suggesting that J_{sc} may not suffer from the larger SubPc ionization potential, IP.[384] Bilayer devices of the architecture ITO/SubPc/C_{60}/BCP/Al were fabricated and compared to their CuPc analogues.[380] The solar cell metrics of the SubPc devices indicate comparable *FF*, a slightly increased J_{sc}, and a significantly higher V_{oc} as compared to the devices having CuPc in the active layer. The increase in V_{oc} from 0.42 to 0.97 V roughly corresponds with the large shift in donor HOMO energy and supports the theory that V_{oc} depends on $E_{g,HJ}$. It has also been shown that the V_{oc} is somewhat associated with a low reverse saturation current density, J_s, in SubPc/C_{60} bilayer devices.[119,125,362] The V_{oc} doubling is largely responsible for the corresponding approximate doubling of the η_p from 0.9% to 2.1% in SubPc-based cells as compared to CuPc devices. Higher values of J_{sc} have further elevated the reported η_p for this device architecture to as high as 3.0%.[381]

Ma et al. fabricated bilayer OPVs from a solution-processable MSC donor and vapor-deposited C_{60} by exploiting the solubility-enhancing nonplanarity of SubPc, and then further enhancing its solubility via the judicious addition of fused benzene rings to the trio of isoindole units.[385] The resultant molecule, chloro[subnaphthalocyanine]boron(III), SubNc, also exhibits a reduced tendency to aggregate and a broader, red-shifted absorption spectrum than its antecedent (Figure 34).[386] The SubNc is solution-processed from chlorobenzene and covered with C_{60} for direct comparison to P3HT/C_{60} bilayer devices. All OPV metrics of the SubNc/C_{60} devices are superior to those of the P3HT/C_{60} devices, with annealed SubNc/C_{60} devices exhibiting $J_{sc} = 5.59$ mA/cm^2, $V_{oc} = 0.55$ V, $FF = 49\%$, and $\eta_p = 1.47\%$.[385] This efficiency rates SubNc/C_{60} bilayer devices among the very highest-performing solution-processed small molecule OPV devices to date.[387] The decreased V_{oc} as compared to that of SubPc-based devices results from greater conjugation imparted by the additional benzene rings in the SubNc, which raises the molecule HOMO energy, thereby decreasing $E_{g,HJ}$.[385] The benzene rings are also responsible, however, for the shift in absorption to longer wavelengths and a resultant increase of J_{sc} as compared to SubPc OPV devices.

Other small molecule donors consist of simple chains of fused benzene rings. Many of these were also employed in some of the earliest demonstrations of organic crystals to generate photovoltaic responses. These polyacenes[39,387] include anthracene,[65,388] tetracene,[31,119,389] and pentacene,[13,390−393] as well as the phenyl-substituted 5,6,11,12-tetraphenyltetracene, rubrene[391,394,395] (see Figure 24 for chemical structures). In addition to their use in OPVs as donor materials, they have also been used as dopants in more common systems, such as CuPc/C_{60} and ZnPc/C_{60}.[61,396−398]

Another family of compounds, squaraines, has recently been reinvestigated and effectively applied to small molecule OPV devices[399,400] after initial appraisals[401,402] produced device efficiencies of only ~0.02%. Squaraines are 1,3-disubstituted derivatives of squaric acid bound to two aryl groups. These molecules exhibit high extinction coefficients of $>10^{-5}$ M^{-1} cm^{-1},[403] good absorption in the near IR spectral region, and acceptable hole mobility for electro-optic devices (FET $\mu_p = 10^{-4}-10^{-5}$ cm^2 V^{-1} s^{-1}),[176,400] making them excellent candidate chromophores for OPV application. Initially, Silvestri et al. utilized a squaraine, Sq, derivative (shown in Figure 24) in a solution-processed BHJ device architecture with PCBM as the electron acceptor.[400] A high η_p of 1.24% was attained for an unannealed ITO/PEDOT:

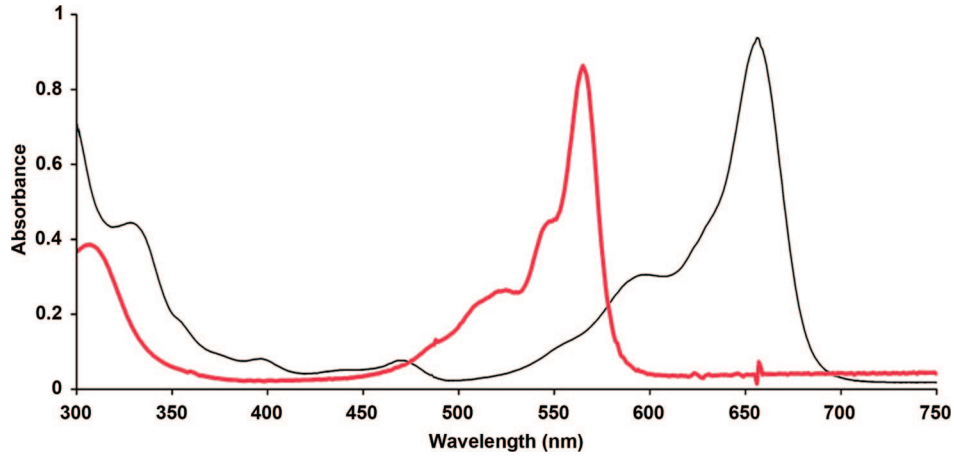

Figure 34. Absorption spectra of SubPc (red line) and SubNc (black line) in toluene. Reprinted with permission from ref 386. Copyright 2002 American Chemical Society.

PSS/Sq:PCBM (1:3)/LiF/Al device when spin-coated in air from $CHCl_3$. Wang et al. followed up this study by making a Sq derivative that is compatible with vapor deposition techniques and fabricating the corresponding devices with planar heterojunction architecture ITO/Sq/C_{60}/BCP/Al.[399] The layer thickness of Sq was varied, and thin layers of 6.5 nm yielded devices with the highest efficiencies, having higher J_{sc} and lower V_{oc} values than devices with thicker Sq layers. Inserting a thin (~5 nm) electron-blocking/hole transport layer of *N*,*N*′-di-1-naphthyl-*N*,*N*′-diphenyl-benzidene, α-NPD (see section 7.3), reduces the charge recombination at the ITO/C_{60} interface, which is present because of incomplete Sq film formation caused by deposition of such a thin layer on ITO. This recombination reduction restores the V_{oc} to 0.82 V, the same value obtained at thicker Sq layers. The best squaraine devices reported here exhibit high η_p of 3.2%, significantly higher than the 1.2% efficiency demonstrated by CuPc/C_{60} devices fabricated in parallel. The Sq/C_{60} devices demonstrate significantly higher V_{oc} values than CuPc/C_{60} devices because of the combination of a higher $E_{g,HJ}$ and a smaller saturation dark current density, J_s.[399]

6.3.4. Perylene Diimides

Fused aromatic rings such as perylene-based cores provide a deep-lying HOMO and a high degree of planarity for strong π-stacking. When perylene cores are combined with tetracarboxylic diimide units and functionalized with aromatic substituents along the main core or linear tails at the carboxydiimide position, a family of perylene diimides, PDIs, is formed (see Figure 24). PDIs have emerged as viable, alternative building blocks to n-type conjugated polymers because they can combine unique liquid crystalline behavior, a large molar absorption coefficient, high electron affinity and mobility, and excellent photochemical and thermal stability together in a single molecular architecture.[16,404,405]

Early organic solar cells consisted of simple Schottky diodes, in which only a single organic layer was located between the metal electrodes.[406] However, these devices suffered from inefficient charge carrier generation because the charge carriers are not only separated but also efficiently quenched at the metal contacts, and thus the achieved power conversion efficiencies were below 0.1%. Tang resolved this issue in 1986 by fabricating a vacuum-deposited organic bilayer, composed of CuPc as electron-donor and 3,4,9,10-perylene tetracarboxylic bis-benzimidazole, PTCBI, as electron-acceptor.[338] A power conversion efficiency of ~1% was achieved in the Tang cell.

In addition, the Armstrong group reported photoelectrochemical studies on heterojunctions based on 3,4,9,10-perylenetetracarboxylic dianhydride, PTCDA, and vanadylphthalocyanine, VOPc, or CuPc.[247] Vacuum-deposited bilayers of these thin films show rectification in their current−voltage behavior over a narrow potential window. It was found that the open-circuit voltage, V_{oc}, appears to be determined by the junction potential formed at the Pc/PTCDA interface and the transient photocurrent was directly proportional to the number of Pc/PTCDA interfaces.

Pentacene has been shown to exhibit large L_{ex} (up to 70 nm) and very high hole mobility (~1−2 cm^2/V^{-1} s^{-1} due to its outstanding crystalline structure and notable coplanar conformation (see section 6.3.3).[13,393] In view of these favorable characteristics, pentacene has been used as donor in combination with C_{60} as acceptor to achieve high-efficiency solar cells. Given the poor light absorption of C_{60}, PTCDI was instead used as acceptor and coevaporated with pentacene in a blend structure for solar cells.[244] The absorption spectrum of this blended photoactive layer covers the whole visible range with an onset at 730 nm. A η_p of 2.0% was obtained under 80 mW/cm^2 AM1.5 illumination with a J_{sc} of 8.6 mA/cm^2. The authors mentioned that the *FF* is expected to improve significantly with better control of the molecular thin-film growth.

Gregg examined the effects of solvent vapor annealing on photophysical and photovoltaic properties of perylene bis(phenethylimide), PPEI, films.[81] It was found that upon treatment with methylene chloride vapor, the PPEI film structure evolved from amorphous to polycrystalline phase, and also the heterojunction barrier height in the CH_2Cl_2 vapor-treated-PPEI/titanyl phthalocyanine, TiOPc, OPV was significantly reduced. Further, Barbara and Gregg employed a combination of near-field scanning optical microscopy, NSOM, and atomic force microscopy, AFM, in conjunction with bulk absorption and fluorescence measurements to spatially resolve the nanoscopic structure and charge transfer-induced fluorescence quenching in molecular semiconductor heterojunctions.[120,121] Studies on PPEI/TiOPc bilayers and respective PPEI and TiOPc single layers, for instance, visually revealed that the layers and bilayers are highly organized containing localized crystalline regions, which are preferentially oriented relative to the substrate and the PPEI/

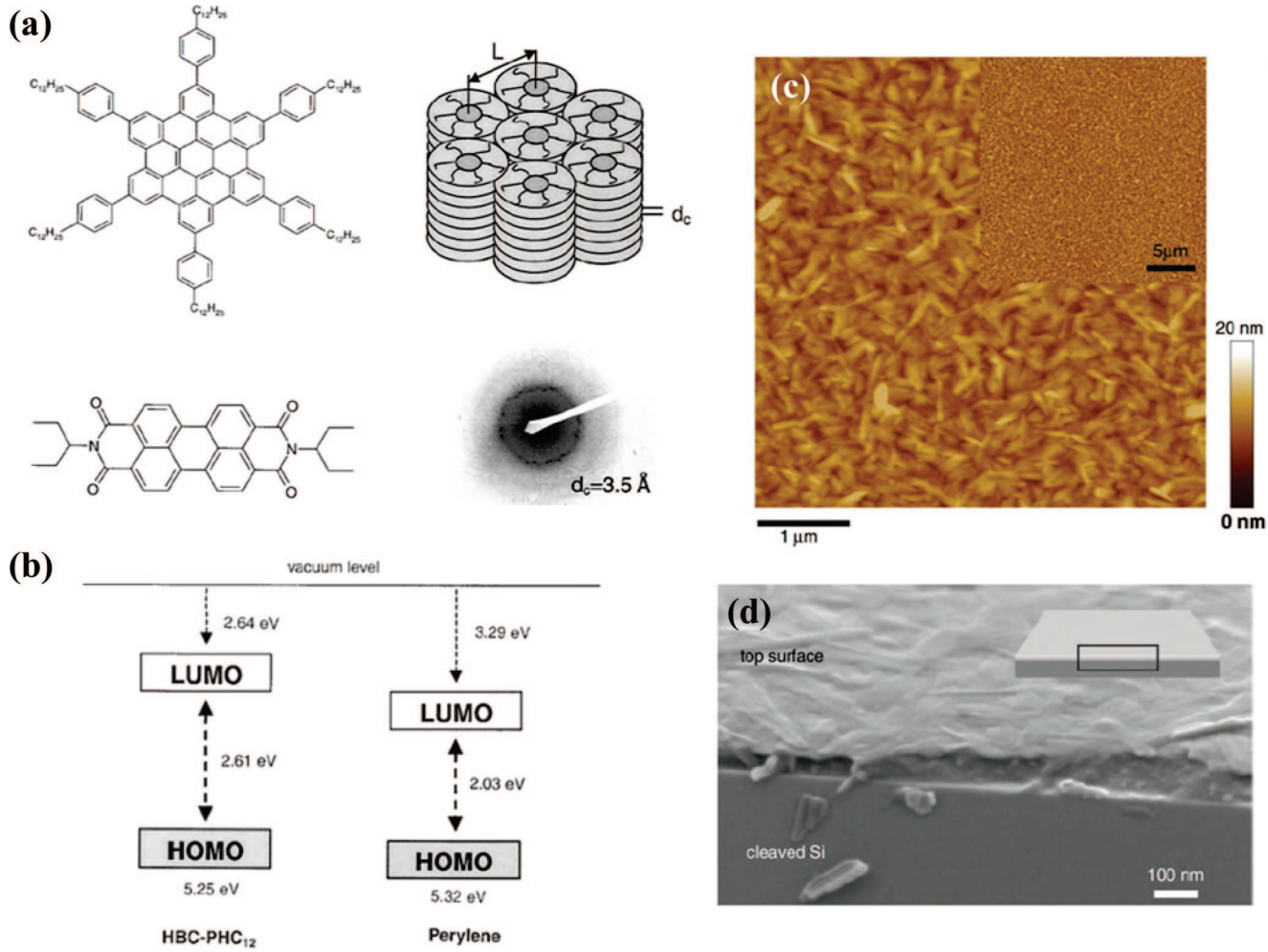

Figure 35. (a) The chemical structures of HBC-PhC_{12} and perylene dye molecule along with a simplified diagram of the $\pi-\pi$ stacking configuration. The intercolumnar distance $L = 34$ Å and cofacial distance $d_c = 3.5$ Å are indicated. An electron diffraction image was taken from a spin-coated xylene film of perylene dyes, and the densest ring of diffraction spots from crystallites corresponds to a spacing of approximately 3.5 Å. (b) HOMO and LUMO energy diagrams for HBC-PhC_{12} and perylene dye. Note that there is a 0.65 eV LUMO offset and a 0.07 eV HOMO offset between the two materials. (c) Tapping-mode AFM image of a film spin-coated from a 40:60 blend solution of HBC-PhC_{12} and perylene diimide. (d) Field-emission scanning electron microscope, SEM, image of a 40% HBC-PhC_{12} blend sample, imaged with the cleaved surface tilted 15° from normal to the incident electron beam (1 kV). Reprinted with permission from ref 102. Copyright 2001 American Association for the Advancement of Science.

TiOPc interface. The authors discovered that the highly solvent-vapor-annealed PPEI/TiOPc interface is comprised of relatively large PPEI crystals making only sporadic contact to small TiOPc nanocrystals. Despite the low density of interfacial contact, the crystalline nature of both layers is not only beneficial in promoting long-range exciton migration but also expected to give rise to more effective generation of free charge carriers and increased charge carrier mobility in both layers.

Müllen and Friend have recently demonstrated that liquid crystalline materials can be solution-processed for high-efficiency OPVs, in which ordered structures can be created through self-organization for photoexciton dissociation and charge transport.[102] In this work (illustrated in Figure 35), the discotic liquid crystal hexa-perihexabenzocoronene, HBC-PhC_{12}, was chosen as a donor in combination with PDI as the acceptor to produce thin films with vertically segregated PDI and HBC-PhC_{12}, which yield large interfacial surface areas. When incorporated into diode structures, these films show photovoltaic response with external quantum efficiencies, EQEs, of more than 34% near 490 nm. High efficiencies result from efficient photoinduced charge transfer between the HBC-PhC_{12} and PDI, as well as from effective transport of charges through vertically segregated PDI and HBC-PhC_{12} π-systems.

6.3.5. Fullerenes

Far and away the most common acceptor molecules in the OPV field, including polymer- and MSC-based solar cells, are fullerenes. Fullerenes are composed of C allotropes and include structures such as C_{60}, C_{70}, C_{76}, C_{78}, C_{84}, etc., with C_{60} and C_{70} being the most common. C_{60} and C_{70} are formed in 75% and 24%, respectively, from the typical arc-discharge method of fullerene production, with a mixture of the other allotropes comprising the remaining 1%.[407,408] The first member of this molecular family, buckminsterfullerene, or C_{60}, was discovered by Kroto et al. in 1985[409] and named after Buckminster Fuller, the man who developed and popularized the architectural geodesic dome design that resembles the C_{60} molecular structure. In 1990, C_{60} solubility in benzene was observed,[408] which allowed for efficient extraction from soot in macroscopic quantities and for functionalization via chemical reaction, in turn enabling an explosion

of research into this fascinating class of molecules.[407,410,411] C_{60} is an aromatic, cage-like, spherical structure having 12 pentagonal rings, each adjacent to 5 of the 20 total hexagonal rings that complete the icosahedral (I_h) geometry.[412] The structure exhibits a host of interesting physical properties, and many of them, such as a high reported n-type mobility of $\sim 10^{-2}-10^{-1}$ cm^2/(V s),[413] are extremely valuable to fullerene application in OPV devices. In electrochemical studies, C_{60} has proven able to withstand reversible electron transfer of up to six electrons, and its frontier energy levels are aligned such that facile and efficient electron transfer is achieved when paired with common MSC and polymer electron donors.[407,410,414,415] In fact, in polymer:fullerene-based devices, photoinduced electron transfer occurs as rapidly as within 100 fs with a quantum efficiency approaching unity.[241,299] In addition, fullerenes have small reorganization energies upon electron transfer, because their robust spherical geometry exhibits relatively small changes in structure and solvation upon electron transfer.[299] This small reorganization energy aids in forming a metastable charge separated state, which lasts up to a few ms at 80 K in polymer:fullerene devices.[241,299] The spherical shape of C_{60} makes it a good acceptor in any direction, and this anisotropy toward electron transfer is advantageous versus two-dimensional molecular structures because it greatly increases the chance for a beneficial alignment with the donor π-system.

For polymer OPVs, which are most often fabricated from solution processes, a soluble fullerene derivative is usually employed as the acceptor in the active layer. Although C_{60} is soluble in many common organic solvents, the fullerene cages tend to aggregate, and the observed solubility is typically rather low.[410,415] Therefore, fullerene derivatives with organic solubilizing groups are synthesized to allow for use in solution-cast OPV devices. Many fullerene derivatives exist, but among these [6,6]-phenyl-C_{61}-butyric acid methyl ester, PCBM (see Figure 24 for structure), is ubiquitous in the present polymer-based OPV literature. It is occasionally employed in solution-processed MSC devices as well.[400,416] The C_{70} analogue of PCBM, $PC_{70}BM$, is also utilized in polymer OPV devices and often exhibits enhanced current density and device performance due to its greater light absorption arising from its reduced symmetry, which allows the lower-energy transitions that are symmetry-forbidden in the C_{60} derivative.[417,418] Polymer:PCBM OPV devices are discussed at length in another review article in this journal (and others) and will not be discussed further here.

Fullerenes dominate the electron-accepting role in MSC-based OPV devices as well. In this case, solubility is not necessarily an issue, because the active layer materials are usually vapor deposited, and therefore C_{60} itself is most commonly used rather than a derivative. C_{60} is so often employed that, except for devices having PDI as an acceptor as discussed above in section 6.3.4, most OPV devices discussed in this review rely on C_{60} as the acceptor. One recent study attempted to improve upon C_{60} in MSC-based BHJ OPV devices by substituting C_{70}.[419] Similar to polymer OPV work in which the extra light absorption of $PC_{70}BM$ was exploited to provide J_{sc} enhancement over devices having $PC_{60}BM$,[417] Pfuetzner et al. realized a >25% improvement in device performance in ZnPc:C_{70} devices over those using ZnPc:C_{60}. The V_{oc} of the small molecule BHJ solar cells made with C_{60} and C_{70} is identical, testament to their identical LUMO energies of $\sim$3.9 eV.[419,420] The *FF* is slightly

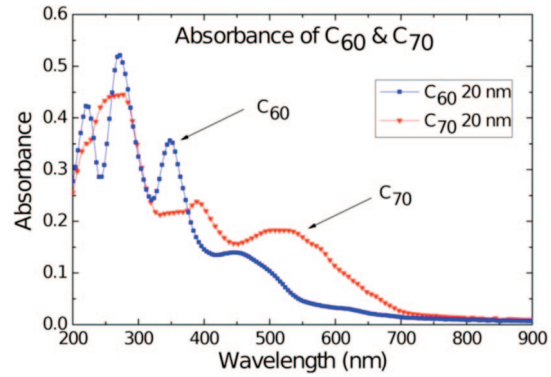

Figure 36. Absorption spectra of C_{60} and C_{70}. Reprinted with permission from ref 419. Copyright 2009 American Institute of Physics.

reduced in the case of C_{70}, which is likely the result of a reduced C_{70} μ_n of $\sim 1.3 \times 10^{-3}$ cm^2/(V s), approximately 2 orders of magnitude below that of C_{60}.[419] The device performance enhancement (2.27 to 2.87%), then, is effected entirely through an increase in photocurrent (7.52 to 9.88 mA/cm^2) due to the greater long-wavelength absorption of C_{70} as compared to C_{60} (Figure 36) brought on by a relaxation of symmetry-forbidden transitions in the C_{70}.[418]

6.3.6. Donor−Acceptor Superstructures

Recently, a new class of photofunctional nanomaterials based on electron donor (D)−acceptor (A) ensembles has been extensively studied for use in light-to-electrical energy conversion.[287,299] In such ensembles, π-electron donors (e.g., porphyrins and phthalocyanines) and π-electron acceptors (e.g., fullerenes and perylene diimides) are covalently linked together or form highly ordered assemblies via noncovalent forces. These molecular π-assemblies have small electron transfer reorganization energies between D and A, which results in fast charge separation yet extremely slow charge recombination, thus holding strong promise for constructing efficient molecular optoelectronic devices. For example, a supramolecular structure covalently binding two ruthenium(II)phthalocyanine, RuPc, molecules and one squaraine, Sq, unit (Pc−Sq−Pc) has been recently demonstrated as an effective sensitizer, because such a triad structure absorbs a large portion of the solar spectrum from 250 to 850 nm.[421] Photophysical studies have revealed a long charge-separated lifetime of 24 ± 2 ms in this triad. BHJ solar cells based on Pc−Sq−Pc and PCBM were fabricated from $CHCl_3$ solution and displayed a η_p of $\sim$0.3%. Main reasons for the low efficiency are high dark leakage current and very low J_{sc}, partly due to low charge carrier mobility in the Pc−Sq−Pc component.

Thelakkat et al. synthesized a novel donor−acceptor dyad consisting of tetraphenylbenzidine, TPD, and PDI linked by a dodecyl spacer.[422] The selective excitation of the TPD donor leads to a highly efficient, nonradiative energy transfer (>90%) to the PDI, evidenced by quenched donor emission and a simultaneous acceptor emission. Such intramolecular energy transfer was 4 times more efficient in the D−A dyad than in the D:A blend. Conversely, direct excitation of the PDI acceptor in the dyad exhibited reduced fluorescence emission of the acceptor, also indicating efficient electron transfer between the moieties. This D−bridge−A is an excellent model system for the study of energy- and electron-transfer processes in organic semiconductors.

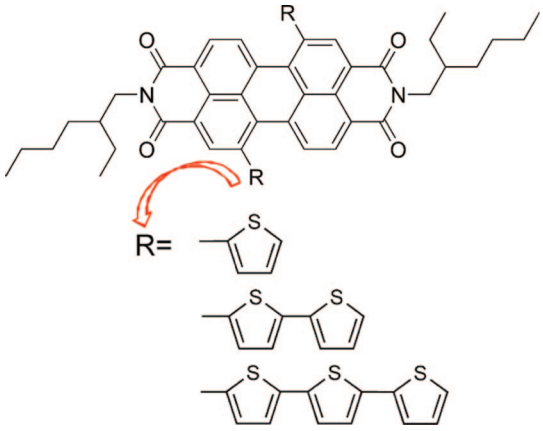

Figure 37. Molecular structures of an oligothiophene-functionalized PDI. Reprinted with permission from ref 432. Copyright 2005 American Chemical Society.

Carbon nanotubes, CNTs, are well-known as one-dimensional electron acceptors, and there have been recently increasing efforts on a new class of D−A nanohybrids based on CNTs and various electron donors such as porphyrin derivatives.[423] Covalent and noncovalent methods have been employed to create these D−A ensemble nanocomposites, in which fast charge separation and slow charge recombination have been observed.[424−431] Long lifetimes of the charge-separated species render these systems promising candidates for the fabrication of high-efficiency photovoltaic devices.

π-Conjugated units can be incorporated into a D−A structure by attaching oligothiophenes (Figure 37), for instance, as substituents at the bay position of a perylene core via Suzuki and Stille coupling reactions.[432] As compared to the original PDI, the thiophene-substituted perylene D−A structure undergoes a bathochromic shift along with considerable band broadening and a less pronounced vibronic fine structure. Moreover, efficient intramolecular electron transfer between the oligothiophene donor and PDI acceptor leads to remarkable fluorescence quenching of the perylene core. The oxidation potential of this D−A structure can be readily tuned by varying the number of thiophene groups. These properties make this D−A structure a promising material for optoelectronic devices such as molecular switches, solar energy harvesters, and supercapacitors for energy storage.

6.3.7. Small Molecule and Polymer Hybrid Structures

Integration of small molecules with polymers enables easy solution-processing of OPVs. Note that the functionalized fullerene derivative PCBM is not discussed in this section, because PCBM in conjunction with semiconducting polymers will be largely reviewed by others in this special issue. For instance, perylene diimides have been actively exploited as the electron-conductive component for n-channel organic thin film transistor, OTFT, applications due to their high electron mobility along with strongly self-assembled $\pi-\pi$ stacks, and they were also recently utilized in combination with p-type hole-transporting polymers for PV cells. Friend et al. initially studied the combination of conjugated polymers and MSCs in BHJ OPVs.[433] For example, in a blend of P3HT and the small-molecule perylene dye *N*,*N*′-bis(1-ethylpropyl)-3,4,9,10-perylene bis(tetracarboxyl diimide), EP-PTC, having high exciton diffusion length and high carrier mobility, it was found that only a small contribution to photocurrent comes from light absorbed in the polymer as a result of electron trapping within perylene domains. The effect of electron trapping can be reduced by controlling PDI crystal growth via thermal annealing.

More recently, the four soluble PDIs shown in Figure 38a have been prepared as electron-accepting and -transporting materials and mixed with P3HT in OPV devices.[434] Among them, *N*,*N*′-di(1-nonadecyl)perylene-3,4,9,10-bis(dicarboximide), PDI-C9, has longer alkyl chains than EP-PTC to give better solubility in solution and to have better miscibility with P3HT in the solid-state. A more planar structure, 2-(1-nonyldecyl)benzimidazo[2,1-*a*]anthra[2,1,9-*def*:6,5,10-*d*′*e*′*f*′]diisoquinoline-1,3,8(2*H*)-trione, PDI-BI, was designed to exhibit superior stacking to PDI-C9 while maintaining reasonable solubility via long swallow-tailed alkyl chains. The 1,7-bis(*N*-pyrrolidinyl)-*N*,*N*′-dicyclohexyl-3,4,9,10-perylenebis(dicarboximide), 5-PDI, introduces the electron-donating pyrrolidinyl group to absorb the longer wavelength (>750 nm) light and also to raise the LUMO energy to render high V_{oc} values up to 0.71 V in the OPV cell. The *N*,*N*′-bis(cyclohexyl)-(1,7 and 1,6)-dicyanoperylene-3,4,9,10-bis(dicarboximide), PDI-CN, has high charge mobility as an OTFT material, which is also desirable for BHJ OPV materials. Figure 38b presents the energy diagram of these PDIs and P3HT in OPV configuration. Both PDI-C9 and PDI-BI have proper HOMO and LUMO energy alignment with P3HT, while the HOMO energy of 5-PDI is too high, and both the HOMO and LUMO energies of PDI-CN are too low. Overall, the PDI-C9-based cell exhibits the highest incident photon-to-current conversion efficiency, IPCE, of 19% at 495 nm and a η_p of 0.18% under AM1.5G light.

In another study, PDI was combined with a highly soluble poly(2,7-carbazole), PCz, for BHJ solar cells.[435] Such a D:A pair shows a broad absorption overlap with the solar spectrum and balanced energy levels for charge separation at the D−A interface. The morphology of PCz:PDI films studied by SEM shows the formation of a favorable microphase separation, which is key for exciton dissociation. The best device exhibits an EQE of 16% at 490 nm and a η_p of 0.6% under simulated solar illumination. By comparison, incorporation of P3HT instead of PCz as donor produced a much lower V_{oc} and thus a lower efficiency in solar cells, mainly due to the improper energy level alignment between the low band gap donor and acceptor. It was concluded that high E_g conjugated polymers can also be employed as donor materials for efficient solar cells if appropriate electron acceptors are chosen.

Large-scale phase separation often occurs within blends of semiconductive polymers and PDI. As an example, the Fréchet group synthesized a novel diblock copolymer as a compatibilizer (Figure 39a) that helps control the phase segregation of a P3HT:PDI blend.[436] Device performance was enhanced in the presence of the compatibilizer with optimized devices exhibiting an efficiency of 0.55% (Figure 40b and c).

Of additional importance is the intermolecular interaction between polymer and small molecule in the blend. For instance, it was recently shown how the photophysical and photovoltaic properties of PDI blends with fluorene copolymers are correlated with their respective film morphologies.[437] Three fluorene copolymers, poly(9,9′-dioctylfluorene-*co*-benzothiadiazole), F8BT, poly[9,9′-dioctylfluorene-*co*-*N*-(4-butylphenyl)diphenylamine], TFB, and poly[9,9′-dioctyfluorene-*co*-bis-*N*,*N*′-(4-butylphenyl)-bis-*N*,*N*-phenyl-1,4-phenylenediamine], PFB, were used as electron donors as shown in Figure 40a. Note that (i) the

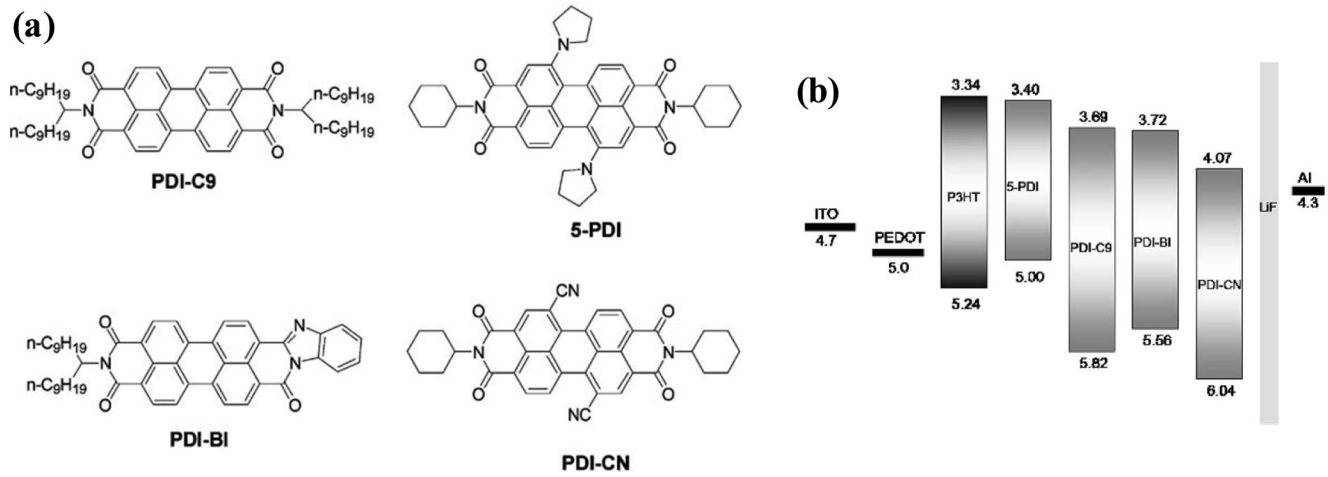

Figure 38. (a) Chemical structures of four PDIs and (b) energy diagram of ITO/PEDOT:PSS/P3HT:PDIs/LiF/Al devices. Reprinted with permission from ref 434. Copyright 2006 Royal Society of Chemistry.

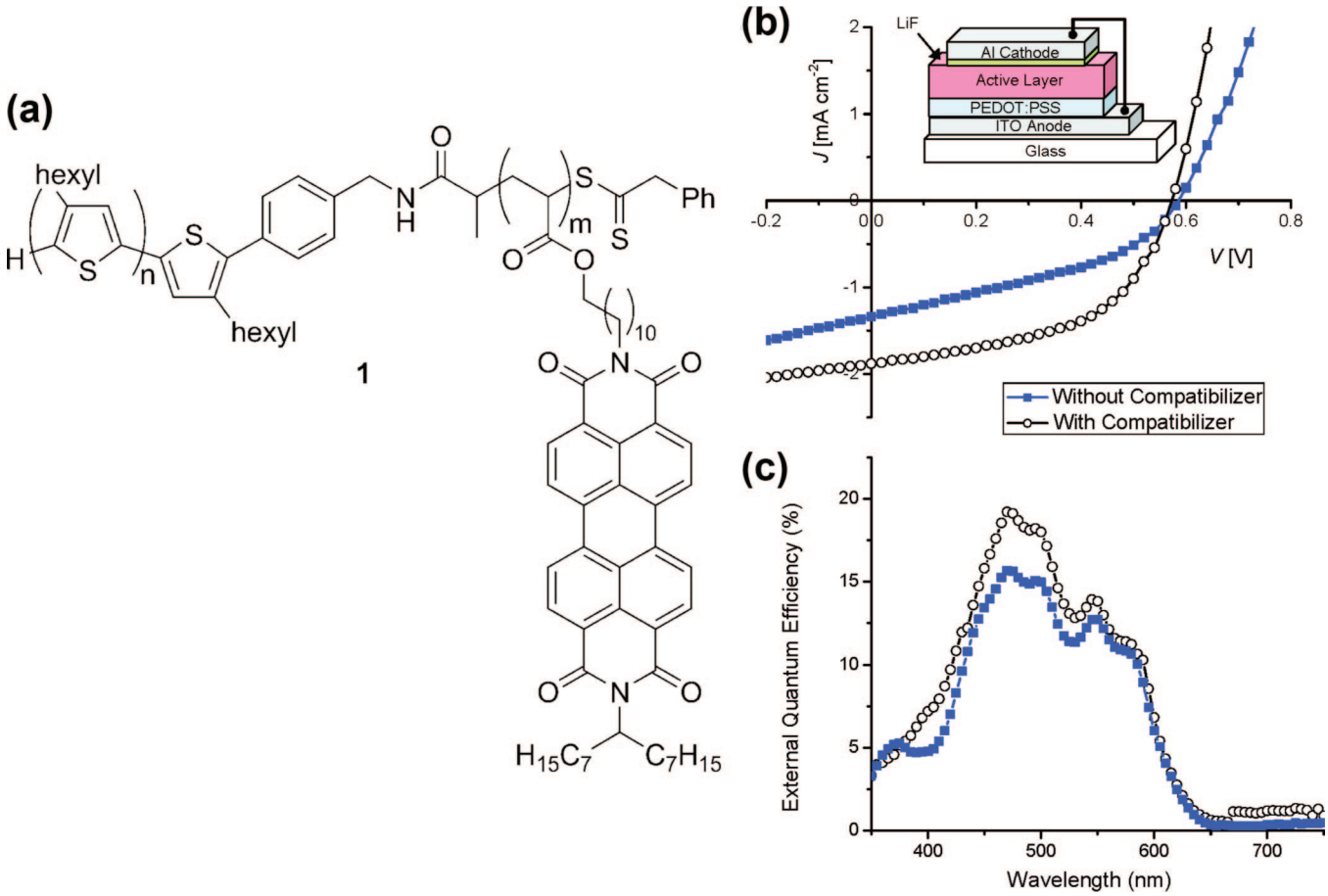

Figure 39. (a) Chemical structure of a diblock copolymer compatibilizer. (b) $J-V$ characteristics of solar cells with the displayed configuration under 100 mW/cm^2 AM1.5G illumination. Both devices utilized an active layer with a 4:1 ratio of PDI:P3HT by mass. Solar cells with the compatibilizer contain 25% by mass in the active layer. (c) External quantum efficiency as a function of wavelength, measured at 0 V bias for devices with and without compatibilizer. Reprinted with permission from ref 436. Copyright 2009 American Chemical Society.

ionization potential of the polymer hosts as well as the extent of long-range order in the solid-state progressively decrease in the order F8BT > TFB > PFB, and (ii) the PDI derivative possesses the smallest electrochemical energy gap of all materials studied. Hence, the trend in the energetic offset between the HOMO energies of the three systems increases following F8BT:PDI < TFB:PDI < PFB:PDI. It was found that PDI-rich domains are formed at the film/air interface in both TFB:PDI and PFB:PDI blends and by contrast at the PEDOT:PSS/blend interface in the F8BT:PDI blend. The device efficiency of these systems is thus limited by the distance that the photogenerated holes must diffuse between the PDI-rich domain and the hole-collecting electrode. With an optimum PDI content of 60 wt %, F8BT exhibits the highest device performance, followed by TFB:PDI and then PFB:PDI. The high efficiency of the F8BT:PDI system is presumably due to the ability of the F8BT matrix to efficiently solubilize the PDI derivative and to promote extensive disorder in the $\pi-\pi$ stacking within the PDI aggregates in the blend. Disordered π-stacks can inhibit the

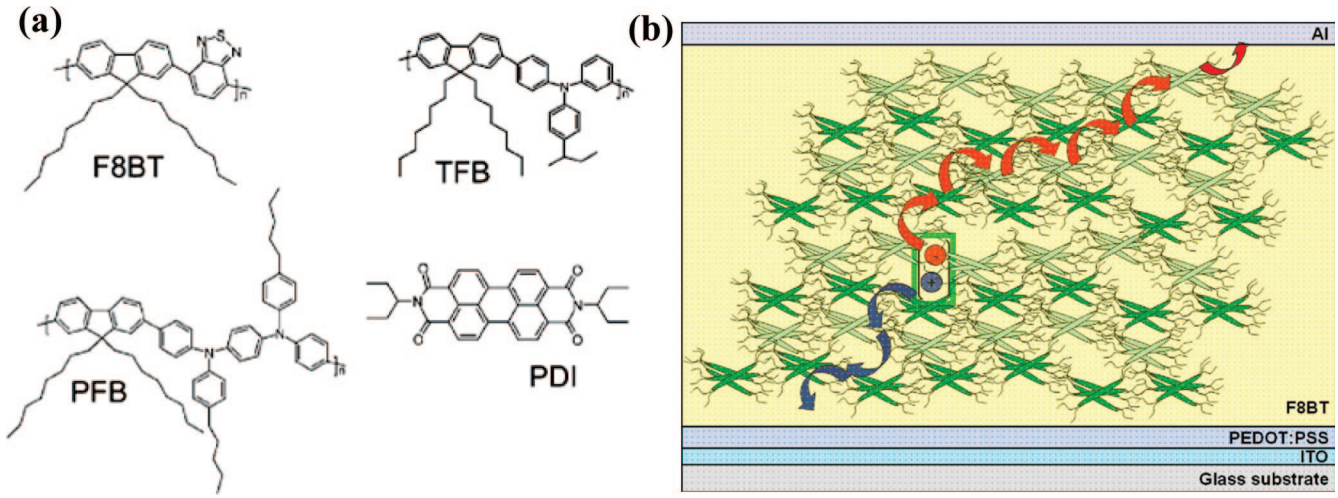

Figure 40. (a) Chemical structures of fluorene copolymers and PDI. (b) A simplified visualization of the proposed mechanism for the balanced extraction of the photogenerated carriers in the as-spun F8BT:PDI (60 wt %) films from $CHCl_3$. The F8BT matrix is proposed to transport holes, whereas efficient electron extraction is suggested to take place via the grain boundaries of disordered PDI aggregates. In this scheme, grain boundaries are proposed to vertically interconnect the PDI superstructures that are formed by the PDI aggregates within the F8BT matrix. The differently colored PDI aggregates correspond to the different PDI layers as seen from the optical microscope in the transmission mode. Reprinted with permission from ref 437. Copyright 2008 Wiley-VCH Verlag GmbH & Co. KGaA.

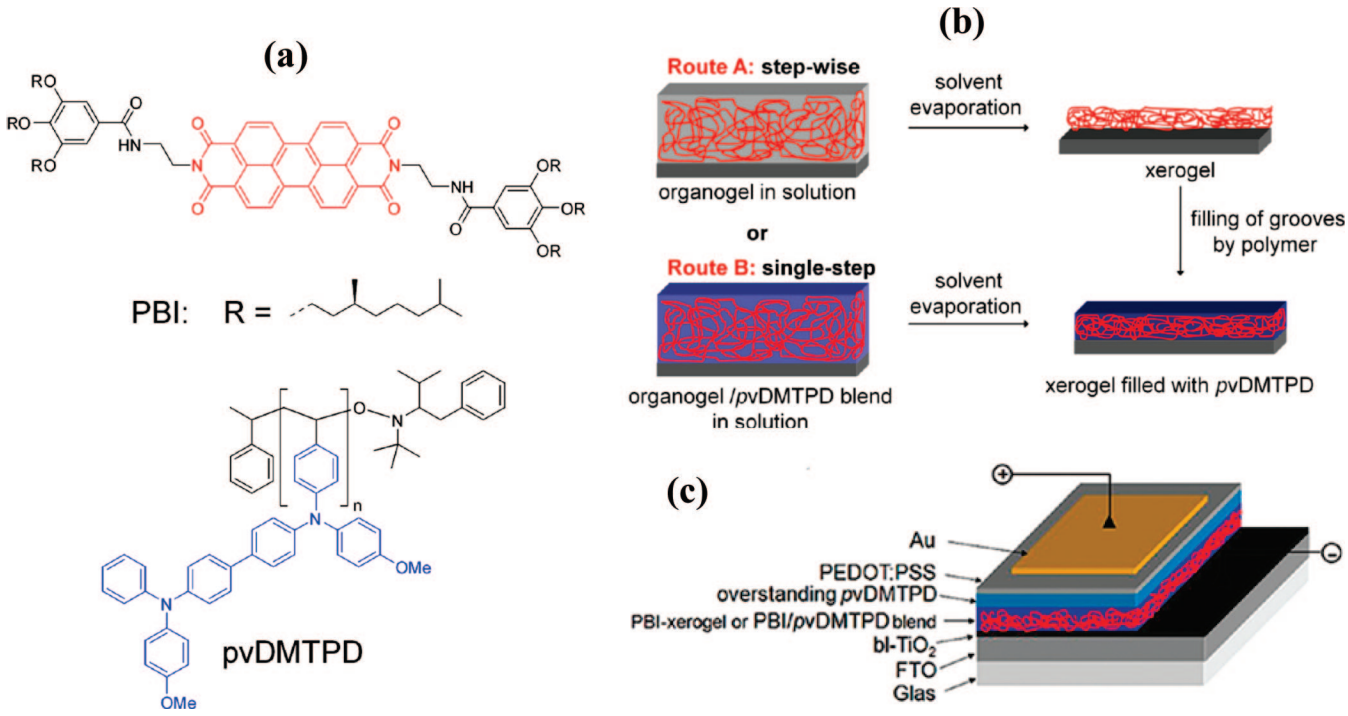

Figure 41. (a) Molecular structures of PBI organogelator and hole-transporting polymer poly[*N*,*N*′-bis(4-methoxyphenyl)-*N*-phenyl-*N*′-4-vinylphenyl-(1,1′-biphenyl)-4,4′-diamine], pvDMTPD. (b) Schematic representation of organogel-polymer concept for realization of an interpenetrating organic bulk heterojunction. Route A: Formation of n-type xerogel with subsequent filling with p-type polymer. Route B: Concomitant embedding of the physical network by a blend approach. (c) Device architecture with inverted cell geometry. Reprinted with permission from ref 438. Copyright 2009 American Chemical Society.

formation of large PDI crystallites, which prevents the trapping of the photogenerated carriers within PDI domains.

Creation of D−A nanostructures will facilitate charge generation and transport. Wicklein et al. found that an electron-conducting perylene bisimide, PBI, organogelator forms nanowires in appropriate solvents during a gelation process.[438] This phenomenon was utilized for PBI self-assembly in an amorphous hole-conducting polymer matrix to realize an interpenetrating D−A interface with inherent morphological stability (Figure 41a). The self-assembly and interface generation were carried out either stepwise or in a single step (Figure 41b). Such D−A nanowires generate large D−A interfacial areas, which is desirable for photoinduced charge separation and charge transport. To test this morphology in a device, an inverted OPV cell (see section 6.4) was fabricated as illustrated in Figure 41c. The device yields J_{sc} of ∼0.28 mA/cm^2, V_{oc} of ∼390 mV, *FF* of ∼38%, and η_p of ∼0.041% under AM1.5G spectral conditions. Although the device would be further improved by utilizing low band gap conjugated polymers, the organogel−polymer concept demonstrates the great potential of nanostructured D−A BHJ devices.

Complementary to the BHJ configuration, Gregg and co-workers have demonstrated that small molecule (PBI)/

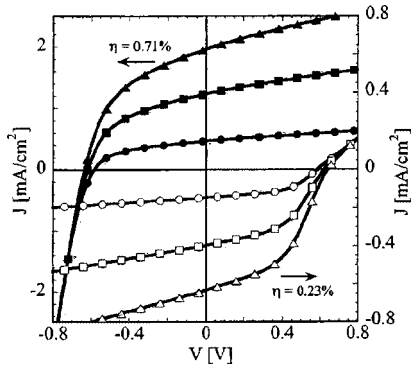

Figure 42. $J-V$ curves taken under white light intensities of 16 mW/cm^2 (circles), 48 mW/cm^2 (squares), and 80 mW/cm^2 (triangles) for device configurations ITO/PDI (~20 nm)/poly[2,5-dimethoxy-1,4-phenylene-1,2-ethenylene-2-methoxy-5-(2-ethylhexyloxy)-1,4-phenylene-1,2-ethenylene], M3EH-PPV (~35 nm)/Au (closed symbols, left-hand-side J scale), and ITO/M3EH-PPV (44 nm)/PDI (24 nm)/Au (open symbols, right-hand-side J scale). Note the different scales for the two current axes. Reprinted with permission from ref 151. Copyright 2002 American Institute of Physics.

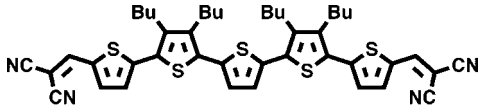

Figure 43. Chemical structure of DCV5T.

polymer (MEH-PPV) hybrid bilayer OPV cells exhibit a η_p of 0.71% under 80 mW/cm^2 white light illumination.[151] Varying the order of the photoactive layers demonstrates that the ordering of the band offsets of the two organic materials plays an important role in determining the polarity of the photocurrent and the photovoltage of the device (Figure 42). Comparison to an analogous pure small molecule device based on a PBI/MgPc bilayer shows that the hybrid device is more than 3.5× more efficient. This work exemplifies that development of a rough, nanostructured interface in bilayer OPVs to increase the dissociation area represents one effective approach to increasing efficiencies.

In a more recent investigation, an efficient vacuum-deposited bilayer OPV device has been fabricated based on a low-band gap oligothiophene, α,α′-bis(2,2-dicyanovinyl)-quinquethiophene, DCV5T (Figure 43), as the donor and C_{60} as the acceptor.[439] Due to electron-accepting cyano groups at both ends, the optical band gap of DCV5T is reduced from about 2.5 to 1.77 eV as compared to that of unsubstituted quinquethiophene. When combined with a p-doped hole-transport layer, HTL, on the anode side and a thin exciton blocking layer, EBL, on the cathode side, the cells exhibit high EQE values, high photovoltages of up to 1 V, and a η_p of 3.4% under 118 mW/cm^2 simulated sunlight. The deep-lying HOMO of DCV5T and the dopant concentration in the p-doped HTL significantly improve V_{oc} and FF.

The transient photoconducting behavior of p/n bilayer OPVs was investigated in cells constructed with the copolymer, poly(3-butylthiophene-*co*-ethylenedioxythiophene), as the p-type material and a PDI as the n-type material.[440] The peak photocurrent response is both field- and temperature-dependent, whereas the decay of the photoresponse, related directly to the carrier lifetime, is nearly independent of both field strength and temperature. The temperature dependence of the peak photocurrent gives an activation energy that is significantly smaller than expected for the binding energy of a Frenkel exciton in a molecular solid, indicating that exciton dissociation occurs predominantly at sites associated with the organic p/n interface and is neither thermally activated nor field-assisted. The low activation energy is concluded to be associated with the mobility.

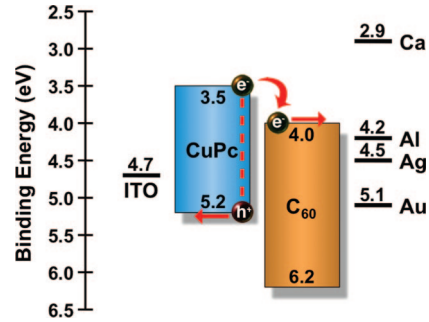

Figure 44. Energy level diagram illustrating the work functions of common cathode materials in relation to ITO, CuPc, and C_{60}.

6.4. Back Electrode

The deposition of an electrode on top of the active layer is the final stage in OPV device fabrication, although often an additional encapsulation step is carried out last to prevent O_2 and moisture in the air from contacting the device and degrading performance over time. Various metals are utilized for the purpose of the back electrode, most of which are vacuum deposited as a thin 50−200 nm layer. The work function, ϕ_f, of the metal is an important consideration for several reasons. The built-in electric field that aids in separating photoinduced charges at the D−A interface is dependent upon the work function differential of the device electrodes. Because the work function of ITO is ~4.7−5.0 eV, a metal with a lower work function (closer to vacuum), such as Al with $\phi_f \approx 4.2$ eV, would provide a field that promotes hole collection at the ITO anode and electron collection at the metal cathode (see Figure 44). A very low work function metal such as Ca ($\phi_f \approx 2.9$ eV) in theory creates a larger field, and similarly Ag creates a somewhat smaller electric field because its work function ($\phi_f \approx 4.3-4.7$ eV) is slightly closer to that of ITO than is the Al work function. Utilizing a metal with a ϕ_f higher than that of ITO, such as gold ($\phi_f \approx 5.1$ eV), reverses the field entirely, supporting charge flow in the opposite direction. The strategy of using a Au electrode in devices with inverse architecture is therefore frequently employed.

A second consideration in the choice of back electrode material is the alignment of the metal work function with respect to the active layer energy levels. To form a desired ohmic contact and effectively collect electrons at the cathode, the metal ϕ_f must be approximately equal to the acceptor LUMO energy. If the ϕ_f is significantly farther from vacuum, the built-in electric field is less than ideal. If ϕ_f is at a level where it depletes majority carriers from the MSC, a Schottky barrier is formed, which inhibits charge transfer and decreases device performance.[441] Together, the electric-field and MSC energy level alignment in Figure 44 support spontaneous electron extraction with both Al and Ag contacts, but Al should give rise to a larger built-in electric field. Gold, however, should form a slightly blocking contact. Experimental work by Mihailetchi et al. corroborates this trend via observation that devices with large built-in electric fields, and therefore a large driving force for charges to separate, exhibit higher J_{sc} than those with low electric fields, that is, J_{sc} for devices using Al > Ag > Au.[442] Calcium electrodes should yield high built-in fields, but they are so chemically

reactive that actual results may vary. While some studies report lower V_{oc} than with other metals,[441] other research groups continue to use Ca with success and achieve high V_{oc}.[443−445] It was suggested that Ca results in "Fermi level pinning" through surface states in the fullerene LUMO.[155,241,446,447] To prevent oxidation of the Ca, a thicker layer of a more inert metal typically covers it. Thus, Ca/Al bilayers are often deposited sequentially without breaking vacuum.

Another common OPV cathode in the literature is achieved by subsequent depositions of LiF and Al. The ultrathin LiF layer is usually ≤ 1 nm, which implies that island formation occurs rather than a contiguous film. The LiF cathode is believed to form an ohmic contact with fullerene acceptors and often improves the performance of OPV devices,[155] and its origins as a cathode interfacial layer derive from its prior use in OLEDs.[37,448−451] Most studies of LiF/Al cathodes in OPV devices to date have employed polymer-based active layers, but recently LiF has also been used with MSC-based OPVs.[452] Several theories have been proposed in the literature as to why such a thin LiF layer is so influential in optoelectronic devices, and these appear applicable to both polymer and MSC OPV devices.[453−456] (i) The LiF acts as a protective layer to the organic material that inhibits hot Al atom bombardment of the organic and subsequent Al−C bond formation during deposition; these disruptions to the organic π-system otherwise act as interfacial trap sites that suppress efficient electron extraction. (ii) Li-doping of the organic material occurs immediately beneath the electrode and contributes to an increase in V_{oc}. (iii) The LiF establishes a dipole that influences charge carrier extraction and (iv) slightly alters the effective Al work function.

An additional role played by the metallic back OPV contact is the reflection of light unabsorbed by the active layer back through the device and out through the transparent electrode. In this way, the effective active layer thickness is essentially doubled, because light can be absorbed traveling through the device in either direction. The wave-like properties of light traveling in either direction through the device, however, introduce optical interference effects, which are addressed in the OPV design with the insertion of an optical spacer, and therefore this effect is discussed more thoroughly below in section 7.3.

7. Device Architectures

Not only are the MSCs used in OPV devices important in governing device function, but the specific device architecture employed is also of utmost importance. In fact, the simple architectural change from a single MSC sandwiched between two electrodes to a bilayer D/A organic heterojunction between electrodes[338] was the innovation that stimulated such intense research into the OPV field and brought it from moderate curiosity to the burgeoning state the field is in today. OPV devices have continued to develop from the simple bilayer and bulk-heterojunction designs to more complex multijunction stacks incorporating charge-blocking layers. In this section, the various device configurations employed will be discussed, and some examples will be cited from the literature to exemplify each case.

7.1. Planar Bilayer

Tang developed the planar bilayer heterojunction in 1986 using CuPc and PTCBI,[338] and the initial discovery is discussed above in section 6.3.2. The realization that a D/A interface is necessary for efficient separation of photogenerated excitons in the organic active layer into free charge carriers is directly responsible for the dramatic observed increase in OPV device efficiency all but obsoleted the prior OPV device configuration consisting of a single organic material sandwiched between two electrodes. The bilayer design has been employed with a wide variety of donor and acceptor species, and it is certainly a straightforward and useful way of gauging the performance of new MSCs. In many cases, this simple design is quite capable of exhibiting relatively high power conversion efficiencies.[13,223,357,389] It also represents a basic and organized configuration, which can be advantageous over the more complicated or disordered systems described below when designing experiments.

Despite its instrumental role in eliciting an improved photovoltaic response compared to a single layer, the bilayer architecture suffers from the short exciton diffusion length in most organic films (section 3.6). In layers thick enough to absorb most light, many excitons will fail to reach the D/A interface before recombining. One solution to this is achieved via interfacial engineering, and the following sections describe various device architectures in which multiple or highly convoluted interfaces are employed to allow use of thicker active layers while still maintaining a short path for exciton diffusion.

7.2. Bulk Heterojunctions

The bulk-heterojunction, BHJ, concept was first proposed by Heeger[124] as well as Friend and Holmes[123] to improve the low efficiencies exhibited by planar bilayer OPVs due to the intrinsically short exciton diffusion length, L_{ex}, of organic semiconducting polymers. This was achieved by blending D and A in solution, coating a film, and allowing the donor and acceptor to phase separate at the nanoscale to form an interpenetrating network. Thus, the distance an exciton travels to reach a D−A interface is significantly reduced, and these numerous D−A interfaces all assist in exciton dissociation. However, the random distribution of D and A materials in such a thermodynamically driven system can lead to charge trapping at bottlenecks and cul-de-sacs in the conducting pathways to the electrodes due to the entropy of the interface formation process. For this reason, Forrest et al. presented a method for growing crystalline organic films of MSCs into a more controlled BHJ, in which the positions and orientations of donor (CuPc) and acceptor (PTCBI) materials are determined during growth by organic vapor-phase deposition, OVPD, thus reducing contorted and resistive conducting pathways while maximizing the interfacial area.[193] This results in a substantial increase in power conversion efficiency as compared to small molecule-based bilayer or BHJ solar cells. One promising solution to the problem of isolated cluster formation proposed by Pfuetzner et al. is to introduce controlled substrate heating during the film deposition, which improves film morphology and results in better charge carrier percolation pathways within the blend, leading to reduced transport losses.[457] This was demonstrated in BHJ solar cells utilizing a 150 nm thick ZnPc:C_{60} (coevaporated at a 1:1 weight ratio) blend layer. When heating the substrate to an optimum temperature of

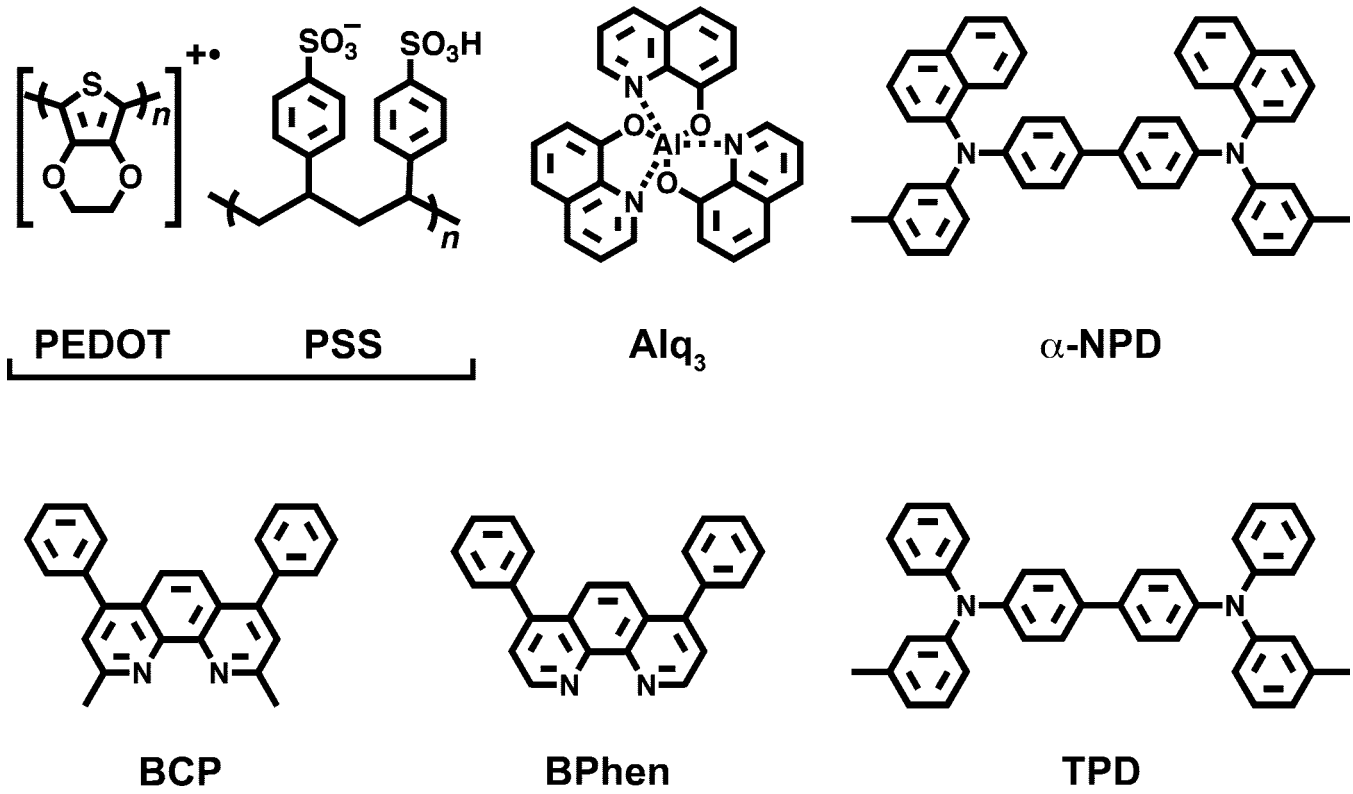

Figure 45. Chemical structures and abbreviations of common charge- and exciton-blocking layer materials in MSC OPV devices. PEDOT = poly(3,4-ethylenedioxythiophene). PSS = poly(styrene sulfonate). Alq_3 = tris(8-hydroxyquinoline) aluminum. α-NPD = *N*,*N*′-di-1-naphthyl-*N*,*N*′-diphenyl-benzidene. BCP = 2,9-dimethyl-4,7-diphenyl-1,10-phenanthroline. BPhen = 4,7-diphenyl-1,10-phenanthroline. TPD = *N*,*N*′-diphenyl-*N*,*N*′-bis(3-methylphenyl)-(1,1′-biphenyl)-4,4′-diamine.

110 °C, the cell attained an efficiency of 2.56% as compared to 1.59% for an identical device prepared at room temperature. The improved efficiency is attributed to higher interaction energies of molecules after heating and hence better charge conduction pathways. In another study by the same authors, the fullerene C_{70} replaced C_{60} and increased visible light absorption, leading to a high EQE of over 50% in the 500−700 nm spectral range.[419] An optimized BHJ solar cell comprising a C_{70}:ZnPc blend exhibits an efficiency of 2.87%, which is a substantial improvement over the cell employing C_{60} having $\eta_p \approx 2.27\%$.

Most MSC-based bilayer or BHJ solar cells are made by vapor deposition of donor and acceptor molecules either successively or together. Novel MSCs that are suitable for low-cost solution-processing, a technique that is regularly employed in polymer solar cells, are highly desired. In contrast to polymer analogues, solution-processed small molecule-based BHJ cells enjoy high-purity molecules and strong molecular organization into ordered structures, leading to high charge carrier mobility, although good film-forming still remains a big challenge. A soluble porphyrin was recently synthesized and exhibited discotic liquid crystalline, LC, phases homotropically aligned into columns normal to the electrode surface, thereby facilitating charge transport and light harvesting.[458] Inspired by this, the LC porphyrin was used as electron donor and blended with PCBM as electron acceptor in chlorobenzene for use in BHJ devices.[110] A J_{sc} of up to 5.02 mA/cm^2 and a η_p of up to 0.775% were achieved in this solution-processed BHJ cell under 100 mW/cm^2 irradiation. It is noteworthy that photoactive layer alignment of the porphyrin leads to significantly improved photocurrent and efficiency. The solution processability of small molecules holds promise for cost-effective fabrication of highly ordered and efficient solar cells.

7.3. Charge- and Exciton-Blocking Layers and Optical Spacers

Although the BHJ design has proven invaluable in the progression of the OPV field, the architecture usually produces a relatively disordered and convoluted active layer both in spin-cast and in coevaporated BHJ devices. Nanodomains of D and A distributed throughout the BHJ active layer cause an electrode contact problem that was not present in bilayer devices. That is, while the bilayer configuration incorporates discrete anode/donor and acceptor/cathode interfaces, the BHJ architecture results in intimate contact with both the D and the A species at both electrodes, which can be responsible for degraded device performance. Charge "leakage" to the electrodes is possible because of the energetically favorable, yet undesirable charge transfer from the donor HOMO to the cathode and from the acceptor LUMO to the anode. Exciton quenching at the organic/electrode interface represents another prevalent loss mechanism in many devices. Clearly, there exists a need for interfacial layer, IFL, incorporation into device design on both sides of the active layer to prevent the aforementioned processes and achieve optimal device performance.

On the anode side of the device, the conventional treatment is to deposit a layer of PEDOT:PSS between the ITO and active layer (Figure 45). This conductive polymer blend is applied by spin-coating a blended aqueous dispersion of PEDOT and PSS onto clean ITO, and its device incorporation has been common practice in OLEDs as well as OPVs.[34,282,459] The resultant 20−80 nm PEDOT:PSS film simultaneously

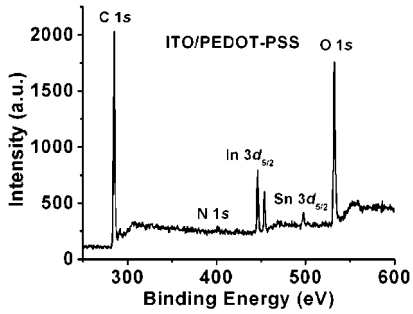

Figure 46. XPS spectrum of a 50 nm PEDOT:PSS film on an ITO substrate baked at 200 °C under vacuum for 1 h demonstrating significant In contamination in PEDOT:PSS. Reprinted with permission from ref 469. Copyright 2005 American Chemical Society.

fulfills many roles. It planarizes the ITO, preventing surface spikes from shorting out the device;[357,460,461] it increases the OPV anode work function to a consistent and reliable ~5.1 eV and forms ohmic contacts with many donor materials;[357,456] it creates a more uniform surface conductivity than that of ITO, which has been shown to have regions of high conductivity intermixed with nonconductive regions,[258,462,463] and can then efficiently shuttle charges into the conductive regions of the ITO surface for collection; and it is modestly able to block electrons and increase the V_{oc} as compared to devices without an IFL.[464−466] Despite these advantages, PEDOT:PSS leaves much room for improvement as well as introducing some new problems. The electron-blocking character in PEDOT:PSS has been demonstrated to be unexceptional and incomplete.[464,466] Although the PEDOT:PSS conductivity in the plane of the film serves to increase the probability that charges succeed in finding conductive ITO regions for charge collection, it also can lead to undesirable cross-talk between multiple devices on a common substrate and is itself still rather inhomogeneous.[467,468] Finally, one of the major problems with PEDOT:PSS is that it is highly acidic, with pH ≈ 1. As confirmed by X-ray photoelectron spectroscopy, XPS, data presented in Figure 46, PEDOT:PSS acidity is sufficient to corrode the underlying ITO substrate, especially at the elevated temperatures inherent to OPV device operation. This corrosion enables indium ion diffusion through the PEDOT:PSS layer and potential subsequent contamination of the semiconducting active layer, causing catastrophic device failure.[466,469−471]

In efforts to replace the ubiquitous PEDOT:PSS, several organic[329,362,399,464,472,473] and inorganic[306,474,475] IFLs have been devised that produce similar or enhanced OPV device performance as compared to PEDOT:PSS when applied as an IFL to the anode of OPV solar cells. Hains et al. recently developed a novel solution-processable silane-based cross-linking IFL for OPVs derived from TPD (Figure 45) that comprises a blend of 4,4′-bis[(*p*-trichlorosilylpropylphenyl)-phenylamino]biphenyl, $TPDSi_2$, and poly[9,9-dioctylfluorene-*co*-*N*-[4-(3-methylpropyl)]-diphenylamine], TFB.[464] The layer is deposited by spin-coating the blend solution from toluene, and upon ambient exposure it forms a robust, cross-linked, insoluble matrix that chemisorbs to the hydroxylated ITO surface, imparting good thermal stability and superior electron-blocking capabilities versus PEDOT:PSS. The high-lying LUMO energies of $TPDSi_2$ and TFB effectively block the electron leakage to the anode and thereby have the effect of increasing the V_{oc} and η_p of polymer-based OPV devices, and similar characteristics may be observed for this layer,

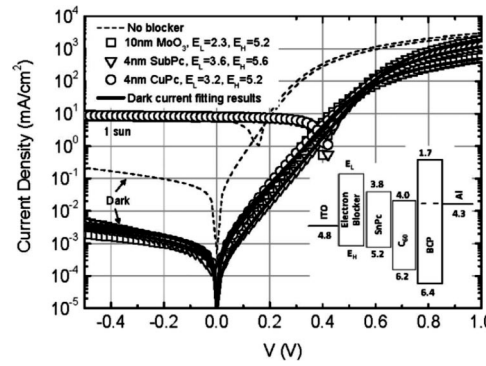

Figure 47. Dark and light $J-V$ plots of ITO/IFL/SnPc/C_{60}/BCP/Al OPV devices where the IFL used is MoO_3 (□), SubPc (▽), or CuPc (○) or is not present (dashed line). The inset shows an energy level diagram of the device components. Reprinted with permission from ref 362. Copyright 2009 American Institute of Physics.

or an analogous one with appropriate HOMO and LUMO energies, when used with MSC active layer components.

Li et al. then adapted the idea of blocking misdirected electrons and reducing dark current to small molecule bilayer OPV devices.[362] CuPc/C_{60} and SnPc/C_{60} active layers were used as control MSC OPV systems that were modified via insertion of an electron-blocking layer between the ITO and the Pc. The SnPc LUMO energy only creates an energetic barrier to electron leakage to the anode of ~0.2 eV when paired with C_{60}, while the CuPc system LUMO energy is closer to vacuum and creates a barrier of ~0.8 eV; therefore, SnPc should have a higher occurrence of electron leakage and receive greater benefit from the IFL insertion. Three IFLs were employed in this study, MoO_3, CuPc, and SubPc. All three IFLs yielded devices with low dark current, and all three restored the low V_{oc} exhibited by SnPc devices without an IFL (~0.16 V) to ~0.41 V, approximately the same value obtained by CuPc devices without a blocking layer (Figure 47). This study emphasizes the importance of charge leakage not only in BHJ devices, but also in bilayer devices where discrete contacts at the electrodes are already present.

Interfacial modification at the cathode side of OPV devices is no less important than at the anode, and again a wide range or inorganic[476−478] and organic[329,353,376,377,443,479−482] buffer layers have been employed to date in OPV devices for this purpose. A buffer layer between the active layer and the cathode needs to display hole blocking characteristics and good electron transport properties. One common electron transport material in OLEDs that displayed such properties, tris(8-hydroxyquinoline) aluminum, Alq_3 (Figure 45), was successfully utilized as an IFL in OPVs. In addition to its role in OPVs as an electron transport layer, Song et al. determined that Alq_3 was actually able to increase the lifetime of unencapsulated solar cells by ~150× as compared to devices using BCP (see section 8).[482] The increase in stability is attributed to formation of a superior barrier against permeation of ambient O_2 and water molecules as well as against metal atom diffusion from the cathode into the active layer.

2,9-Dimethyl-4,7-diphenyl-1,10-phenanthroline, BCP, is the most widely employed IFL on the cathode side of MSC OPV devices today. Like Alq_3, BCP too was originally used in OLEDs[483] before being adapted for use in OPVs in the Forrest group.[353] It is typically deposited as a ~10 nm film and is said to act as an "exciton blocking layer" that prevents excitons from quenching at the active layer/cathode interface. The excitons in the active layer cannot transfer to the BCP

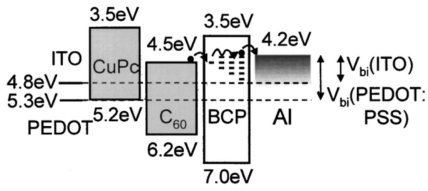

Figure 48. Energy level diagram of a bilayer CuPc/C_{60} OPV device illustrating electron transport through BCP defect states to collection at cathode. Reprinted with permission from ref 357. Copyright 2001 American Institute of Physics.

because the BCP has a significantly larger energy gap ($E_g \approx 3.5$ eV) than the active layer materials. Additionally, BCP acts to protect the active layer from hot metal atoms during cathode deposition. Although the BCP energy levels are aligned such that it would appear to cause a significant energetic barrier to both holes and electrons when perylene derivatives or fullerenes are employed as acceptors, it is proposed that defect states formed at the BCP/cathode interface during cathode deposition allow electrons to traverse this IFL for collection at the cathode without the apparent ~1.0 eV barrier, as illustrated in Figure 48.[357,481,484] BCP crystallization in air has been reported to pose serious stability problems,[377,485] especially at high illumination intensities, but doping the BCP with ~10 wt % PTCBI has prevented recrystallization in some instances.[353,354]

A substitute for BCP in MSC OPV devices, 4,7-diphenyl-1,10-phenanthroline, BPhen (Figure 45), was recently developed and demonstrated to enhance OPV performance.[479,480] It has essentially the same frontier orbital energies as BCP, but exhibits an electron mobility 2 orders of magnitude higher.[486,487] Because of the facilitated electron transport through the IFL while retaining the same high optical transparency and energy level arrangement, an increase in J_{sc} and η_p is realized in solar cells having BPhen as an IFL as compared to those fabricated in parallel containing BCP, as portrayed in Figure 49.[480]

A separate, but often simultaneous, function fulfilled by a cathode-side IFL is that of an optical spacer, as briefly alluded to in section 6.4. A reflective metal cathode directs light unabsorbed by the active layer back through the device, providing a second opportunity for absorption and also causing an optical interference pattern in the device owing to the overlapping incident and reflected light waves (Figure 50).[324] An efficient device design centers the positive interference in the active layer region, near the D/A interface, to maximize possible light absorption and photocurrent generation. If this region of the interference pattern does not naturally reside near the D/A interface, then the addition of an "optical spacer" to the device architecture between the active layer and the cathode can add thickness to the device, shifting the positive overlap of the incident and backreflected light so that it falls within the active region.[13,324,476,478,488] Figure 50 illustrates that by simply varying the thickness of the C_{60} acceptor in a bilayer OPV device, a wavelength-dependent periodic photocurrent arises, demonstrating the existence and importance of the optical interference phenomenon.[324] An optical spacer should be both transparent to wavelengths of light absorbed in the active layer and electrically conductive to minimize the added series resistance associated with its presence. The ability of a cathode-side IFL to control the light intensity distribution within the various regions of an OPV device in addition to hole- and/or exciton-blocking character and active layer protection from cathode deposition makes this layer of utmost importance in achieving the maximum efficiency from an optimized solar cell. Serving as an example, Figure 51 depicts TiO_x incorporation into a polymer-based OPV device and shows the shift in the squared optical electric-field maximum to the active layer.[478]

7.4. Trilayer p−i−n Cells

An ideal p−i−n OPV structure for an organic solar cell is illustrated in Figure 52 (left).[37,358,489] In a typical p−i−n cell, only the middle intrinsic layer (i-layer), comprising a bilayer or blended layer of two highly absorbing materials, absorbs visible light to generate excitons. The p- and n-type transport layers are made of controllably doped wide-gap materials. Such a heterojunction has a vast number of heteromolecular D−A interfacial contacts acting as efficient photocarrier generation sites. However, a proper alignment of energy levels between photoactive layer and transport layers as illustrated in Figure 52 (right) is critical to attain the transport of photogenerated carriers across the p/i/n interfaces without losing free energy. One advantage for such a trilayer configuration is that the thicknesses of both the photoactive and transport layers can be independently optimized to reach the maximum optical absorption and hence high IPCE.

Due to the doped transport layer, the series resistance of a trilayer OPV device is significantly lowered, and hence the photocurrent and *FF* are increased. Gebeyehu et al. reported a highly efficient p−i−n-type BHJ OPV device based on (i) a blend of ZnPc as electron donor and C_{60} as electron acceptor, and (ii) doped wide-gap charge transport layers, which were formed using a high vacuum coevaporation deposition technique, that is, cosublimation of matrix and dopant.[490] A neat layer of perylene dye, PTCBI, can be added to extend the absorption spectrum of the active layer system. The power conversion efficiency of this cell under 1 sun reaches ~1.9%, which represents an almost 2-fold improvement as compared to the conventional OPV architecture.

Hiramoto et al. have also demonstrated a three-layered OPV that contains a sandwiched interlayer of codeposited p-type Pc pigment and n-type perylene derivative, PTC, along with neat Pc and PTC layers. This trilayer cell exhibits considerable photocurrent enhancement when compared to the bilayer cell without the interlayer.[343,344] A large number of Pc/PTC molecular contacts within the interlayer serve as active sites for effective charge carrier photogeneration. In such a p−i−n structure, two unique characteristics can be derived: (i) the built-in potential produced by Fermi level differences in the respective layers is mainly distributed across the codeposited interlayer, and (ii) efficient carrier photogeneration in the codeposited layer occurs via an exciplex, $(PTC^- \cdots Pc^+)^*$. More recently, the same group reported another three-layered OPV cell incorporating an amorphous C_{60}:crystalline H_2Pc nanocomposite interlayer, achieving a η_p of 2.5%.[491]

Solution-processing of trilayer p−i−n cells was enabled by employing tetrabenzoporphyrin, BP, as donor, which is thermally converted from the soluble precursor bearing four bicyclo rings and is insoluble in conventional organic solvents.[492] A p−i−n heterojunction of BP/BP:fullerene/fullerene, where the p-layer is crystalline BP, the i-layer consists of both BP and fullerene, and fullerene acts as the n-layer, was fabricated from organic solution and achieved a η_p as high as 3.4%. The efficiency was further improved to 4.1% by introducing a new fullerene derivative, 1,4-

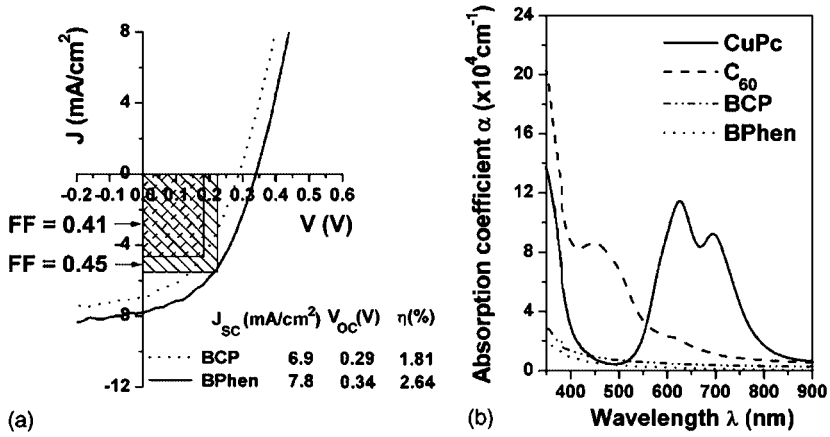

Figure 49. (a) Comparison of $J-V$ characteristics of ITO/CuPc/C_{60}/*BPhen*/Al and ITO/CuPc/C_{60}/*BCP*/Al OPV devices demonstrating enhanced device performance with BPhen. (b) Absorption coefficients of OPV device components. Reprinted with permission from ref 480. Copyright 2006 American Institute of Physics.

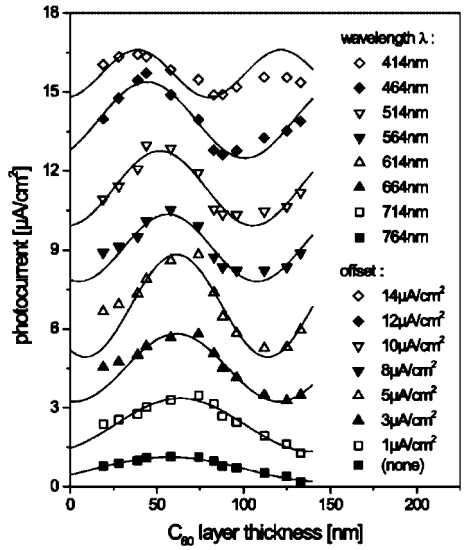

Figure 50. Dependence of the photocurrent on the C_{60} layer thickness at a fixed wavelength in ITO/CuPc/C_{60}/Al OPV devices verifies the presence of the optical interference due to light reflecting off the back metal electrode. Reprinted with permission from ref 324. Copyright 2001 American Institute of Physics.

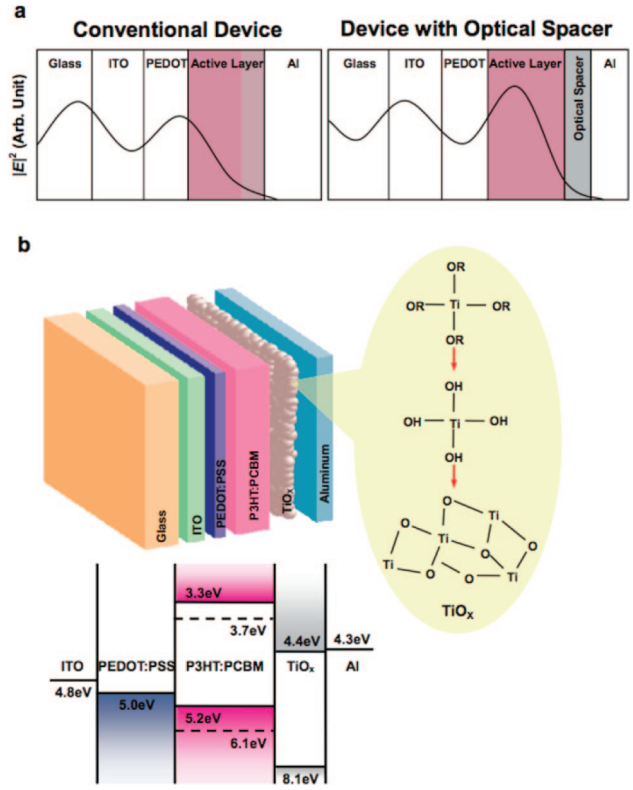

Figure 51. (a) Squared optical electric-field strength inside OPV devices without (left) and with (right) an optical spacer. (b) (top) Schematic representation of OPV device architecture with optical spacer inserted between active layer and cathode and (bottom) energy level diagram of device components. Reprinted with permission from ref 478. Copyright 2006 Wiley-VCH Verlag GmbH & Co. KGaA.

bis(dimethylphenylsilylmethyl)[60] fullerene, SIMEF, for use in the i- and n-layers, which greatly increases V_{oc}. When a very thick (~1 mm) i-layer of codeposited H_2Pc:single crystalline C_{60} is introduced, the cell attains nearly 100% utilization of solar light in the visible region and hence a high J_{sc} of 18.3 mA/cm^2, giving rise to a η_p of 5.3%.[493] It was specifically noted in this report that the *FF* hardly decreases, even for the very thick 1.2 mm interlayer.

Forrest et al. studied a kind of small-molecule p−i−n cell that was fabricated in a confined geometry.[352] The layer structure was ITO/CuPc (100 Å)/CuPc:PTCBI (600 Å, 3:4 by weight)/PTCBI (100 Å), where the mixed-layer was made through codeposition and annealed afterward. They found that when the film is uncapped by metal, the annealing step results in a high density of pinholes and phase-separation in the mixed-layer, which leads to a rough surface morphology and eventually to short-circuited devices. A metal contact was thus proposed for confining the organic materials during the annealing process to prevent stress relief during morphological relaxation, thereby giving rise to a η_p of 50% higher than comparable bilayer devices.

Peumans et al. studied the control of electrical field strength and orientation at the D−A interface in OPVs.[117] Figure 53a shows an energy level diagram of the metal−insulator−metal, MIM, model adopted by most OPV operation, where the built-in electric field is established by the electrode work function differential. The MIM model assumes negligible doping in the active organic layers and predicts a uniform electric field, F, throughout the device thickness in the absence of space charge. In many MSC OPVs, however, unintentional electrical doping is present, which has a dominant effect on the built-in electric field at the D−A interface and as a result on the efficiency of exciton

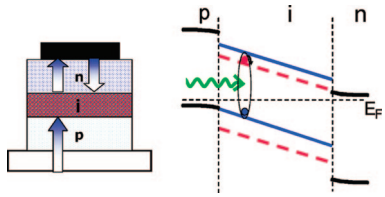

Figure 52. Schematic illustration of an ideal p−i−n solar cell structure (left) and an energy diagram containing a bulk heterojunction as the photoactive region (right). The arrows indicate incoming and reflected light. Reprinted with permission from ref 37. Copyright 2007 American Chemical Society.

dissociation and overall power conversion efficiency. Figure 53b displays a similar energy level diagram, in which the acceptor and donor were n- and p-doped, respectively, leading to a concentration of the built-in potential drop at the D−A interface and strong electric fields that assist the charge carrier separation. The potential drop is no longer dominated by the alignment of the electrode Fermi levels within the organic semiconductor band gap and is instead determined by the position of the Fermi level in the donor and acceptor layer, which is a function of the electrically active doping concentration. If the doping is absent or of the wrong type, as shown in Figure 53c, the electric field at the D−A interface prevents the charges from separating, leading to low efficiencies. In a CuPc/BPE-PTCDI, *N*,*N*′-bis(2-phenylethyl)-perylene-3,4,9,10-tetracarbonicacid-diimide, bilayer OPV (Figure 53d), the device employing impure PTCDI shows improvement in all cell characteristics as opposed to the one using pure PTCDI. This indicates that a strong electric field at the D−A interface is essential to high-efficiency OPVs, due to the strong Coulomb attraction of photogenerated excitons.

7.5. Multilayer Molecular Junctions

The Forrest group first demonstrated small molecule multilayer junctions for organic photodetectors. Donor/acceptor (CuPc/PTCBI) alternating multilayer stacks were used as photoactive layers, exhibiting an EQE of 75% and response times of 720 ± 70 ps at a reverse bias of ∼10 V.[354] As shown in Figure 54a, photogenerated excitons efficiently dissociate into free electrons and holes, followed by carrier separation via tunneling across several closely spaced organic layer interfaces. Figure 54b shows the quantum efficiency dependence on applied voltage and layer thickness, suggesting that the escape of photogenerated carriers from potential wells formed by the multilayers due to tunneling prior to recombination leads to the high efficiencies observed. An energy diagram is shown in Figure 54c to illustrate the charge transport across successive layers. The devices are useful for molecular organic photonics and visible and near-infrared spectral detection.

In two successive reports, Xue and Forrest discussed carrier transport in multilayer organic photodetectors in detail. In the first part,[351] effects of a multilayer structure on dark current and photoresponse were discussed by analyzing carrier tunneling both within the organic active region and at the anode/organic interface. To achieve a high quantum efficiency and a fast response speed, individual layers in the active region must be thin enough for photogenerated carriers to tunnel through the adjacent barriers and ultimately be collected at the electrodes. Next, in the second part,[259] the effects of anode preparation on device performance were discussed. ITO substrates undergoing oxygen plasma or UV ozone treatment showed an increased work function, which is preferable for reducing the tunneling current of electrons from the anode into the organic layers, thereby lowering the dark current under reverse bias. However, the ITO/organic interface was found to have a high density of defect states. One solution to this was to coat the ITO with a doped organic layer such as PEDOT:PSS, which may provide an anode with both a high work function and a low defect density.

As one more example, Hong and Leo et al. demonstrated an improved ZnPc/C_{60} heterojunction by alternately depositing ultrathin active layers between the two bulk layers.[479] The PV cell based on such ultrathin multilayer structures shows a 60% improvement in PCE under AM1.5G illumination over flat heterojunctions. An effective phase-separation of ZnPc and C_{60} and a high degree of crystalline ordering of C_{60} were observed in electron microscope studies on this system. The authors then proposed that an interpenetrating interface between ZnPc and C_{60} is formed, thus facilitating both exciton separation and charge transport given the short L_{ex}, and enhancing the photocurrent from ZnPc due to an extended photoactive region.

7.6. Tandem Cells

As discussed in section 7.5, the use of doped wide-gap charge transport layers with high conductivity and low absorption in the visible range enables one to achieve high internal quantum efficiency, IQE, and to optimize devices with respect to optical interference effects via adjusting the film thickness. This inspired the concept of stacking several cells on top of each other to form tandem structures, which enables one to resolve two limiting factors existing intrinsically among organic semiconductor molecules, poor charge carrier mobility and a narrow light absorption range. With this method, two or even more organic solar cells can be stacked together, and the components of each device can be tailored to exhibit complementary absorption spectra. As a proof-of-concept, a double p−i−n architecture was recently proposed to achieve efficient OPVs.[494] As shown in Figure 55, stacking two p−i−n-type cells, both having a ZnPc:C_{60} blend as the photoactive layer, yields a tandem OPV device that exhibits a power conversion efficiency of 3.8 ± 0.2% under simulated AM1.5G illumination, as compared to 2.1% for the respective single p−i−n cell. Note that gold clusters were introduced between cells as recombination centers. The concept may yield even higher efficiency devices by stacking several p−i−n cells with complementary absorption spectra to achieve panchromatic absorption through the visible and near-infrared portions of the solar spectrum.

Additionally, Xue et al. demonstrated a high-efficiency OPV tandem cell in which two hybrid planar-mixed molecular heterojunction cells are stacked in series as shown in Figure 56.[359] Absorption of incident light was maximized by positioning the subcell tuned to absorb long-wavelength light nearest the transparent anode, and situating the second subcell closest to the reflecting metal cathode to preferentially absorb short-wavelength solar energy. By using such an asymmetric tandem cell structure that offers to incorporate different D and A material combinations in the individual subcells to cover a broader solar spectral region, the authors achieved a V_{oc} of 1.2 V (doubling that of a single cell) and a maximum PCE of ∼5.7 ± 0.3% under 1 sun simulated AM1.5G solar illumination based on the system of CuPc and C_{60}. It can be further projected that (i) by

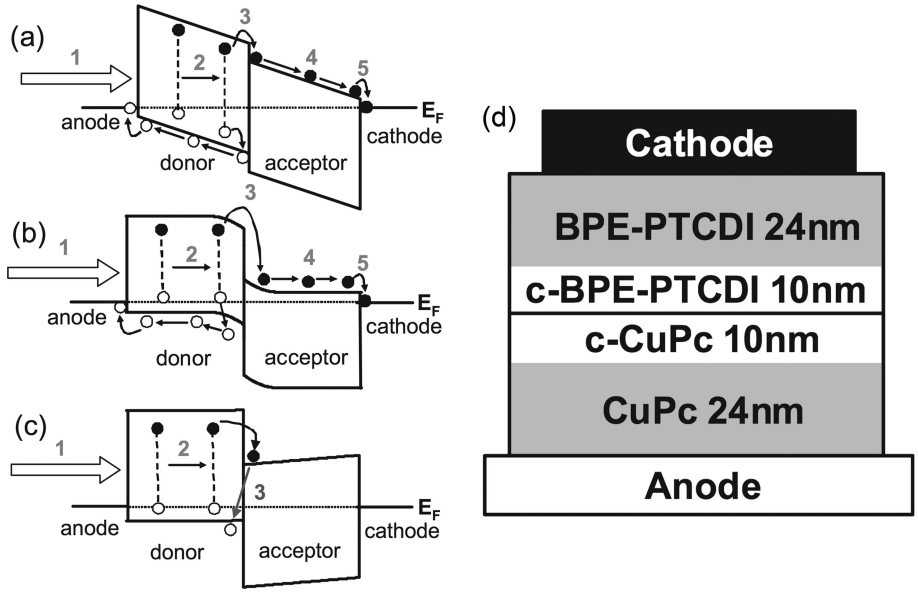

Figure 53. Energy level diagrams of a D/A solar cell at 0 V for (a) the conventional metal−insulator−metal (MIM) model (the five steps of photocurrent generation are illustrated), (b) the p-type doped donor and n-type doped acceptor with each layer 30 nm thick and with a doping concentration of 10^{18} cm^{-3}, (c) the donor having p-type doping of 10^{17} cm^{-3} and acceptor with n-type doping of 10^{7} cm^{-3}, and (d) schematic of the device structure used for modeling. Reprinted with permission from ref 117. Copyright 2008 Wiley-VCH Verlag GmbH & Co. KGaA.

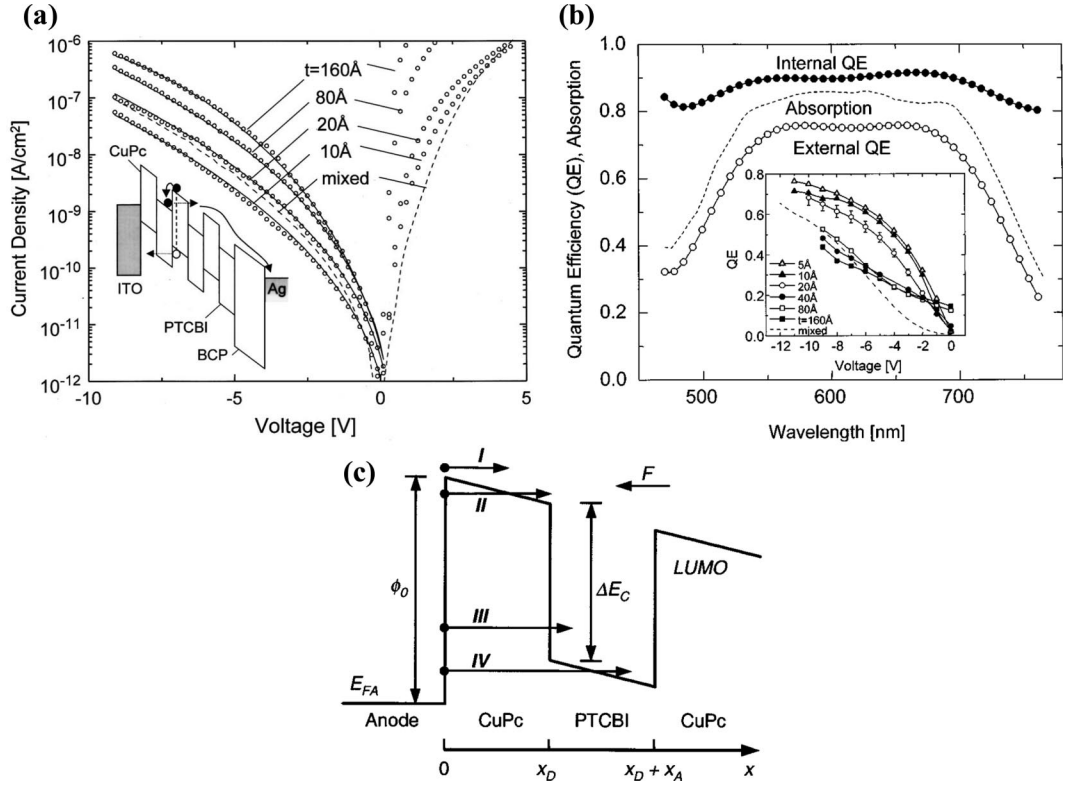

Figure 54. (a) $J-V$ characteristics of 2-, 4-, 16-, and 32-layer (○) and mixed-layer (- - -) ITO/(CuPc/PTCBI)$_n$/BCP/Ag devices with a 1 mm diameter (t is the individual layer thickness). Fits of the data to theory are also shown (−). Inset schematically illustrates an energy-level diagram of an alternating donor−acceptor multilayer photodetector device under reverse bias. (b) External quantum efficiency (○), internal quantum efficiency (●), and absorption (- - -) of a 64-layer device as a function of wavelength. Inset is the peak external quantum efficiency of different devices as a function of the thickness of the molecular layers with the applied voltage as a parameter. (c) Energy level diagram illustrating the several electron injection components at the anode/organic interface. E_{FA} is the Fermi level of the anode, Φ_0 is the barrier height for electron injection from the anode into CuPc, ΔE_C is the LUMO level offset between CuPc and PTCBI, F is the external electric field, and x_D and x_A are the thicknesses of the CuPc and PTCBI layers, respectively. Numerals I−IV represent different components of the electron injection current. Parts a and b reprinted with permission from ref 354. Copyright 2000 American Institute of Physics. Part c reprinted with permission from ref 351. Copyright 2004 American Institute of Physics.

applying antireflection coatings to the glass substrates, an additional 10% improvement to efficiencies is possible, and (ii) by employing a three-subcell device, with two subcells absorbing across the blue to red, and a third primarily absorbing in the near-infrared range, efficiencies in excess of 7% can potentially be attained.

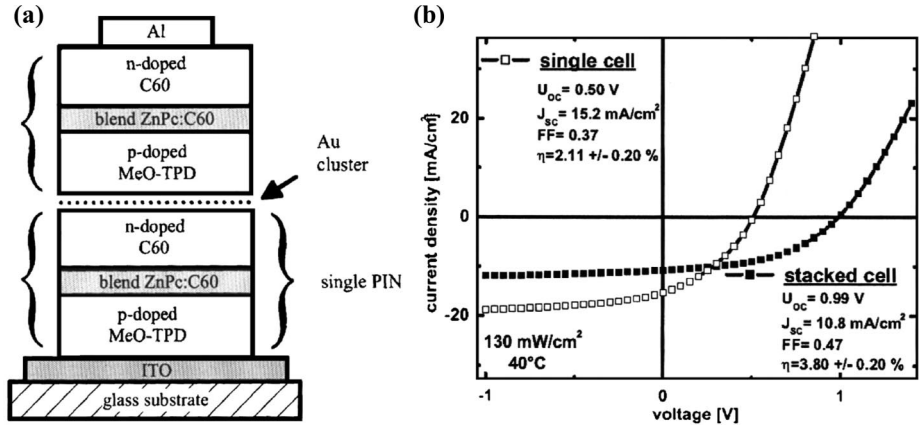

Figure 55. (a) Schematic of the double p−i−n solar cell and (b) $J-V$ characteristics of single and tandem p−i−n solar cells under 130 mW/cm^2 simulated AM1.5G solar illumination. Reprinted with permission from ref 494. Copyright 2005 American Institute of Physics.

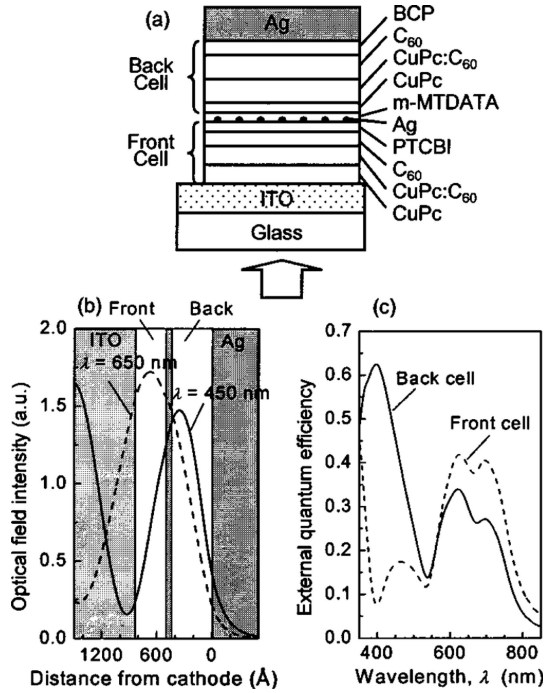

Figure 56. (a) Structure of an organic tandem PV cell formed by stacking two hybrid planar mixed-heterojunction cells in series. Each subcell (front or back, with respect to the incident light direction as indicated) employs a mixed CuPc:C_{60} layer sandwiched between homogeneous CuPc and C_{60} layers as the photoactive region, with a PTCBI (front) or BCP (back) layer serving as the EBL. (b) Optical field intensities at $\lambda = 450$ nm (−) and $\lambda = 650$ nm (- - -) calculated as functions of the distance from the cathode in an asymmetric organic tandem cell. (c) Calculated external quantum efficiencies for the front (- - -) and back (−) subcells. The asymmetric spectral responses from the two subcells result from the placement of the layers within the asymmetric tandem cell structure. Reprinted with permission from ref 359. Copyright 2004 American Institute of Physics.

Yan et al. succeeded in fabricating a tandem OPV device without relying on metal clusters between the subcells for recombination. The purely organic connecting units impart enhanced optical transparency and require a lower sublimation temperature than Au or Ag.[495] The organic heterojunction film becomes an effective recombination center for electrons and holes generated in front cell and back cell, respectively. In an optimized tandem solar cell (illustrated in Figure 57) comprising a tin phthalocyanine dichloride, $SnCl_2Pc$/copper hexadecafluorophthalocyanine, $F_{16}CuPc$, heterojunction as the connecting unit, the V_{oc} is about 1.04 V (double of the single unit cells) and the η_p is ∼1.8% (60% higher than each subcell). Moreover, the all-organic connecting units can be continuously deposited and designed in such a way as to cover a broad light absorption range.

An additional charge recombination region in tandem OPV devices is composed of a bilayer of Al and MoO_3 with optimized respective thicknesses of 1 and 15 nm (Figure 58).[496] Such an intermediate layer has high visible transparency (∼98%) and efficient charge collection to realize electric connection in series. For a polymer−small molecule tandem cell having a P3HT:PCBM blend as the front cell and a CuPc/C_{60} bilayer as the back cell, a η_p of 2.8% was obtained under 100 mW/cm^2 illumination, which is larger than that of either individual cell. In this polymer−small molecule cell, the role of MoO_3 is 2-fold: hole transporting and exciton blocking. Similar examples were also recently shown by using a 1 nm thick Au recombination layer[497] or using two doped MSC layers along with a thin noble metal interlayer as an intermediate recombination zone in tandem OPVs.[498]

A monolithic tandem OPV cell was demonstrated with subcells in parallel connections, where transparent multiwalled carbon nanotube, MWCNT, sheets are used as an interlayer anode (Figure 59).[280] The parallel tandem cell exhibits the superposition spectrum of the two spectral sensitivities of the front and back cells, and therefore yields a J_{sc} larger than that of either individual cell.

8. OPV Device Stability

Few studies have been conducted on degradation mechanisms in OPVs, and even fewer have focused on MSC-based devices. As OPV efficiencies improve, however, long-term device stability becomes a more relevant and important issue to consider. A review article by Jørgensen et al. was recently published that summarizes the progress researchers have made in understanding OPV stability.[499] The review highlights the importance of focusing research efforts not only on raising efficiencies, as is the current trend, but also on improving processing techniques and understanding and solving device stability issues. Without advances in all three areas, OPVs will not find commercial application. This realization has even led to the development of a web portal for reporting stability studies by commercial OPV ventures.[500] This section will discuss some of these emerging stability investigations and touch briefly on the mechanisms proposed to be responsible for the degradation, some possible

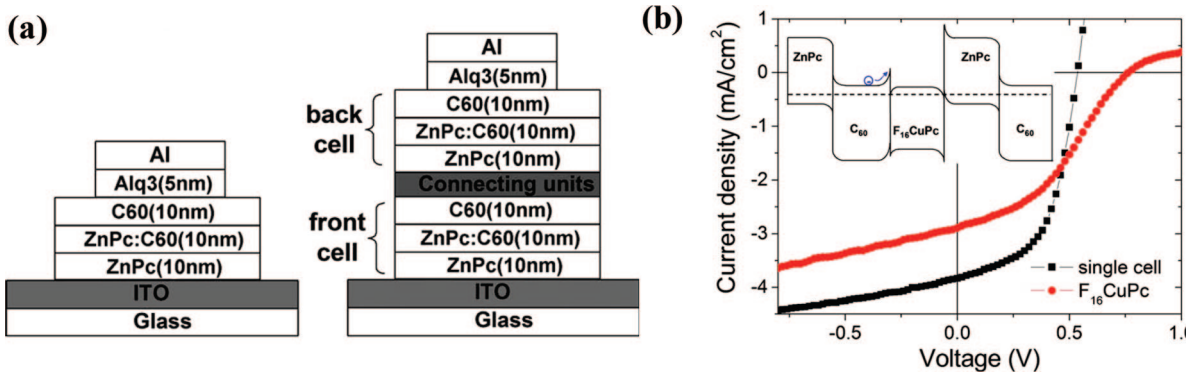

Figure 57. (a) Schematic of device configurations of a single cell and a tandem organic solar cell. (b) $J-V$ characteristics of a single cell and a tandem cell with a $F_{16}CuPc$ layer as a connecting unit under 100 mW/cm^2 AM1.5G illumination. The inset gives the schematic diagram of the energy levels of the tandem cell based on aligned Fermi levels. Reprinted with permission from ref 495. Copyright 2008 American Institute of Physics.

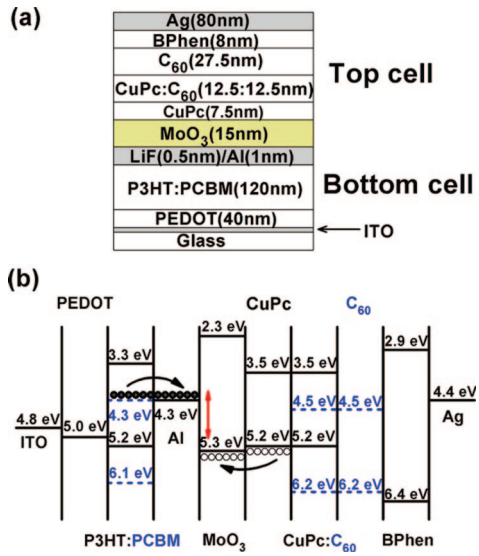

Figure 58. Schematic illustrating (a) device configuration and (b) energy level diagram of a small molecule−polymer tandem OPV with an optimized intermediate layer. Reprinted with permission from ref 496. Copyright 2008 American Institute of Physics.

solutions, and what it all means in the context of OPV commercialization.

The dominant degradation mechanism in OPVs derives from reaction of the active layer materials with water and oxygen from the air. The detailed mechanisms are complex and not completely understood, but developing their understanding marks the first crucial step toward preventing device degradation. An example is provided in fullerenes, which are common acceptor species to both MSC and polymer devices in the form of C_{60} and PCBM, respectively. Fullerenes have been well documented to exhibit diminished conductivity upon oxygen absorption,[482,501−503] and this detrimental effect doubtlessly carries through to yield a reduced overall device performance. Heutz et al. have suggested that in the case of CuPc/C_{60} bilayered or CuPc:C_{60} BHJ devices, n-type C_{60} reaction with oxygen is responsible for the observed degraded device performance over time illustrated in Figure 60.[485]

Water and O_2 can become incorporated into the device during fabrication or can diffuse into the finished device. Therefore, ambient exposure during device fabrication is often minimized by conducting as much work as possible in a glovebox. The inert atmosphere prevents active layer contamination with water and oxygen during fabrication, and some method of encapsulation (discussed below) can be applied before removing the device from this protective environment into air. To maximize published efficiencies, many cited OPV efficiency measurements are made immediately following device fabrication,[360] and often the $J-V$ plots are even recorded under inert environment. While this procedure is not technically incorrect, it should be noted that this level of performance is not always representative of how OPV devices would function in commercial applications with requisite ambient exposure and/or prolonged operation.

In addition to the O_2 and water ingress that leads to degraded device performance, other instances of OPV instability stem from photoinitiated radicals that react with organic materials,[499] thermal stress,[504] and also the various device interfaces.[445] PEDOT:PSS, for example, has been associated in the literature with device temporal instability.[282,466,469−471] It is acidic and may etch the underlying ITO, potentially lead to dewetting and delamination causing catastrophic device failure. PEDOT:PSS is also generally spin-cast as an aqueous dispersion, and it is hygroscopic. As the IFL absorbs water, the series resistance rises, reducing FF and current.[505,506] Metal−organic interfaces are not free from problems either.[445] Thin Al electrodes could be prone to oxidation[504] and also allow significant oxygen permeation into the active layer.[507]

Because many stability issues are shared between MSC- and polymer-based OPVs, the Jørgensen review[499] that focuses on OPV degradation in polymer solar cells contains many references that exemplify and expand upon the OPV degradation mechanisms that are also relevant in MSC OPVs, and the interested reader is referred to that review for a more in-depth discussion. There are, however, some differences between MSC and polymer OPV stability. For example, there appear to be fewer problems associated with photobleaching in MSCs than in polymer systems, but crystallization appears to be a more prominent complication in MSCs. Crystallization has been a major concern for the common cathode-side IFL BCP. BCP as an exciton-blocking IFL is discussed above (section 7.3), and it is often used in MSC OPV devices. Despite its popularity, BCP has been shown to increase the rate of degradation of devices as compared to those not having the IFL such that unencapsulated solar cells tested in air that incorporate BCP into the device architecture exhibit a η_p of only one-half the initial value after a brief 20 min.[377] Wu et al. attribute this decline in efficiency in part to large gaps induced by BCP crystallization that allows more efficient O_2 permeation into the device. An image of ITO/

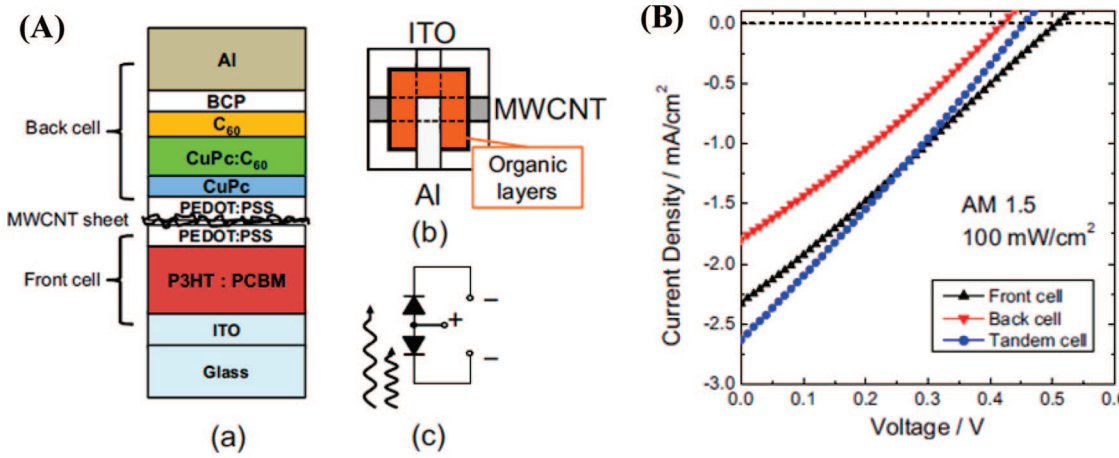

Figure 59. (A) Schematic device structure of the monolithic parallel tandem OPV cell. (a) Cross-section view of stacked layers. (b) Top-view of a typical tandem OPV cell. (c) Equivalent circuit. Three electrodes are accessible for an external circuit connection independently. (B) $J-V$ characteristics for the front cell (▲), the back cell (▼), and the total tandem parallel connection (●). All measurements were performed in a glovebox in N_2 atmosphere. Reprinted with permission from ref 280. Copyright 2009 American Institute of Physics.

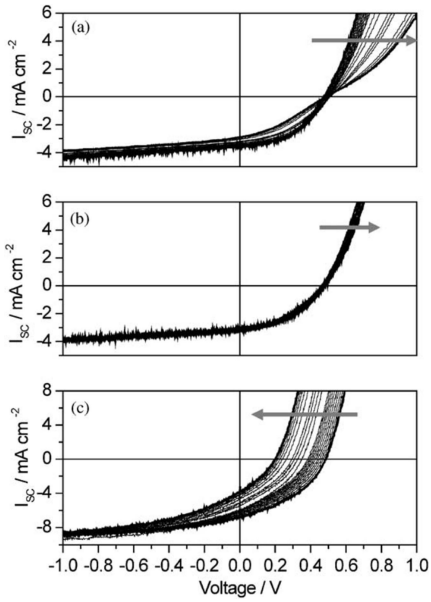

Figure 60. Current−voltage curves of a bilayer ITO/CuPc (15 nm)/C_{60} (40 nm)/BCP (12 nm)/Al OPV device (a) in air and (b) under vacuum and of (c) an ITO/CuPc (3.5 nm)/CuPc:C_{60} (50 nm)/C_{60} (5 nm)/BCP (12 nm)/Al BHJ OPV device in air under 1 sun illumination as a function of time, from 0 to 120 min (with time progression shown by the gray arrows). Reprinted with permission from ref 485. Copyright 2004 Elsevier.

C_{60}/BCP in air shows obvious BCP crystal formation (Figure 61),[377] which is believed to occur at an increased rate in the presence of water.[6,482] In several reports from the Forrest group, doping the BCP with 5−15% (by wt) PTCBI via coevaporation is claimed to prevent the micrometer-sized BCP crystals from forming,[6,353,354] but many later publications continue to utilize pure BCP instead of the coevaporated blend.[223,352,359]

In an attempt to find a more stable alternative to BCP, Song et al. focused their efforts on Alq_3.[376,482] This material has a reduced propensity to crystallize as compared to BCP, and it is reported to improve unencapsulated device lifetimes in air ∼150-fold as compared to devices having BCP due to superior blocking of water and O_2 permeation.[482] Carrying this idea further, inverted devices of architecture ITO/Alq_3/C_{60}/CuPc/Au were fabricated to better protect the C_{60} from water/O_2 permeation through the metal back electrode.[376] In this configuration, device lifetimes were significantly improved, achieving a shelf lifetime of ∼1500 h for an unencapsulated device in air, as compared to ∼61 h for an analogous device with conventional architecture.

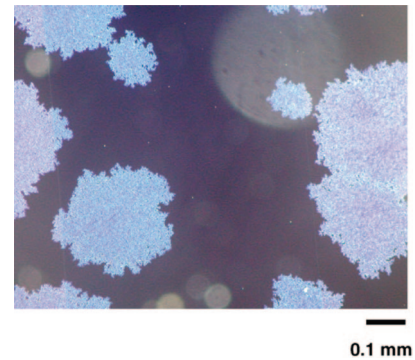

Figure 61. Image of ITO/C_{60} (100 nm)/BCP (10 nm) in air taken by polarized light microscopy. Reprinted with permission from ref 377. Copyright 2007 Elsevier.

Encapsulation methods can further inflate OPV device lifetimes. For example, Franke et al. accomplished an efficiency decrease of only ∼3% after 1400 h of continuous white light illumination.[508] The encapsulants do add cost to the device, but may prove essential for attaining sufficient long-term performance. The best, most impermeable barriers include a glass-on-glass edge seal,[445,508] but other flexible alternatives exist and are under investigation.

Whether stability issues will ultimately limit OPV implementation in commercial applications remains to be seen. It is a positive sign, however, that OLEDs have been commercialized for application in various technologies, including portable electronic device displays. The first commercial OPV cells may be employed in consumer applications that do not require a long lifetime, but with further research, cells stable for many years should be achievable.

9. Conclusions and Outlook

The understanding of molecular semiconductors is progressing rapidly, as is the field of organic photovoltaics. Major practical issues remain, however, such as minimizing interfacial recombination, preventing both chemical and morphological instabilities, and learning to employ cleaner, more crystalline materials. New MSCs and new cell designs

may be needed to achieve a higher level of performance. Nevertheless, the remarkable improvements in OPV cell efficiency in recent years bode well for the future of this exciting field.

10. Abbreviations

A	electron acceptor
Alq_3	tris(8-hydroxyquinoline) aluminum
AM1.5G	air mass 1.5, global
BCP	2,9-dimethyl-4,7-diphenyl-1,10-phenanthroline
BHJ	bulk heterojunction
CT	charge transfer
CuPc	copper phthalocyanine
D	electron donor
DSSC	dye-sensitized solar cell
EBL	exciton blocking layer
EQE	external quantum efficiency
FET	field-effect transistor
H_2Pc	metal-free phthalocyanine
HJ	heterojunction
HOMO	highest occupied molecular orbital
HTL	hole transport layer
IFL	interfacial layer
IPCE	incident photon to current efficiency
ISC	inorganic semiconductor
ITO	tin-doped indium oxide
LC	liquid crystal
LUMO	lowest unoccupied molecular orbital
m-MTDATA	4,4′,4″-tris(3-methylphenylphenylamino)triphenylamine
MEH-PPV	poly[2-methoxy-5-(2′-ethylhexyloxy)-1,4-phenylene vinylene]
MPc	metallophthalocyanine
MSC	molecular semiconductor
OLED	organic light-emitting diode
OPV	organic photovoltaic
OSC	organic semiconductor
P3HT	poly(3-hexylthiophene)
PBI	perylene bisimide; also PDI
Pc	phthalocyanine
PCBM	[6,6]-phenyl-C_{61}-butyric acid methyl ester
PDI	perylene diimide; also PBI
PEDOT:PSS	poly(3,4-ethylenedioxythiophene):poly(styrene sulfonate)
PET	poly(ethylene terephthalate)
PPEI	perylene bis(phenylethylimide)
PTCBI	3,4,9,10-perylenetetracarboxylic bis-benzimidazole
PTCDI	3,4,9,10-perylenetetracarboxylic diimide
PV	photovoltaic
SC	semiconductor
SEM	scanning electron microscope
SubPc	chloro[subphthalocyanine]boron(III)
TCO	transparent conducting oxide
XSC	excitonic semiconductor

Symbols

α	absorption coefficient
η_p	power conversion efficiency
λ_{max}	wavelength of maximum absorption
$\mu_{n,p}$	electron, hole mobility
$\nabla\mu$	gradient of the chemical potential
A	active area of solar cell
E_f	Fermi energy
∇E_f	gradient of the electrochemical potential, or quasi-Fermi level
E_g	electrical band gap, or transport gap
$E_{g,HJ}$	difference between the LUMO of the A and the HOMO of the D; $E_{g,HJ} = E_{vb,D} - E_{cb,A}$
F	electric field
FF	fill factor
J_{sc}	short-circuit current density
L_{ex}	exciton diffusion length
M	spectral mismatch factor
n_d	dopant concentration
n_f	free electron density
q	electronic charge
R_s	series resistance
R_{sh}	shunt resistance, or parallel resistance
∇U	gradient of the electric potential
V_{oc}	open-circuit voltage

11. Acknowledgments

We thank the U.S. Department of Energy, Office of Science, Basic Energy Science, Division of Chemical Sciences, Geosciences and Biosciences, under Contract No. DE-AC36-08GO28308 to NREL for funding this research.

12. References

(1) BES Workshop on Solar Energy Utilization, 2005.
(2) BES Report from the BES Advisory Committee, 2007.
(3) Smalley, R. E. *MRS Bull.* **2005**, *30*, 412.
(4) Lewis, N. S.; Nocera, D. G. *Proc. Natl. Acad. Sci. U.S.A.* **2006**, *103*, 15729.
(5) *Organic-Based Photovoltaics. MRS Bull*. **2005**, *30*, 1.
(6) Peumans, P.; Yakimov, A.; Forrest, S. R. *J. Appl. Phys.* **2003**, *93*, 3693.
(7) *Organic Photovoltaics: Mechanisms, Materials, and Devices*; Sun, S.-S., Sariciftci, N. S., Eds.; Taylor and Francis: Boca Raton, FL, 2005.
(8) Günes, S.; Neugebauer, H.; Sariciftci, N. S. *Chem. Rev.* **2007**, *107*, 1324.
(9) McGehee, M. D. *MRS Bull.* **2009**, *34*, 95.
(10) Shaheen, S. E.; Ginley, D. S. *Dekker Encyclopedia of Nanoscience and Nanotechnology*; Marcel Dekker: New York, 2004.
(11) Placencia, D.; Wang, W.; Shallcross, R. C.; Nebesny, K. W.; Brumbach, M.; Armstrong, N. R. *Adv. Funct. Mater.* **2009**, *19*, 1913.
(12) Yang, F.; Shtein, M.; Forrest, S. R. *Nat. Mater.* **2005**, *4*, 37.
(13) Yoo, S.; Domercq, B.; Kippelen, B. *Appl. Phys. Lett.* **2004**, *85*, 5427.
(14) Jenekhe, S. *Chemistry of Materials, Special Issue on "Organic Electronics"*, 2004; Vol. 16.
(15) Law, K.-Y. *Chem. Rev.* **1993**, *93*, 449.
(16) Gregg, B. A. *J. Phys. Chem. B* **2003**, *107*, 4688.
(17) Coropceanu, V.; Cornil, J.; da Silvo Filho, D. A.; Olivier, Y.; Silbey, R.; Brédas, J.-L. *Chem. Rev.* **2007**, *107*, 926.
(18) Giaimo, J. M.; Lockard, J. V.; Sinks, L. E.; Scott, A. M.; Wilson, T. M.; Wasielewski, M. R. *J. Phys. Chem. A* **2008**, *112*, 2322.
(19) Hagfeldt, A.; Grätzel, M. *Acc. Chem. Res.* **2000**, *33*, 269.
(20) Heeger, A. J. *J. Phys. Chem. B* **2001**, *105*, 8475.
(21) Ohkita, H.; Cook, S.; Astuti, Y.; Duffy, W.; Tierney, S.; Zhang, W.; Heeney, M.; McCulloch, I.; Nelson, J.; Bradley, D. D. C.; Durrant, J. R. *J. Am. Chem. Soc.* **2008**, *130*, 3030.
(22) Kearns, D. R.; Tollin, G.; Calvin, M. *J. Phys. Chem.* **1960**, *32*, 1020.
(23) Leempoel, P.; Castro-Acuna, M.; Fan, F.-R. F.; Bard, A. J. *J. Phys. Chem.* **1982**, *86*, 1396.
(24) Leempoel, P.; Fan, F.-R. F.; Bard, A. J. *J. Phys. Chem.* **1983**, *87*, 2948.
(25) Meier, H.; Tschirwitz, U. *Ber. Bunsen-Ges. Phys. Chem.* **1969**, *73*, 795.
(26) Tollin, G.; Kearns, D. R.; Calvin, M. *J. Chem. Phys.* **1960**, *32*, 1013.
(27) Braun, C. B. In *Handbook on Semiconductors*; Keller, S. P., Ed.; North-Holland: Amsterdam, 1980; Vol. 3.
(28) Davydov, A. S. *Theory of Molecular Excitons*; Plenum: New York, 1971.
(29) Pope, M.; Swenberg, C. E. *Electronic Processes in Organic Crystals and Polymers*, 2nd ed.; Oxford University Press: New York, 1999.
(30) Charlé, K.-P.; Willig, F. *Chem. Phys. Lett.* **1978**, *57*, 253.
(31) Geacintov, N.; Pope, M.; Kallmann, H. *J. Chem. Phys.* **1966**, *45*, 2639.
(32) Bloom, C. J.; Elliott, C. M.; Schroeder, P. G.; France, C. B.; Parkinson, B. A. *J. Phys. Chem. B* **2003**, *107*, 2933.
(33) Murata, H.; Kafafi, Z. H.; Uchida, M. *Appl. Phys. Lett.* **2002**, *80*, 189.
(34) Armstrong, N. R.; Wang, W.; Alloway, D. M.; Placencia, D.; Ratcliff, E.; Brumbach, M. *Macromol. Rapid Commun.* **2009**, *30*, 717.
(35) Forrest, S. R. *Chem. Rev.* **1997**, *97*, 1793.

(36) Forrest, S. R. *Nature* **2004**, *428*, 911.
(37) Walzer, K.; Maennig, B.; Pfeiffer, M.; Leo, K. *Chem. Rev.* **2007**, *107*, 1233.
(38) Facchetti, A. *Mater. Today* **2007**, *10*, 28.
(39) Rand, B. P.; Genoe, J.; Heremans, P.; Poortmans, J. *Prog. Photovoltaics: Res. Appl.* **2007**, *15*, 659.
(40) Chwang, A. B.; Frisbie, C. D. *J. Phys. Chem. B* **2000**, *104*, 12202.
(41) Katz, H. E.; Bau, Z. *J. Phys. Chem. B* **2000**, *104*, 671.
(42) Lonergan, M. *Science* **1997**, *278*, 2103.
(43) Babel, A.; Jenehke, S. A. *J. Phys. Chem. B* **2002**, *106*, 6129.
(44) Chesterfield, R. J.; McKeen, J. C.; Newman, C. R.; Ewbank, E. C.; da Silva Filho, D. A.; Bredas, J.-L.; Miller, L. L.; Mann, K. R.; Frisbie, C. D. *J. Phys. Chem. B* **2004**, *108*, 19281.
(45) Jones, B. A.; Facchetti, A.; Wasielewski, M. R.; Marks, T. J. *J. Am. Chem. Soc.* **2007**, *129*, 15259.
(46) Katz, H. E.; Bao, Z.; Gilat, S. L. *Acc. Chem. Res.* **2001**, *34*, 359.
(47) Newman, C. R.; Frisbie, C. D.; da Silva Filho, D. A.; Bredas, J. L.; C, E. P.; Mann, K. R. *Chem. Mater.* **2004**, *16*, 4436.
(48) Sirringhaus, H.; Tessler, N.; Friend, R. H. *Science* **1998**, *280*, 1741.
(49) McGehee, M. D.; Heeger, A. J. *Adv. Mater.* **2000**, *12*, 1655.
(50) Herbst, W.; Hunger, K. *Industrial Organic Pigments: Production, Properties, Applications*, 3rd ed.; Wiley-VCH: Weinheim, 2004.
(51) Popovic, Z. D. *Mol. Cryst. Liq. Cryst.* **1989**, *171*, 103.
(52) Kazmaier, P. M.; Hoffmann, R. *J. Am. Chem. Soc.* **1994**, *116*, 9684.
(53) Klebe, G.; Graser, F.; Hädicke, E.; Berndt, J. *Acta Crystallogr., Sect. B* **1989**, *B45*, 69.
(54) Brumbach, M.; Placencia, D.; Armstrong, N. R. *J. Phys. Chem. C* **2008**, *112*, 3142.
(55) Konarka Technologies Inc. Retrieved on May 5, 2009 from http://www.konarka.com/index.php/site/newsdetail.
(56) Sze, S. M. *Physics of Semiconductor Devices*, 2nd ed.; Wiley-Interscience: New York, 1981.
(57) Bard, A. J.; Faulkner, L. R. *Electrochemical Methods*; Wiley & Sons: New York, 1980.
(58) Pearson, G. L.; Bardeen, J. *Phys. Rev.* **1949**, *75*, 865.
(59) Chen, S.-G.; Stradins, P.; Gregg, B. A. *J. Phys. Chem. B* **2005**, *109*, 13451.
(60) Gregg, B. A. In *Organic Photovoltaics*; Sun, S. S., Sariciftci, N. S., Eds.; Marcell Dekker: New York, 2005.
(61) Gregg, B. A.; Cormier, R. A. *J. Am. Chem. Soc.* **2001**, *123*, 7959.
(62) Frenkel, J. *Phys. Rev.* **1938**, *54*, 647.
(63) Simmons, J. G. *Phys. Rev.* **1967**, *155*, 657.
(64) Zakhidov, A. A.; Yoshino, K. *Synth. Met.* **1994**, *64*, 155.
(65) Kallmann, H.; Pope, M. *J. Chem. Phys.* **1959**, *30*, 585.
(66) *Spectroscopy and Excitation Dynamics of Condensed Molecular Systems*; Agranovich, V. M., Hochstrasser, R. M., Eds.; North Holland: Amsterdam, 1983.
(67) Zhu, X.-Y.; Yang, Q.; Muntwiler, M. *Acc. Chem. Res.* **2009**, *42*, 1779.
(68) Popovic, Z. D.; Hor, A.-M.; Loutfy, R. O. *Chem. Phys.* **1988**, *127*, 451.
(69) Powell, R. C.; Soos, Z. G. *J. Lumin.* **1975**, *11*, 1.
(70) Gregg, B. A.; Chen, S.-G.; Cormier, R. A. *Chem. Mater.* **2004**, *16*, 4586.
(71) Debye, P. P.; Conwell, E. M. *Phys. Rev.* **1954**, *93*, 693.
(72) Smith, R. A. *Semiconductors*; Cambridge University Press: Cambridge, 1978.
(73) Gregg, B. A.; Hanna, M. C. *J. Appl. Phys.* **2003**, *93*, 3605.
(74) Brédas, J.-L.; Beljonne, D.; Coropceanu, V.; Cornil, J. *Chem. Rev.* **2004**, *104*, 4971.
(75) Gregg, B. A.; Kose, M. E. *Chem. Mater.* **2008**, *2008*, 5235.
(76) Feng, X.; Marcon, V.; Pisula, W.; Hansen, M. R.; Kirkpatrick, J.; Grozema, F.; Andienko, D.; Kremer, K.; Mullen, K. *Nat. Mater.* **2009**, *8*, 421.
(77) Brédas, J.-L.; Norton, J. E.; Cornil, J.; Coropceanu, V. *Acc. Chem. Res.* **2009**, *42*, 1691.
(78) Perlstein, J. *Chem. Mater.* **1994**, *6*, 319.
(79) Gregg, B. A.; Fox, M. A.; Bard, A. J. *J. Phys. Chem.* **1989**, *93*, 4227.
(80) Cormier, R. A.; Gregg, B. A. *J. Phys. Chem.* **1997**, *101*, 11004.
(81) Gregg, B. A. *J. Phys. Chem.* **1996**, *100*, 852.
(82) Liu, S.-G.; Sui, G.; Cormier, R. A.; Leblanc, R. M.; Gregg, B. A. *J. Phys. Chem. B* **2002**, *106*, 1307.
(83) Hennessy, M. H.; Soos, Z. G.; Pascal, R. A., Jr.; Girlando, A. *Chem. Phys.* **1999**, *245*, 199.
(84) Hoffmann, M.; Schmidt, K.; Fritz, T.; Hasche, T.; Agranovich, V. M.; Leo, K. *Chem. Phys.* **2000**, *258*, 73.
(85) Saito, T.; Liu, C.-Y.; Lynch, V. M.; Bard, A. J. *Chem. Mater.* **1997**, *9*, 1318.
(86) Yamao, T.; Miki, T.; Akagami, H.; Nishimoto, Y.; Ota, S.; Hotta, S. *Chem. Mater.* **2007**, *19*, 3748.
(87) Tseng, R. J.; Chan, R.; Tung, V. C.; Yang, Y. *Adv. Mater.* **2008**, *20*, 435.
(88) Fahrenbruch, A. L.; Bube, R. H. *Fundamentals of Solar Cells. Photovoltaic Solar Energy Conversion*; Academic Press: New York, 1983.
(89) Landsberg, P. T.; Tonge, G. *J. Appl. Phys.* **1980**, *51*, R1.
(90) Witte, G.; Wöll, C. *J. Mater. Res.* **2004**, *19*, 1889.
(91) Hsiao, Y.-S.; Whang, W.-T.; Suen, S.-C.; Shiu, J.-Y.; Chen, C.-P. *Nanotechnology* **2008**, *19*, 415603.
(92) Sakurai, T.; Fukasawa, R.; Saito, K.; Akimoto, K. *Org. Electron.* **2007**, *8*, 702.
(93) Lunt, R. R.; Benziger, J. B.; Forrest, S. R. *Adv. Mater.* **2007**, *19*, 4229.
(94) Sullivan, P.; Jones, T. S.; Ferguson, A. J.; Heutz, S. *Appl. Phys. Lett.* **2007**, *91*, 233114.
(95) Gregg, B. A.; Sprague, J.; Peterson, M. *J. Phys. Chem. B* **1997**, *101*, 5362.
(96) Briseno, A. L.; Aizenberg, J.; Han, Y.-J.; Penkala, R. A.; Moon, H.; Lovinger, A. J.; Kloc, C.; Bao, Z. *J. Am. Chem. Soc.* **2005**, *127*, 12164.
(97) Liu, C.-Y.; Lynch, V. M.; Bard, A. J. *Chem. Mater.* **1997**, *9*, 943.
(98) Klofta, T. J.; Danziger, J.; Lee, P.; Pankow, J.; Nebesny, K. W.; Armstrong, N. R. *J. Phys. Chem.* **1987**, *91*, 5646.
(99) Klofta, T. J.; Rieke, P. C.; Linkous, C. A.; Buttner, W. J.; Nanthakumar, A.; Mewborn, T. D.; Armstrong, N. R. *J. Electrochem. Soc.* **1985**, *132*, 2134.
(100) Gregg, B. A.; Fox, M. A.; Bard, A. J. *J. Phys. Chem.* **1990**, *94*, 1586.
(101) Simon, J.; Andre, J.-J. *Molecular Semiconductors*; Springer Verlag: Berlin, 1985.
(102) Schmidt-Mende, L.; Fechtenkötter, A.; Müllen, K.; Moons, E.; Friend, R. H.; MacKenzie, J. D. *Science* **2001**, *293*, 1119.
(103) Li, J.; Kastler, M.; Pisula, W.; Robertson, J. W. F.; Wasserfallen, D.; Grimsdale, A. C.; Wu, J.; Mullen, K. *Adv. Funct. Mater.* **2007**, *17*, 2528.
(104) Doherty, W. J., III; Simmonds, A. G.; Mendes, S. B.; Armstrong, N. R.; Saavedra, S. S. *Appl. Spectrosc.* **2005**, *59*, 1248.
(105) Drager, A. S.; Zangmeister, R. A. P.; Armstrong, N. R.; O'Brien, D. F. *J. Am. Chem. Soc.* **2001**, *123*, 3595.
(106) Flora, W. H.; Mendes, S. B.; Doherty, W. J.; Saavedra, S. S.; Armstrong, N. R. *Langmuir* **2005**, *21*, 360.
(107) Osburn, E. J.; Schmidt, A.; Chau, L. K.; Chen, S. Y.; Smolenyak, P.; Armstrong, N. R.; O'Brian, D. F. *Adv. Mater.* **1996**, *8*, 926.
(108) Gregg, B. A.; Fox, M. A.; Bard, A. J. *J. Am. Chem. Soc.* **1989**, *111*, 3024.
(109) Kim, J. Y.; Bard, A. J. *Chem. Phys. Lett.* **2004**, *383*, 11.
(110) Sun, Q.; Dai, L.; Zhou, X.; Li, L.; Li, Q. *Appl. Phys. Lett.* **2007**, *91*, 253505.
(111) Schouten, P. G.; Warman, J. M.; de Haas, M. P.; Fox, M. A.; Pan, H.-L. *Nature* **1991**, *353*, 736.
(112) Warman, J. M.; de Haas, M. P.; van der Pol, J. F.; Drenth, W. *Chem. Phys. Lett.* **1989**, *164*, 581.
(113) Warman, J. M.; Schouten, P. G. *Appl. Organomet. Chem.* **1996**, *10*, 637.
(114) Warman, J. M.; van de Craats, A. M. *Mol. Cryst. Liq. Cryst.* **2003**, *396*, 41.
(115) Gregg, B. A. *Soft Matter* **2009**, *5*, 2985.
(116) Liang, Z.; Nardes, A.; Wang, D.; Berry, J. J.; Gregg, B. A. *Chem. Mater.* **2009**, *21*, 4914.
(117) Liu, A.; Zhao, S.; Rim, S.-B.; Wu, J.; Könemann, M.; Erk, P.; Peumans, P. *Adv. Mater.* **2008**, *20*, 1065.
(118) Wang, D.; Reese, M. O.; Kopidakis, N.; Gregg, B. A. *Chem. Mater.* **2008**, *20*, 6307.
(119) Perez, M. D.; Borek, C.; Forrest, S. R.; Thompson, M. E. *J. Am. Chem. Soc.* **2009**, *131*, 9281.
(120) Conboy, J. C.; Olson, E. J. C.; Adams, D. M.; Kerimo, J.; Zaban, A.; Gregg, B. A.; Barbara, P. F. *J. Phys. Chem. B* **1998**, *102*, 4516.
(121) Adams, D. M.; Kerimo, J.; Olson, E. J. C.; Zaban, A.; Gregg, B. A.; Barbara, P. F. *J. Am. Chem. Soc.* **1997**, *119*, 10608.
(122) Zhao, W.; Kahn, A. *J. Appl. Phys.* **2009**, *105*, 123711.
(123) Halls, J. J. M.; Walsh, C. A.; Greenham, N. C.; Marseglia, E. A.; Friend, R. H.; Moratti, S. C.; Holmes, A. B. *Nature* **1995**, *376*, 498.
(124) Yu, G.; Gao, J.; Hummelen, J. C.; Wudl, F.; Heeger, A. J. *Science* **1995**, *270*, 1789.
(125) Rand, B. P.; Burk, D. P.; Forrest, S. R. *Phys. Rev. B* **2007**, *75*, 115327.
(126) Popovic, Z. D. *J. Phys. Chem.* **1983**, *78*, 1552.
(127) Veldman, D.; Meskers, S. C. J.; Janssen, R. A. J. *Adv. Funct. Mater.* **2009**, *19*, 1.
(128) Peumans, P.; Forrest, S. R. *Chem. Phys. Lett.* **2004**, *398*, 27.
(129) Gregg, B. A. *J. Phys. Chem. B* **2004**, *108*, 17285.
(130) O'Regan, B.; Grätzel, M. *Nature* **1991**, *353*, 737.
(131) Gregg, B. A. *Coord. Chem. Rev.* **2004**, *248*, 1215.
(132) *Coord. Chem. Rev. Special Issue for Michael Grätzel*; Lever, A. P. B., Ed., 2004.
(133) Pichot, F.; Gregg, B. A. *J. Phys. Chem. B* **2000**, *104*, 6.
(134) Gregg, B. A. *J. Phys. Chem. B* **2003**, *107*, 13540.

(135) Schwarzburg, K.; Willig, F. *J. Phys. Chem. B* **1999**, *103*, 5743.
(136) Schwarzburg, K.; Willig, F. *J. Phys. Chem. B* **2003**, *107*, 3552.
(137) Cahen, D.; Hodes, G.; Grätzel, M.; Guillemoles, J. F.; Riess, I. *J. Phys. Chem. B* **2000**, *104*, 2053.
(138) Chen, F.-C.; Xu, Q.; Yang, Y. *Appl. Phys. Lett.* **2004**, *84*, 3181.
(139) Ramsdale, C. M.; Barker, J. A.; Arias, A. C.; MacKenzie, J. D.; Friend, R. H.; Greenham, N. C. *J. Appl. Phys.* **2002**, *92*, 4266.
(140) Cheyns, D.; Poortmans, J.; Heremans, P.; Deibel, C.; Verlaak, S.; Rand, B. P.; Genoe, J. *Phys. Rev. B: Condens. Matter* **2008**, *77*, 165332.
(141) Gregg, B. A.; Pichot, F.; Ferrere, S.; Fields, C. L. *J. Phys. Chem. B* **2001**, *105*, 1422.
(142) Kron, G.; Egerter, T.; Werner, J. H.; Rau, U. *J. Phys. Chem. B* **2003**, *107*, 3556.
(143) Augustynski, J. *J. Phys. Chem. B* **2003**, *107*, 13544.
(144) Bisquert, J. *J. Phys. Chem. B* **2003**, *107*, 13541.
(145) Rau, U.; G, K.; Werner, J. H. *J. Phys. Chem. B* **2003**, *107*, 13547.
(146) Turrion, M.; Macht, B.; Tributsch, H.; Salavadore, P. *J. Phys. Chem. B* **2001**, *105*, 9732.
(147) Vanmaekelbergh, D.; de Jongh, P. E. *J. Phys. Chem. B* **1999**, *103*, 747.
(148) Gerischer, H. In *Photoelectrochemistry, Photocatalysis and Photoreactors*; Schiavello, M., Ed.; D. Reidel: Dordrecht, 1985.
(149) Gregg, B. A.; Kim, Y. I. *J. Phys. Chem.* **1994**, *98*, 2412.
(150) Gregg, B. A. *Appl. Phys. Lett.* **1995**, *67*, 1271.
(151) Breeze, A. J.; Salomon, A.; Ginley, D. S.; Gregg, B. A. *Appl. Phys. Lett.* **2002**, *81*, 3085.
(152) Reiss, H. *J. Phys. Chem.* **1985**, *89*, 3783.
(153) Koster, L. J. A.; Mihailetchi, V. D.; Blom, P. W. M. *Appl. Phys. Lett.* **2006**, *88*, 093511.
(154) Shockley, W.; Queisser, H. J. *J. Appl. Phys.* **1961**, *32*, 510.
(155) Blom, P. W. M.; Mihailetchi, V. D.; Koster, L. J. A.; Markov, D. E. *Adv. Mater.* **2007**, *19*, 1551.
(156) Blom, P. W. M.; Tanase, C.; de Leeuw, D. M.; Coehoorn, R. *Appl. Phys. Lett.* **2005**, *86*, 092105.
(157) Jain, S. C.; Geens, W.; Mehra, A.; Kumar, V.; Aernouts, T.; Poortmans, J.; Mertens, R.; Willander, M. *J. Appl. Phys.* **2001**, *89*, 3804.
(158) Reynaert, J.; Arkhipov, V. I.; Borghs, G.; Heremans, P. *Appl. Phys. Lett.* **2004**, *85*, 603.
(159) Helfrich, W. In *Physics and Chemistry of the Organic Solid State*; Fox, D., Labes, M. M., Weissberger, A., Eds.; Interscience: New York, 1967; Vol. 3.
(160) Gregg, B. A. *J. Phys. Chem. C* **2009**, *113*, 5899.
(161) Gregg, B. A.; Gledhill, S. E.; Scott, B. *J. Appl. Phys.* **2006**, *99*, 116104.
(162) *Organic Molecular Aggregates*; Reineker, P., Haken, H., Wolf, H. C., Eds.; Springer: Berlin, 1983.
(163) Borsenberger, P. M.; Pautmeier, L.; Bässler, H. *J. Chem. Phys.* **1991**, *94*, 5447.
(164) Kreouzis, T.; Poplavskyy, D.; Tuladhar, S. M.; Campoy-Quiles, M.; Nelson, J.; Campbell, A. J.; Bradley, D. D. C. *Phys. Rev. B: Condens. Matter* **2006**, *73*, 235201.
(165) Choulis, S. A.; Nelson, J.; Kim, Y.; Poplavskyy, D.; Kreouzis, T.; Durrant, J. R.; Bradley, D. D. C. *Appl. Phys. Lett.* **2003**, *83*, 3812.
(166) Kopidakis, N.; Schiff, E. A.; Park, N.-G.; van de Lagemaat, J.; Frank, A. J. *J. Phys. Chem. B* **2000**, *104*, 3930.
(167) Yuan, Y.; Gregg, B. A.; Lawrence, M. F. *J. Mater. Res.* **2000**, *15*, 2494.
(168) Juška, G.; Genevičius, K.; Arlauskas, K.; Österbacka, R.; Stubb, H. *Phys. Rev. B: Condens. Matter* **2002**, *65*, 233208.
(169) Mozer, A. J.; Saraciftci, N. S.; Lutsen, L.; Vanderzande, D.; Österbacka, R.; Westerling, M.; Juška, G. *Appl. Phys. Lett.* **2005**, *86*, 112104.
(170) Mozer, A. J.; Sariciftci, N. S.; Pivrikas, A.; Österbacka, R.; Juška, G.; Brassat, L.; Bässler, H. *Phys. Rev. B: Condens. Matter* **2005**, *71*, 035214.
(171) Schroder, D. K. *Semiconductor Material and Device Characterization*, 3rd ed.; John Wiley and Sons: Hoboken, 2006.
(172) Ferguson, A. J.; Kopidakis, N.; Shaheen, S. E.; Rumbles, G. *J. Phys. Chem. C* **2008**, *112*, 9865.
(173) Hoofman, R. J. O. M.; de Haas, M. P.; Siebbeles, L. D. A.; Warman, J. M. *Nature* **1998**, *392*, 54.
(174) Ai, X.; Beard, M. C.; Knutsen, K. P.; Shaheen, S. E.; Rumbles, G.; Ellingson, R. J. *J. Phys. Chem. B* **2006**, *110*, 25462.
(175) Beard, M. C.; Turner, G. M.; Schuttenmaer, C. A. *Phys. Rev. B* **2000**, *62*, 15764.
(176) Shirota, Y.; Kageyama, H. *Chem. Rev.* **2007**, *107*, 953.
(177) Bässler, H. *Phys. Status Solidi B* **1993**, *175*, 15.
(178) Arkhipov, V. I.; Heremans, P.; Emilianova, E. V.; Adriaenssens, G. J.; Bässler, H. *Appl. Phys. Lett.* **2003**, *82*, 3245.
(179) Arkhipov, V. I.; Heremans, P.; Emilianova, E. V.; Bässler, H. *Phys. Rev. B* **2005**, *71*, 045214.
(180) Novikov, S. V.; Dunlap, D. H.; Kenkre, V. M.; Parris, P. E.; Vannikov, A. V. *Phys. Rev. Lett.* **1998**, *81*, 4472.
(181) Rakhmanova, S. V.; Conwell, E. M. *Appl. Phys. Lett.* **2000**, *76*, 3822.
(182) Van der Auweraer, M.; De Schryver, F. C.; Borsenberger, P. M.; Bässler, H. *Adv. Mater.* **1994**, *6*, 199.
(183) Novikov, S. V. *Phys. Status Solidi B* **2003**, *236*, 119.
(184) Kenkre, V. M.; Parris, P. E.; Schmidt, D. *Phys. Rev. B: Condens. Matter* **1985**, *32*, 4946.
(185) Kenkre, V. M.; Wong, Y. M. *Phys. Rev. B: Condens. Matter* **1980**, *22*, 5716.
(186) Scully, S. R.; McGehee, M. D. *J. Appl. Phys.* **2006**, *100*, 034907.
(187) Theander, M.; Yartsev, A.; Zigmantas, D.; Sundström, V.; Mammo, W.; Andersson, M. R.; Inganäs, O. *Phys. Rev. B: Condens. Matter* **2000**, *61*, 12957.
(188) Bulović, V.; Burrows, P. E.; Forrest, S. R.; Cronin, J. A.; Thompson, M. E. *Chem. Phys.* **1996**, *210*, 1.
(189) Bulović, V.; Forrest, S. R. *Chem. Phys.* **1996**, *210*, 13.
(190) Lunt, R. R.; Giebink, N. C.; Belak, A. A.; Benziger, J. B.; Forrest, S. R. *J. Appl. Phys.* **2009**, *105*, 053711.
(191) Huijser, A.; Suijkerbuijk, B. M. J. M.; Gebbink, R. J. M. K.; Savenije, T. J.; Siebbeles, L. D. A. *J. Am. Chem. Soc.* **2008**, *130*, 2485.
(192) Haugeneder, A.; Neges, M.; Kallinger, C.; Spirkl, W.; Lemmer, U.; Feldman, J.; Scherf, U.; Harth, E.; Gügel, A.; Müllen, K. *Phys. Rev. B: Condens. Matter* **1999**, *59*, 15346.
(193) Yang, F.; Shtein, M.; Forrest, S. R. *Nat. Mater.* **2004**, *4*, 37.
(194) Lim, S.-H.; Bjorglund, T. G.; Spano, F. C.; Bardeen, C. J. *Phys. Rev. Lett.* **2004**, *92*, 107402.
(195) Markovitsi, D.; Lecuyer, I.; Simon, J. *J. Phys. Chem.* **1991**, *95*, 3620.
(196) Sigal, H.; Markovitsi, D.; Gallos, L. K.; Argyrakis, P. *J. Phys. Chem.* **1996**, *100*, 10999.
(197) *Exciton Dynamics in Molecular Crystals and Aggregates*; Höhler, G., Ed.; Springer: Berlin, 1982.
(198) Nguyen, T. P. *Phys. Status Solidi A* **2008**, *205*, 162.
(199) Ivory, D. M.; Miller, G. G.; Sowa, J. M.; Shacklette, L. W.; Chance, R. R.; Baughman, R. H. J. *J. Chem. Phys.* **1979**, *71*, 1506.
(200) Parthasarathy, G.; Shen, C.; Kahn, A.; Forrest, S. R. *J. Appl. Phys.* **2001**, *89*, 4986.
(201) Kido, J.; Matsumoto, T. *Appl. Phys. Lett.* **1998**, *73*, 2866.
(202) Marks, T. J. *Science* **1985**, *227*, 881.
(203) Anthopoulos, T. D.; Sharai, T. S. *Appl. Phys. Lett.* **2003**, *82*, 1628.
(204) Hiramoto, M.; Ihara, K.; Fukusumi, H.; Yokoyama, M. J. *J. Appl. Phys.* **1995**, *78*, 7153.
(205) Endo, J.; Matsumoto, T.; Kido, J. *Jpn. J. Appl. Phys., Part 2* **2002**, *41*, L358.
(206) Chan, C. K.; Amy, F.; Zhang, Q.; Barlow, S.; Marder, S.; Kahn, A. *Chem. Phys. Lett.* **2006**, *431*, 67.
(207) Pfeiffer, M.; Beyer, A.; Fritz, T.; Leo, K. *Appl. Phys. Lett.* **1998**, *73*, 3202.
(208) Maennig, B.; Pfeiffer, M.; Nollau, A.; Zhou, X.; Leo, K.; Simon, P. *Phys. Rev. B: Condens. Matter* **2001**, *64*, 195208.
(209) Maitrot, M.; Guillaud, G.; Boudjema, B.; Andre, J. J.; Simon, J. J. *J. Appl. Phys.* **1986**, *60*, 2396.
(210) Andre, J. J.; Simon, J.; Even, R.; Boudjema, B.; Guillaud, G.; Maitrot, M. *Synth. Met.* **1987**, *18*, 683.
(211) Pfeiffer, M.; Beyer, A.; Plönnigs, B.; Nollau, A.; Fritz, T.; Leo, K.; Schlettwein, D.; Hiller, S.; Wörhle, D. *Sol. Energy Mater. Sol. Cells* **2000**, *63*, 83.
(212) Werner, A. G.; Li, F.; Harada, K.; Pfeiffer, M.; Fritz, T.; Leo, K. *Appl. Phys. Lett.* **2003**, *82*, 4495.
(213) Chan, C. K.; Zhao, W.; Kanh, A.; Hill, I. G. *Appl. Phys. Lett.* **2009**, *94*, 203306.
(214) Gao, W.; Kahn, A. *Appl. Phys. Lett.* **2001**, *79*, 4040.
(215) Harada, K.; Werner, A. G.; Pfeiffer, M.; Bloom, C. J.; Elliott, C. M.; Leo, K. *Phys. Rev. Lett.* **2005**, *94*, 036601.
(216) Chen, S.-G.; Branz, H. M.; Eaton, S. S.; Taylor, P. C.; Cormier, R. A.; Gregg, B. A. *J. Phys. Chem. B* **2004**, *108*, 17329.
(217) Gregg, B. A.; Chen, S.-G.; Branz, H. M. *Appl. Phys. Lett.* **2004**, *84*, 1707.
(218) Dicker, G.; de Haas, M. P.; Warman, J. M.; de Leeuw, D. M.; Siebbeles, L. D. A. *J. Phys. Chem. B* **2004**, *108*, 17818.
(219) Wang, D.; Reese, M. O.; Kopidakis, N.; Gregg, B. A. *Proc. 33rd IEEE Photovoltaics Specialist Conference*, 2008.
(220) Green, M. A.; Emery, K.; Hishikawa, Y.; Warta, W. *Prog. Photovoltaics: Res. Appl.* **2009**, *17*, 85.
(221) Shrotriya, V.; Li, G.; Yao, Y.; Moriarty, T.; Emery, K.; Yang, Y. *Adv. Funct. Mater.* **2006**, *16*, 2016.
(222) Heliatek. Retrieved on December 14, 2009 from http://www.heliatek.com/en/page/index.php and http://www.heliatek.com/en/page/upload/Heliatek_press_release_2009_08_31.pdf.
(223) Xue, J.; Uchida, S.; Rand, B. P.; Forrest, S. R. *Appl. Phys. Lett.* **2004**, *84*, 3013.
(224) Taylor, F. W. *Elementary Climate Physics*; Oxford University Press: New York, 2005.

(225) National Renewable Energy Laboratory. Retrieved on July 31, 2009 from http://rredc.nrel.gov/solar/spectra/am1.5.
(226) Case, M. A.; Owusu, Y. A.; Chapman, H.; Dargan, T.; Ruscher, P. *Renewable Energy* **2008**, *33*, 2645.
(227) Myers, D. R.; Emery, K.; Gueymard, C. *J. Sol. Energy Eng.* **2004**, *126*, 567.
(228) Sommeling, P. M.; Rieffe, H. C.; Roosmalen, J. A. M. v.; Schonecker, A.; Kroon, J. M.; Wienke, J.; Hinsch, A. *Sol. Energy Mater. Sol. Cells* **2000**, *62*, 399.
(229) Ito, S.; Matsui, H.; Okada, K.; Kusano, S.; Kitamura, T.; Wada, Y.; Yanagida, S. *Sol. Energy Mater. Sol. Cells* **2004**, *82*, 421.
(230) Currie, M. J.; Mapel, J. K.; Heidel, T. D.; Goffri, S.; Baldo, M. A. *Science* **2008**, *321*, 226.
(231) Park, S. H.; Roy, A.; Beaupré, S.; Cho, S.; Coates, N.; Moon, J. S.; Moses, D.; Leclerc, M.; Lee, K.; Heeger, A. J. *Nat. Photon.* **2009**, *3*, 297.
(232) Luque, A.; Hegedus, S. *Handbook of Photovoltaic Science and Engineering*; John Wiley & sons Ltd.: chichester, U.K., 2003.
(233) Signerski, R. *J. Non-Cryst. Solids* **2008**, *354*, 4465.
(234) Ooi, Z. E.; Tam, T. L.; Sellinger, A.; deMello, J. C. *Energy Environ. Sci.* **2008**, *1*, 300.
(235) Cheyns, D.; Gommans, H.; Odijk, M.; Poortmans, J.; Heremans, P. *Sol. Energy Mater. Sol. Cells* **2007**, *91*, 399.
(236) Nanditha, D. M.; Dissanayake, M.; Hatton, R. A.; Curry, R. J.; Silva, S. R. P. *Appl. Phys. Lett.* **2007**, *90*, 113505.
(237) Nelson, J.; Kirkpatrick, J.; Ravirajan, P. *Phys. Rev. B: Condens. Matter* **2004**, *69*, 035337.
(238) Hains, A. W.; Liu, J.; Martinson, A. B. F.; Irwin, M. D.; Marks, T. J. *Adv. Funct. Mater.* **2010**, *20*, 595.
(239) Glatthaar, M.; Riede, M.; Keegan, N.; Sylvester-Hvid, K.; Zimmermann, B.; Niggemann, M.; Hinsch, A.; Gombert, A. *Sol. Energy Mater. Sol. Cells* **2007**, *91*, 390.
(240) *Clean Electricity from Photovoltaics*; Archer, M. D., Hill, R., Eds.; Imperial College Press: London, 2001.
(241) Brabec, C. J.; Sariciftci, N. S.; Hummelen, J. C. *Adv. Funct. Mater.* **2001**, *11*, 15.
(242) Ding, J. M.; de la Fuente Vornbrock, A.; Ting, C.; Subramanian, V. *Sol. Energy Mater. Sol. Cells* **2009**, *93*, 459.
(243) Huang, J.; Wang, X.; Kim, Y.; deMello, A. J.; Bradley, D. D. C.; deMello, J. C. *Phys. Chem. Chem. Phys.* **2006**, *8*, 3904.
(244) Pandey, A. K.; Nunzi, J.-M. *Appl. Phys. Lett.* **2006**, *89*, 213506.
(245) Kushto, G. P.; Kim, W.; Kafafi, Z. H. *Appl. Phys. Lett.* **2005**, *86*, 093502.
(246) Pagliaro, M.; Ciriminna, R.; Palmisano, G. *Chem. Sus. Chem.* **2008**, *1*, 880.
(247) Danziger, J.; Dodelet, J.-P.; Lee, P.; Nebesny, K. W.; Armstrong, N. R. *Chem. Mater.* **1991**, *3*, 821.
(248) Danziger, J.; Dodelet, J.-P.; Armstrong, N. R. *Chem. Mater.* **1991**, *3*, 812.
(249) Gu, G.; Burrows, P. E.; Venkatesh, S.; Forrest, S. R. *Opt. Lett.* **1997**, *22*, 172.
(250) Al-Ibrahim, M.; Roth, H. K.; Sensfuss, S. *Appl. Phys. Lett.* **2004**, *85*, 1481.
(251) Weaver, M. S.; Michalski, L. A.; Rajan, K.; Silvernail, M. A.; Brown, J. J. *Appl. Phys. Lett.* **2002**, *81*, 2929.
(252) Antony, A.; Nisha, M.; Manoj, R.; Jayaraj, M. K. *Appl. Surf. Sci.* **2004**, *225*, 294.
(253) Han, H.; Mayer, J. W.; Alford, T. L. *J. Appl. Phys.* **2006**, *100*, 083715.
(254) Hamberg, I.; Granqvist, C. G.; Berggren, K.-F.; Sernelius, B. E.; Engström, L. *Phys. Rev. B* **1984**, *30*, 3240.
(255) Yang, Y.; Huang, Q.; Metz, A. W.; Ni, J.; Jin, S.; Marks, T. J.; Madsen, M. E.; DiVenere, A.; Ho, S.-T. *Adv. Mater.* **2004**, *16*, 321.
(256) Chen, C.-P.; Tien, T.-C.; Ko, B.-T.; Chen, Y.-D.; Ting, C. *ACS Appl. Mater. Interfaces* **2009**, *1*, 741.
(257) Rider, D. A.; Harris, K. D.; Wang, D.; Bruce, J.; Fleischauer, M. D.; Tucker, R. T.; Brett, M. J.; Buriak, J. M. *ACS Appl. Mater. Interfaces* **2009**, *1*, 279.
(258) Brumbach, M.; Veneman, P. A.; Marrikar, F. S.; Schulmeyer, T.; Simmonds, A.; Xia, W.; Lee, P.; Armstrong, N. R. *Langmuir* **2007**, *23*, 11089.
(259) Xue, J.; Forrest, S. R. *J. Appl. Phys.* **2004**, *95*, 1869.
(260) Kim, J. S.; Granström, M.; Friend, R. H.; Daik, R.; Feast, W. J.; Cacialli, F. *J. Appl. Phys.* **1998**, *84*, 6859.
(261) Christou, V.; Etchells, M.; Renault, O.; Dobson, P. J.; Salata, O. V.; Beamson, G.; Egdell, R. G. *J. Appl. Phys.* **2000**, *88*, 5180.
(262) Ko, C.-J.; Lin, Y.-K.; Chen, F.-C.; Chu, C.-W. *Appl. Phys. Lett.* **2007**, *90*, 063509.
(263) Roy, B.; Perkins, J. D.; Kaydanova, T.; Young, D. L.; Taylor, M.; Miedaner, A.; Curtis, C.; Kleebe, H.-J.; Readey, D. W.; Ginley, D. S. *Thin Solid Films* **2008**, *516*, 4093.
(264) Sheng, S.; Fang, G.; Li, C.; Xu, S.; Zhao, X. *Phys. Status Solidi A* **2006**, *203*, 1891.
(265) Banerjee, A. N.; Chattopadhyay, K. K. *Prog. Cryst. Growth Charact. Mater.* **2005**, *50*, 52.
(266) Teplin, C. W.; Kaydanova, T.; Young, D. L.; Perkins, J. D.; Ginley, D. S.; Ode, A.; Ready, D. W. *Appl. Phys. Lett.* **2004**, *85*, 3789.
(267) Ginley, D.; Roy, B.; Ode, A.; Warmsingh, C.; Yoshida, Y.; Parilla, P.; Teplin, C.; Kaydanova, T.; Miedaner, A.; Curtis, C.; Martinson, A.; Coutts, T.; Readey, D.; Hosono, H.; Perkins, J. *Thin Solid Films* **2003**, *445*, 193.
(268) Kawazoe, H.; Yasukawa, M.; Hyodo, H.; Kurita, M.; Yanagi, H.; Hosono, H. *Nature* **1997**, *389*, 939.
(269) Sato, H.; Minami, T.; Takata, S.; Yamada, T. *Thin Solid Films* **1993**, *236*, 27.
(270) Salazar, K. Mineral Commodity Summary; U.S. Department of the Interior-U.S. Geologic Survey; U.S. Government Printing Office, 2009.
(271) Green, M. A. *Prog. Photovoltaics: Res. Appl.* **2009**, *17*, 347.
(272) Kim, H.; Kushto, G. P.; Auyeung, R. C. Y.; Piqué, A. *Appl. Phys. A: Mater. Sci. Process.* **2008**, *93*, 521.
(273) Yang, F.; Forrest, S. R. *Adv. Mater.* **2006**, *18*, 2018.
(274) Bernède, J. C.; Cattin, L.; Morsli, M.; Berredjem, Y. *Sol. Energy Mater. Sol. Cells* **2008**, *92*, 1508.
(275) Bernède, J. C.; Berredjem, Y.; Cattin, L.; Morsli, M. *Appl. Phys. Lett.* **2008**, *92*, 083304.
(276) Kim, J.-S.; Cacialli, F.; Friend, R. *Thin Solid Films* **2003**, *445*, 358.
(277) Liu, J.; Hains, A. W.; Wang, L.; Marks, T. J. *Thin Solid Films*, in press.
(278) Liu, J.; Hains, A. W.; Servaites, J. D.; Ratner, M. A.; Marks, T. J. *Chem. Mater.* **2009**, *21*, 5258.
(279) Tenent, R. C.; Barnes, T. M.; Bergeson, J. D.; Ferguson, A. J.; To, B.; Gedvilas, L. M.; Heben, M. J.; Blackburn, J. L. *Adv. Mater.* **2009**, *21*, 1.
(280) Tanaka, S.; Mielczarek, K.; Ovalle-Robles, R.; Wang, B.; Hsu, D.; Zakhidov, A. A. *Appl. Phys. Lett.* **2009**, *94*, 113506.
(281) Rowell, M. W.; Topinka, M. A.; McGehee, M. D.; Prall, H.-J.; Dennler, G.; Sariciftci, N. S.; Hu, L.; Gruner, G. *Appl. Phys. Lett.* **2006**, *88*, 233506.
(282) Greczynski, G.; Kugler, T.; Keil, M.; Osikowicz, W.; Fahlman, M.; Salaneck, W. R. *J. Electron Spectrosc. Relat. Phenom.* **2001**, *121*, 1.
(283) Groenendaal, L.; Jonas, F.; Freitag, D.; Pielartzik, H.; Reynolds, J. R. *Adv. Mater.* **2000**, *12*, 481.
(284) Heywang, G.; Jonas, F. *Adv. Mater.* **1992**, *4*, 116.
(285) Snaith, H. J.; Kenrick, H.; Chiesa, M.; Friend, R. H. *Polymer* **2005**, *46*, 2573.
(286) Zhang, F.; Johansson, M.; Andersson, M. R.; Hummelen, J. C.; Inganäs, O. *Adv. Mater.* **2002**, *14*, 662.
(287) Fukuzumi, S.; Kojima, T. *J. Mater. Chem.* **2008**, *18*, 1427.
(288) Umeyama, T.; Takamatsu, T.; Tezuka, N.; Matano, Y.; Araki, Y.; Wada, T.; Yoshikawa, O.; Sagawa, T.; Yoshikawa, S.; Imahori, H. *J. Phys. Chem. C* **2009**, *113*, 10798.
(289) Kadish, K. M.; Caemelbecke, E. V.; Royal, G. In *The Porphyrin Handbook*, 1st ed.; Kadish, K. M., Smith, K. M., Guilard, R., Eds.; Academic Press: New York City, NY, 1999; Vol. 8.
(290) Huijser, A.; Savenije, T. J.; Shalav, A.; Siebbeles, L. D. A. *J. Appl. Phys.* **2008**, *104*, 034505.
(291) Martinson, A. B. F.; Massari, A. M.; Lee, S. J.; Gurney, R. W.; Splan, K. E.; Hupp, J. T.; Nguyen, S. T. *J. Electrochem. Soc.* **2006**, *153*, A527.
(292) Hasobe, T.; Imahori, H.; Kamat, P. V.; Fukuzumi, S. *J. Am. Chem. Soc.* **2003**, *125*, 14962.
(293) Takahashi, K.; Goda, T.; Yamaguchi, T.; Komura, T.; Murata, K. *J. Phys. Chem. B* **1999**, *103*, 4868.
(294) Kerp, H. R.; Donker, H.; Koehorst, R. B. M.; Schaafsma, T. J.; van Faassen, E. E. *Chem. Phys. Lett.* **1998**, *298*, 302.
(295) Savenije, T. J.; Moons, E.; Boschloo, G. K.; Goossens, A.; Schaafsma, T. J. *Phys. Rev. B* **1997**, *55*, 9685.
(296) Marée, C. H. M.; Roosendaal, S. J.; Savenije, T. J.; Schropp, R. E. I.; Schaafsma, T. J.; Habraken, F. H. P. M. *J. Appl. Phys.* **1996**, *80*, 3381.
(297) Lawrence, M. F.; Huang, Z.; Langford, C. H.; Ordonez, I. *J. Phys. Chem.* **1993**, *97*, 944.
(298) Günster, S.; Siebentritt, S.; Elbe, J.; Kreienhoop, L.; Tennigkeit, B.; Wöhrle, D.; Memming, R.; Meissner, D. *Mol. Cryst. Liq. Cryst.* **1992**, *218*, 117.
(299) Imahori, H.; Fukuzumi, S. *Adv. Funct. Mater.* **2004**, *14*, 525.
(300) Burke, K. B.; Belcher, W. J.; Thomsen, L.; Watts, B.; McNeill, C. R.; Ade, H.; Dastoor, P. C. *Macromolecules* **2009**, *42*, 3098.
(301) Belcher, W. J.; Wagner, K. I.; Dastoor, P. C. *Sol. Energy Mater. Sol. Cells* **2007**, *91*, 447.
(302) Dastoor, P. C.; McNeill, C. R.; Frohne, H.; Foster, C. J.; Dean, B.; Fell, C. J.; Belcher, W. J.; Campbell, W. M.; Officer, D. L.; Blake, I. M.; Thordarson, P.; Crossley, M. J.; Hush, N. S.; Reimers, J. R. *J. Phys. Chem. C* **2007**, *111*, 15415.

(303) Li, G.; Shrotriya, V.; Huang, J.; Yao, Y.; Moriarty, T.; Emery, K.; Yang, Y. *Nat. Mater.* **2005**, *4*, 864.
(304) Ma, W.; Yang, C.; Gong, X.; Kwanghee, L.; Heeger, A. *Adv. Funct. Mater.* **2005**, *15*, 1617.
(305) Kim, Y.; Cook, S.; Tuladhar, S. M.; Choulis, S. A.; Nelson, J.; Durrant, J. R.; Bradley, D. D. C.; Giles, M.; McCulloch, I.; Ha, C.-K.; Ree, M. *Nat. Mater.* **2006**, *5*, 197.
(306) Irwin, M. D.; Buchholz, D. B.; Hains, A. W.; Chang, R. P. H.; Marks, T. J. *Proc. Natl. Acad. Sci. U.S.A.* **2008**, *105*, 2783.
(307) Vilmercati, P.; Castellarin-Cudia, C.; Gebauer, R.; Ghosh, P.; Lizzit, S.; Petaccia, L.; Cepek, C.; Larciprete, R.; Verdini, A.; Floreano, L.; Morgante, A.; Goldoni, A. *J. Am. Chem. Soc.* **2009**, *131*, 644.
(308) Nierengarten, J.-F.; Eckert, J.-F.; Felder, D.; Nicoud, J.-F.; Armaroli, N.; Marconi, G.; Vicinelli, V.; Boudon, C.; Gisselbrecht, J.-P.; Gross, M.; Hadziioannou, G.; Krasnikov, V.; Ouali, L.; Echegoyen, L.; Liu, S.-G. *Carbon* **2000**, *38*, 1587.
(309) Liddell, P. A.; Sumida, J. P.; Macpherson, A. N.; Noss, L.; Seely, G. R.; Clark, K. N.; Moore, A. L.; Moore, T. A.; Gust, D. *Photochem. Photobiol.* **1994**, *60*, 537.
(310) Yamada, H.; Imahori, H.; Nishimura, Y.; Yamazaki, I.; Fukuzumi, S. *Adv. Mater.* **2002**, *14*, 892.
(311) Yamada, H.; Imahori, H.; Nishimura, Y.; Yamazaki, I.; Ahn, T. K.; Kim, S. K.; Kim, D.; Fukuzumi, S. *J. Am. Chem. Soc.* **2003**, *125*, 9129.
(312) Xu, Z.-X.; Xiang, H.-F.; Roy, V. A. L.; Chui, S. S.-Y.; Che, C.-M.; Lai, P. T. *Appl. Phys. Lett.* **2008**, *93*, 223305.
(313) Grozema, F. C.; Houarner-Rassin, C.; Prins, P.; Siebbeles, L. D. A.; Anderson, H. L. *J. Am. Chem. Soc.* **2007**, *129*, 13370.
(314) Shea, P. B.; Kanicki, J.; Ono, N. *J. Appl. Phys.* **2005**, *98*, 014503.
(315) Checcoli, P.; Conte, G.; Salvatori, S.; Paolesse, R.; Bolognesi, A.; Berliocchi, M.; Brunetti, F.; D'Amico, A.; Carlo, A. D.; Lugli, P. *Synth. Met.* **2003**, *138*, 261.
(316) Harima, Y.; Furusho, S.; Okazaki, K.; Kunugi, Y.; Yamashita, K. *Thin Solid Films* **1997**, *300*, 213.
(317) Savenije, T. J.; Koehorst, R. B. M.; Schaafsma, T. J. *J. Phys. Chem. B* **1997**, *101*, 720.
(318) Harima, Y.; Furusho, S.; Kunugi, Y.; Yamashita, K. *Chem. Phys. Lett.* **1996**, *258*, 213.
(319) Kocherzhenko, A. A.; Patwardhan, S.; Grozema, F. C.; Anderson, H. L.; Siebbeles, L. D. A. *J. Am. Chem. Soc.* **2009**, *131*, 5522.
(320) *The Porphyrin Handbook*; Kadish, K. M., Smith, K. M., Guilard, R., Eds.; Academic Press: San Diego, CA, 2003; Vols. *11*−*20*.
(321) Senge, M. O.; Fazekas, M.; Notaras, E. G. A.; Blau, W. J.; Zawadzka, M.; Locos, O. B.; Mhuircheartaigh, E. M. N. *Adv. Mater.* **2007**, *19*, 2737.
(322) Bayiyr, Z.; Merey, S.; Hamuryudan, E. *Monatsh. Chem.* **2003**, *134*, 1027.
(323) Vivo, P.; Ojala, M.; Chukharev, V.; Efimov, A.; Lemmetyinen, H. *J. Photochem. Photobiol., A* **2009**, *203*, 125.
(324) Stübinger, T.; Brütting, W. *J. Appl. Phys.* **2001**, *90*, 3632.
(325) Banerjee, S.; Parhi, A. P.; Iyer, S. S. K.; Kumar, S. *Appl. Phys. Lett.* **2009**, *94*, 223303.
(326) Yang, L.-G.; Chen, H.-Z.; Wang, M. *Thin Solid Films* **2008**, *516*, 7701.
(327) Kurrle, D.; Pflaum, J. *Appl. Phys. Lett.* **2008**, *92*, 133306.
(328) Terao, Y.; Sasabe, H.; Adachi, C. *Appl. Phys. Lett.* **2007**, *90*, 103515.
(329) Osasa, T.; Matsui, Y.; Matsumura, T.; Matsumura, M. *Sol. Energy Mater. Sol. Cells* **2006**, *90*, 3136.
(330) Salzman, R. F.; Xue, J.; Rand, B. P.; Alexander, A.; Thompson, M. E.; Forrest, S. R. *Org. Electron.* **2005**, *6*, 242.
(331) Gould, R. D. *Thin Solid Films* **1985**, *125*, 63.
(332) Kitamura, M.; Imada, T.; Kako, S.; Arakawa, Y. *Jpn. J. Appl. Phys., Part 1* **2004**, *43*, 2326.
(333) Xiao, K.; Liu, Y. Q.; Yu, G.; Zhu, D. B. *Synth. Met.* **2003**, *137*, 991.
(334) Kudo, K.; Sumimoto, T.; Hiraga, K.; Kuniyoshi, S.; Tanaka, K. *Jpn. J. Appl. Phys., Part 1* **1997**, *36*, 6994.
(335) Gould, R. D. *J. Phys. D: Appl. Phys.* **1986**, *19*, 1785.
(336) Lozzi, L.; Santucci, S.; Rosa, S. L.; Picozzi, S. *J. Chem. Phys.* **2004**, *121*, 1883.
(337) Heutz, S.; Jones, T. S. *J. Appl. Phys.* **2002**, *92*, 3039.
(338) Tang, C. W. *Appl. Phys. Lett.* **1986**, *48*, 183.
(339) Panayotatos, P.; Bird, G.; Sauers, R.; Piechowski, A.; Husain, S. *Sol. Cells* **1987**, *21*, 301.
(340) Forrest, S. R.; Leu, L. Y.; So, F. F.; Yoon, W. Y. *J. Appl. Phys.* **1989**, *66*, 5908.
(341) Wöhrle, D.; Meissner, D. *Adv. Mater.* **1990**, *3*, 129.
(342) Arbour, C.; Armstrong, N. R.; Brina, R.; Collins, G.; Danziger, J.; Dodelet, J.-P.; Lee, P.; Nebesny, K. W.; Pankow, J.; Waite, S. *Mol. Cryst. Liq. Cryst.* **1990**, *183*, 307.
(343) Hiramoto, M.; Fujiwara, H.; Yokoyama, M. *Appl. Phys. Lett.* **1991**, *58*, 1062.
(344) Hiramoto, M.; Fujiwara, H.; Yokoyama, M. *J. Appl. Phys.* **1992**, *72*, 3781.
(345) Schlettwein, D.; Wöhrle, D.; Karmann, E.; Melville, U. *Chem. Mater.* **1994**, *6*, 3.
(346) Schmidt, A.; Chau, L.-K.; Valencia, V. S.; Armstrong, N. R. *Chem. Mater.* **1995**, *7*, 657.
(347) Kudo, T.; Kimura, M.; Hanabusa, K.; Shirai, H. *J. Porphyrins Phthalocyanines* **1998**, *2*, 231.
(348) Rudiono; Kaneko, F.; Takeuchi, M. *Appl. Surf. Sci.* **1999**, *142*, 598.
(349) Kudo, T.; Kimura, M.; Hanabusa, K.; Shirai, H. *J. Porphyrins Phthalocyanines* **1999**, *3*, 310.
(350) Petritsch, K.; Friend, R. H.; Lux, A.; Rozenberg, G.; Moratti, S. C.; Holmes, A. B. *Synth. Met.* **1999**, *102*, 1776.
(351) Xue, J.; Forrest, S. R. *J. Appl. Phys.* **2004**, *95*, 1859.
(352) Peumans, P.; Uchida, S.; Forrest, S. R. *Nature* **2003**, *425*, 158.
(353) Peumans, P.; Bulović, V.; Forrest, S. R. *Appl. Phys. Lett.* **2000**, *76*, 2650.
(354) Peumans, P.; Bulović, V.; Forrest, S. R. *Appl. Phys. Lett.* **2000**, *76*, 3855.
(355) Rim, S.-B.; Zhao, S.; Scully, S. R.; McGehee, M. D. *Appl. Phys. Lett.* **2008**, *91*, 243501.
(356) Bailey-Salzman, R. F.; Rand, B. P.; Forrest, S. R. *Appl. Phys. Lett.* **2006**, *88*, 223502.
(357) Peumans, P.; Forrest, S. R. *Appl. Phys. Lett.* **2001**, *79*, 126.
(358) Xue, J.; Rand, B. P.; Uchida, S.; Forrest, S. R. *Adv. Mater.* **2005**, *17*, 66.
(359) Xue, J.; Uchida, S.; Rand, B. P.; Forrest, S. R. *Appl. Phys. Lett.* **2004**, *85*, 5757.
(360) Peumans, P.; Forrest, S. R. *Appl. Phys. Lett.* **2002**, *80*, 338.
(361) Dai, J.; Jiang, X.; Wang, H.; Yan, D. *Appl. Phys. Lett.* **2007**, *91*, 253503.
(362) Li, N.; Lassiter, B. E.; Lunt, R. R.; Wei, G.; Forrest, S. R. *Appl. Phys. Lett.* **2009**, *94*, 023307.
(363) Yang, F.; Lunt, R. R.; Forrest, S. R. *Appl. Phys. Lett.* **2008**, *92*, 053310.
(364) Inoue, J.; Yamagishi, K.; Yamashita, M. *J. Cryst. Growth* **2007**, *298*, 782.
(365) Rand, B. P.; Xue, J.; Yang, F.; Forrest, S. R. *Appl. Phys. Lett.* **2005**, *87*, 233508.
(366) Iyechika, Y.; Yakushi, K.; Ikemoto, I.; Kuroda, H. *Acta Crystallogr., Sect. B* **1982**, *B38*, 766.
(367) Ukei, K. *Acta Crystallogr., Sect. B* **1973**, *B29*, 2290.
(368) Friedel, M. K.; Hoskins, B. F.; Martin, R. L.; Mason, S. A. *J. Chem. Soc. D* **1970**, 400.
(369) Kubiak, R.; Janczak, J. *J. Alloys Compd.* **1992**, *189*, 107.
(370) Papageorgiou, N.; Salomon, E.; Angot, T.; Layet, J.-M.; Giovanelli, L.; Lay, G. L. *Prog. Surf. Sci.* **2004**, *77*, 139.
(371) West, A. R. *Basic Solid State Chemistry*; John Wiley & Sons Ltd.: New York, 1984.
(372) Bailey-Salzman, R. F.; Rand, B. P.; Forrest, S. R. *Appl. Phys. Lett.* **2007**, *91*, 013508.
(373) Klofta, T. J.; Sims, T. D.; Pankow, J. W.; Danziger, J.; Nebesny, K. W.; Armstrong, N. R. *J. Phys. Chem.* **1987**, *91*, 5651.
(374) Wynne, K. J. *Inorg. Chem.* **1984**, *23*, 4658.
(375) Ng, T. W.; Lo, M. F.; Zhou, Y. C.; Liu, Z. T.; Lee, C. S.; Kwon, O.; Lee, S. T. *Appl. Phys. Lett.* **2009**, *94*, 199304.
(376) Song, Q. L.; Wang, M. L.; Obbard, E. G.; Sun, X. Y.; Ding, X. M.; Hou, X. Y. *Appl. Phys. Lett.* **2006**, *89*, 251118.
(377) Wu, H. R.; Song, Q. L.; Wang, M. L.; Li, F. Y.; Yang, H.; Wu, Y.; Huang, C. H.; Ding, X. M.; Hou, X. Y. *Thin Solid Films* **2007**, *515*, 8050.
(378) Tanaka, Y.; Kanai, K.; Ouchi, Y.; Seki, K. *Chem. Phys. Lett.* **2007**, *441*, 63.
(379) Rusu, M.; Strotmann, J.; Vogel, M.; Lux-Steiner, M. C.; Fostiropoulos, K. *Appl. Phys. Lett.* **2007**, *90*, 153511.
(380) Mutolo, K. L.; Mayo, E. I.; Rand, B. P.; Forrest, S. R.; Thompson, M. E. *J. Am. Chem. Soc.* **2006**, *128*, 8108.
(381) Gommans, H.; Cheyns, D.; Aernouts, T.; Girotto, C.; Poortmans, J.; Heremans, P. *Adv. Funct. Mater.* **2007**, *17*, 2653.
(382) Verreet, B.; Schols, S.; Cheyns, D.; Rand, B. P.; Gommans, H.; Aernouts, T.; Heremans, P.; Genoe, J. *J. Mater. Chem.* **2009**, *19*, 5295.
(383) Mattheus, C. C.; Michaelis, W.; Kelting, C.; Durfee, W. S.; Wöhrle, D.; Schlettwein, D. *Synth. Met.* **2004**, *146*, 335.
(384) Claessens, C. G.; González-Rodríguez, D.; Torres, T. *Chem. Rev.* **2002**, *102*, 835.
(385) Ma, B.; Woo, C. H.; Miyamoto, Y.; Fréchet, J. M. J. *Chem. Mater.* **2009**, *21*, 1413.
(386) Martín, G.; Rojo, G.; Agulló-López, F.; Ferro, V. R.; García de la Vega, J. M.; Martínez-Díaz, M. V.; Torres, T.; Ledoux, I.; Zyss, J. *J. Phys. Chem. B* **2002**, *106*, 13139.
(387) Lloyd, M. T.; Anthony, J. E.; Malliaras, G. C. *Mater. Today* **2007**, *10*, 34.
(388) Pochettino, A. *Acad. Lincei Rend.* **1906**, *15*, 355.

(389) Chu, C.-W.; Shao, Y.; Shrotriya, V.; Yang, Y. *Appl. Phys. Lett.* **2005**, *86*, 243506.
(390) Pandey, A. K.; Shaw, P. E.; Samuel, I. D. W.; Nunzi, J.-M. *Appl. Phys. Lett.* **2009**, *94*, 103303.
(391) Kinoshita, Y.; Hasobe, T.; Murata, H. *Appl. Phys. Lett.* **2007**, *91*, 083518.
(392) Lloyd, M. T.; Mayer, A. C.; Tayi, A. S.; Bowen, A. M.; Kasen, T. G.; Herman, D. J.; Mourey, D. A.; Anthony, J. E.; Malliaras, G. G. *Org. Electron.* **2006**, *7*, 243.
(393) Mayer, A. C.; Lloyd, M. T.; Herman, D. J.; Kasen, T. G.; Malliaras, G. G. *Appl. Phys. Lett.* **2004**, *85*, 6272.
(394) Sarangerel, K.; Ganzorig, C.; Fujihira, M.; Sakomura, M.; Ueda, K. *Chem. Lett.* **2008**, *37*, 778.
(395) Pandey, A. K.; Nunzi, J.-M. *Adv. Mater.* **2007**, *19*, 3613.
(396) Taima, T.; Sakai, J.; Yamanari, T.; Saito, K. *Sol. Energy Mater. Sol. Cells* **2009**, *93*, 742.
(397) Chan, M. Y.; Lai, S. L.; Fung, M. K.; Lee, C. S.; Lee, S. T. *Appl. Phys. Lett.* **2007**, *90*, 023504.
(398) Chen, W.-B.; Xiang, H.-F.; Xu, Z.-X.; Yan, B.-P.; Roy, V. A. L.; Che, C.-M.; Lai, P.-T. *Appl. Phys. Lett.* **2007**, *91*, 191109.
(399) Wang, S.; Mayo, E. I.; Perez, M. D.; Griffe, L.; Wei, G.; Djurovich, P. I.; Forrest, S. R.; Thompson, M. E. *Appl. Phys. Lett.* **2009**, *94*, 233304.
(400) Silvestri, F.; Irwin, M. D.; Beverina, L.; Facchetti, A.; Pagani, G. A.; Marks, T. J. *J. Am. Chem. Soc.* **2008**, *130*, 17640.
(401) Piechowski, A. P.; Bird, G. R.; Morel, D. L.; Stogryn, E. L. *J. Phys. Chem.* **1984**, *88*, 934.
(402) Merritt, V. Y.; Hovel, H. J. *Appl. Phys. Lett.* **1976**, *29*, 414.
(403) Law, K.-Y. *J. Phys. Chem.* **1987**, *91*, 5184.
(404) Katz, H. E.; Johnson, J.; Lovinger, A. J.; Li, W. *J. Am. Chem. Soc.* **2000**, *122*, 7787.
(405) Struijk, C. W.; Sieval, A. B.; Dakhorst, J. E. J.; van Dijk, M.; Kimkes, P.; Koehorst, R. B. M.; Donker, H.; Schaafsma, T. J.; Picken, S. J.; van de Craats, A. M.; Warman, J. M.; Zuilhof, H.; Sudhölter, E. J. R. *J. Am. Chem. Soc.* **2000**, *122*, 11057.
(406) Chamberlain, G. A. *Sol. Cells* **1983**, *8*, 47.
(407) *Fullerenes: Principles and Applications*; Langa, F., Nierengarten, J.-F., Eds.; Royal Society of Chemistry: Cambridge, 2007.
(408) Krätschmer, W.; Lamb, L. D.; Fostiropoulos, K.; Huffman, D. R. *Nature* **1990**, *347*, 354.
(409) Kroto, H. W.; Heath, J. R.; O'Brien, S. C.; Curl, R. F.; Smalley, R. E. *Nature* **1985**, *318*, 162.
(410) Bonifazi, D.; Enger, O.; Diederich, F. *Chem. Soc. Rev.* **2007**, *36*, 390.
(411) Giacalone, F.; Martín, N. *Chem. Rev.* **2006**, *106*, 5136.
(412) Raghavachari, K.; Rohlfing, C. M. *J. Phys. Chem.* **1992**, *96*, 2463.
(413) Haddock, J. N.; Zhang, X.; Domercq, B.; Kippelen, B. *Org. Electron.* **2005**, *6*, 182.
(414) Carano, M.; Ros, T. D.; Fanti, M.; Kordatos, K.; Marcaccio, M.; Paolucci, F.; Prato, M.; Roffia, S.; Zerbetto, F. *J. Am. Chem. Soc.* **2003**, *125*, 7139.
(415) *Fullerenes: Chemistry, Physics, and Technology*; Kadish, K. M., Ruoff, R. S., Eds.; Wiley-IEEE: New York, 2000.
(416) Koeppe, R.; Sariciftci, N. S.; Troshin, P. A.; Lyubovskaya, R. N. *Appl. Phys. Lett.* **2005**, *87*, 244102.
(417) Wienk, M. M.; Kroon, J. M.; Verhees, W. J. H.; Knol, J.; Hummelen, J. C.; van Hal, P. A.; Janssen, R. A. J. *Angew. Chem., Int. Ed.* **2003**, *42*, 3371.
(418) Arbogast, J. W.; Foote, C. S. *J. Am. Chem. Soc.* **1991**, *113*, 8886.
(419) Pfuetzner, S.; Meiss, J.; Petrich, A.; Riede, M.; Leo, K. *Appl. Phys. Lett.* **2009**, *94*, 223307.
(420) Dresselhaus, M. S.; Dresselhaus, G.; Eklund, P. C. *Science of Fullerenes and Carbon Nanotubes*; Academic Press: San Diego, CA, 1996.
(421) Silvestri, F.; López-Duarte, I.; Seitz, W.; Beverina, L.; Martínez-Díaz, M. V.; Marks, T. J.; Guldi, D. M.; Pagani, G. A.; Torres, T. *Chem. Commun.* **2009**, 4500.
(422) Bauer, P.; Wietasch, H.; Lindner, S. M.; Thelakkat, M. *Chem. Mater.* **2007**, *19*, 88.
(423) Guldi, D. M.; Rahman, G. M. A.; Prato, M.; Jux, N.; Qin, S.; Ford, W. *Angew. Chem., Int. Ed.* **2005**, *44*, 2015.
(424) Guldi, D. M.; Rahman, G. N. A.; Ramey, J.; Marcaccio, M.; Paolucci, D.; Paolucci, F.; Qin, S.; Ford, W. T.; Balbinot, D.; Jux, N.; Tagmatarchisf, N.; Prato, M. *Chem. Commun.* **2004**, 2034.
(425) Li, H.; Martin, R. B.; Harruff, B. A.; Carino, R. A.; Allard, L. F.; Sun, Y.-P. *Adv. Mater.* **2004**, *16*, 896.
(426) Baskaran, D.; Mays, J. W.; Zhang, X. P.; Bratcher, M. S. *J. Am. Chem. Soc.* **2005**, *127*, 6916.
(427) Alvaro, M.; Atienzar, P.; de la Cruz, P.; Delgado, J. L.; Troiani, V.; Garcia, H.; Langa, F.; Palkar, A.; Echegoyen, L. *J. Am. Chem. Soc.* **2006**, *128*, 6626.
(428) Tanaka, H.; Yajima, T.; Matsumoto, T.; Otsuka, Y.; Ogawa, T. *Adv. Mater.* **2006**, *18*, 1411.
(429) Guldi, D. M.; Rahman, G. M. A.; Jux, N.; Tagmatarchis, N.; Prato, M. *Angew. Chem., Int. Ed.* **2004**, *43*, 5526.
(430) Guldi, D. M.; Taieb, H.; Rahman, G. M. A.; Tagmatarchis, N.; Prato, M. *Adv. Mater.* **2005**, *17*, 871.
(431) Ehli, C.; Rahman, G. M. A.; N. Jux, D. B.; Guldi, D. M.; Paolucci, F.; Marcaccio, M.; Paolucci, D.; Melle-Franco, M.; Zerbetto, F.; Campidelli, S.; Prato, M. *J. Am. Chem. Soc.* **2006**, *128*, 11222.
(432) Chen, S.; Liu, Y.; Qiu, W.; Sun, X.; Ma, Y.; Zhu, D. *Chem. Mater.* **2005**, *17*, 2208.
(433) Dittmer, J. J.; Marseglia, E. A.; Friend, R. H. *Adv. Mater.* **2000**, *12*, 1270.
(434) Shin, W. S.; Jeong, H.-H.; Kim, M.-K.; Jin, S.-H.; Kim, M.-R.; Lee, J.-K.; Leec, J. W.; Gal, Y.-S. *J. Mater. Chem.* **2006**, *16*, 384.
(435) Li, J.; Dierschke, F.; Wu, J.; Grimsdale, A. C.; Müllen, K. *J. Mater. Chem.* **2006**, *16*, 96.
(436) Rajaram, S.; Armstrong, P. B.; Kim, B. J.; Fréchet, J. M. J. *Chem. Mater.* **2009**, *21*, 1775.
(437) Keivanidis, P. E.; Howard, I. A.; Friend, R. H. *Adv. Funct. Mater.* **2008**, *18*, 3189.
(438) Wicklein, A.; Ghosh, S.; Sommer, M.; Würthner, F.; Thelakkat, M. *ACS Nano* **2009**, *3*, 1107.
(439) Schulze, K.; Uhrich, C.; Schüppel, R.; Leo, K.; Pfeiffer, M.; Brier, E.; Reinold, E.; Bäuerle, P. *Adv. Mater.* **2006**, *18*, 2872.
(440) Tan, L.; Curtis, M. D.; Francis, A. H. *Chem. Mater.* **2004**, *16*, 2134.
(441) Eo, Y. S.; Rhee, H. W.; Chin, B. D.; Yu, J. W. *Synth. Met.* **2009**, *159*, 19100.
(442) Mihailetchi, V. D.; Koster, L. J. A.; Blom, P. W. M. *Appl. Phys. Lett.* **2004**, *85*, 970.
(443) Na, S.-I.; Oh, S.-H.; Kim, S.-S.; Kim, D.-Y. *Org. Electron.* **2009**, *10*, 496.
(444) Liang, Y.; Wu, Y.; Feng, D.; Tsai, S.-T.; Son, H.-J.; Li, G.; Yu, L. *J. Am. Chem. Soc.* **2009**, *131*, 56.
(445) Reese, M. O.; Morja, A. J.; White, M. S.; Kopidakis, N.; Shaheen, S. E.; Rumbles, G.; Ginley, D. S. *Sol. Energy Mater. Sol. Cells* **2008**, *92*, 746.
(446) Mihailetchi, V. D.; Blom, P. W. M.; Hummelen, J. C.; Rispens, M. T. *J. Appl. Phys.* **2003**, *94*, 6849.
(447) Ishii, H.; Sugiyama, K.; Ito, E.; Seki, K. *Adv. Mater.* **1999**, *11*, 605.
(448) *Organic Light-Emitting Devices: Synthesis, Properties, and Applications*; Müllen, K., Scherf, U., Eds.; Wiley-VCH: Weinheim, Germany, 2006.
(449) Brown, T. M.; Friend, R. H.; Millard, I. S.; Lacey, D. J.; Butler, T.; Burroughes, J. H.; Cacialli, F. *J. Appl. Phys.* **2003**, *93*, 6159.
(450) Hung, L. S.; Zhang, R. Q.; He, P.; Mason, G. *J. Phys. D: Appl. Phys.* **2002**, *35*, 103.
(451) Hung, L. S.; Tang, C. W.; Mason, M. G. *Appl. Phys. Lett.* **1997**, *70*, 152.
(452) Wen, F. S.; Li, W. L.; Liu, Z.; Wei, H. Z. *Mater. Chem. Phys.* **2006**, *95*, 94.
(453) Ahlswede, E.; Hanisch, J.; Powalla, M. *Appl. Phys. Lett.* **2007**, *90*, 163504.
(454) *Handbook of Conducting Polymers: Conjugated Polymers: Processing and Applications*, 3rd ed.; Skotheim, T. A., Reynolds, J. R., Eds.; CRC Press: Boca Raton, FL, 2007.
(455) Jönsson, S. K. M.; Carlegrim, E.; Zhang, F.; Salaneck, W. R.; Fahlman, M. *Jpn. J. Appl. Phys.* **2005**, *44*, 3695.
(456) Brabec, C. J.; Shaheen, S. E.; Winder, C.; Sariciftci, N. S. *Appl. Phys. Lett.* **2002**, *80*, 1288.
(457) Pfuetzner, S.; Meiss, J.; Petrich, A.; Riede, M.; Leo, K. *Appl. Phys. Lett.* **2009**, *94*, 253303.
(458) Kang, S.-W.; Li, Q.; Chapman, B. D.; Pindak, R.; Cross, J. O.; Li, L.; Nakata, M.; Kumar, S. *Chem. Mater.* **2007**, *19*, 5657.
(459) *Organic Photovoltaics*; Brabec, C., Dyakonov, V., Scherf, U., Eds.; Wiley-VCH: Weinheim, Germany, 2008.
(460) Lee, T.-W.; Chung, Y. *Adv. Funct. Mater.* **2008**, *18*, 2246.
(461) de Kok, M. M.; Buechel, M.; Vulto, S. I. E.; van de Weijer, P.; Meulenkamp, E. A.; de Winter, S. H. P. M.; Mank, A. J. G.; Vorstenbosch, H. J. M.; Weijtens, C. H. L.; van Elsbergen, V. *Phys. Status Solidi A* **2004**, *201*, 1342.
(462) Carter, C.; Brumbach, M.; Donley, C.; Hreha, R. D.; Marder, S. R.; Domercq, B.; Yoo, S.; Kippelen, B.; Armstrong, N. R. *J. Phys. Chem. B* **2006**, *110*, 25191.
(463) Donley, C.; Dunphy, D.; Paine, D.; Carter, C.; Nebesny, K.; Lee, P.; Alloway, D.; Armstrong, N. R. *Langmuir* **2002**, *18*, 450.
(464) Hains, A. W.; Marks, T. J. *Appl. Phys. Lett.* **2008**, *92*, 023504.
(465) Takahashi, K.; Suzaka, S.; Sigeyama, Y.; Yamaguchi, T.; Nakamura, J.; Murata, K. *Chem. Lett.* **2007**, *36*, 762.
(466) Yan, H.; Lee, P.; Armstrong, N. R.; Graham, A.; Evmenenko, G. A.; Dutta, P.; Marks, T. J. *J. Am. Chem. Soc.* **2005**, *127*, 3172.
(467) Ionescu-Zanetti, C.; Mechler, A.; Carter, S. A.; Lal, R. *Adv. Mater.* **2004**, *16*, 385.
(468) Kemerink, M.; Timpanaro, S.; de Kok, M. M.; Meulenkamp, E. A.; Touwslager, F. J. *J. Phys. Chem. B* **2004**, *108*, 18820.

(469) Ni, J.; Yan, H.; Wang, A.; Yang, Y.; Stern, C. L.; Metz, A. W.; Jin, S.; Wang, L.; Marks, T. J.; Ireland, J. R.; Kannewurf, C. R. *J. Am. Chem. Soc.* **2005**, *127*, 5613.
(470) Wong, K. W.; Yip, H. L.; Luo, Y.; Wong, K. Y.; Lau, W. M.; Low, K. H.; Chow, H. F.; Gao, Z. Q.; Yeung, W. L.; Chang, C. C. *Appl. Phys. Lett.* **2002**, *80*, 2788.
(471) de Jong, M. P.; van IJzendoorn, L. J.; de Voigt, M. J. A. *Appl. Phys. Lett.* **2000**, *77*, 2255.
(472) Hains, A. W.; Ramanan, C.; Irwin, M. D.; Liu, J.; Wasielewski, M. R.; Marks, T. J. *ACS Appl. Mater. Interfaces* **2010**, *2*, 175.
(473) Johnev, B.; Fostiropoulos, K. *Sol. Energy Mater. Sol. Cells* **2008**, *92*, 393.
(474) Han, S.; Shin, W. S.; Seo, M.; Gupta, D.; Moon, S.-J.; Yoo, S. *Org. Electron.* **2009**, *10*, 791.
(475) Shrotriya, V.; Li, G.; Yao, Y.; Chu, C.-W.; Yang, Y. *Appl. Phys. Lett.* **2006**, *88*, 073508.
(476) Gilot, J.; Barbu, I.; Wienk, M. M.; Janssen, R. A. J. *Appl. Phys. Lett.* **2007**, *91*, 113520.
(477) Hayakawa, A.; Yoshikawa, O.; Fujieda, T.; Uehara, K.; Yoshikawa, S. *Appl. Phys. Lett.* **2007**, *90*, 163517.
(478) Kim, J. Y.; Kim, S. H.; Lee, H.-H.; Lee, K.; Ma, W.; Gong, X.; Heeger, A. J. *Adv. Mater.* **2006**, *18*, 572.
(479) Hong, Z. R.; Maennig, B.; Lessmann, R.; Pfeiffer, M.; Leo, K.; Simon, P. *Appl. Phys. Lett.* **2007**, *90*, 203505.
(480) Chan, M. Y.; Lee, C. S.; Lai, S. L.; Fung, M. K.; Wong, F. L.; Sun, H. Y.; Lau, K. M.; Lee, S. T. *J. Appl. Phys.* **2006**, *100*, 094506.
(481) Rand, B. P.; Li, J.; Xue, J.; Holmes, R. J.; Thompson, M. E.; Forrest, S. R. *Adv. Mater.* **2005**, *17*, 2714.
(482) Song, Q. L.; Li, F. Y.; Yang, H.; Wu, H. R.; Wang, X. Z.; Zhou, W.; Zhao, J. M.; Ding, X. M.; Huang, C. H.; Hou, X. Y. *Chem. Phys. Lett.* **2005**, *416*, 42.
(483) O'Brien, D. F.; Baldo, M. A.; Thompson, M. E.; Forrest, S. R. *Appl. Phys. Lett.* **1999**, *74*, 442.
(484) Hirose, Y.; Kahn, A.; Aristov, V.; Soukiassian, P.; Bulovic, V.; Forrest, S. R. *Phys. Rev. B* **1996**, *54*, 13748.
(485) Heutz, S.; Sullivan, P.; Sanderson, B. M.; Schultes, S. M.; Jones, T. S. *Sol. Energy Mater. Sol. Cells* **2004**, *83*, 229.
(486) Ichikawa, M.; Amagai, J.; Horiba, Y.; Koyama, T.; Taniguchi, Y. *J. Appl. Phys.* **2003**, *94*, 7796.
(487) Naka, S.; Okada, H.; Onnagawa, H.; Tsutsui, T. *Appl. Phys. Lett.* **2000**, *76*, 197.
(488) Chan, M. Y.; Lai, S. L.; Lau, K. M.; Lee, C. S.; Lee, S. T. *Appl. Phys. Lett.* **2006**, *89*, 163515.
(489) Maennig, B.; Drechse, J.; Gebeyehu, D.; Simon, P.; Kozlowski, F.; Werner, A.; Li, F.; Grundmann, S.; Sonntag, S.; Koch, M.; Leo, K.; Pfeiffer, M.; Hoppe, H.; Meissner, D.; Sariciftci, N. S.; Riedel, I.; Dyakonov, V.; Parisi, J. *Appl. Phys. A: Mater. Sci. Process.* **2004**, *79*, 1.
(490) Gebeyehu, D.; Pfeiffer, M.; Maennig, B.; Drechsel, J.; Werner, A.; Leo, K. *Thin Solid Films* **2004**, *451*−*452*, 29.
(491) Suemori, K.; Miyata, T.; Yokoyama, M.; Hiramoto, M. *Appl. Phys. Lett.* **2005**, *86*, 063509.
(492) Sato, Y.; Niinomi, T.; Abe, Y.; Matsuo, Y.; Nakamura, E. *Proc. SPIE* **2008**, *7052*, 70520J/1.
(493) Hiramoto, M.; Sakai, K. *Mol. Cryst. Liq. Cryst.* **2008**, *491*, 284.
(494) Drechsel, J.; Mannig, B.; Kozlowski, F.; Pfeiffer, M.; Leo, K.; Hoppe, H. *Appl. Phys. Lett.* **2005**, *86*, 244102.
(495) Yu, B.; Zhu, F.; Wang, H.; Li, G.; Yan, D. *J. Appl. Phys.* **2008**, *104*, 114503.
(496) Zhao, D. W.; Sun, X. W.; Jiang, C. Y.; Kyaw, A. K. K.; Lo, G. Q.; Kwong, D. L. *Appl. Phys. Lett.* **2008**, *93*, 083305.
(497) Dennler, G.; Prall, H.-J.; Koeppe, R.; Egginger, M.; Autengruber, R.; Sariciftci, N. S. *Appl. Phys. Lett.* **2006**, *89*, 073502.
(498) Colsmann, A.; Junge, J.; Kayser, C.; Lemmer, U. *Appl. Phys. Lett.* **2006**, *89*, 203506.
(499) Jørgensen, M.; Normann, K.; Krebs, F. C. *Sol. Energy Mater. Sol. Cells* **2008**, *92*, 686.
(500) Reese, M. O. Retrieved on May 29, 2008 from http://www.wikispaces.com/opvlifetime.
(501) Könenkamp, R.; Priebe, G.; Pietzak, B. *Phys. Rev. B: Condens. Matter* **1999**, *60*, 11804.
(502) Hamed, A.; Sun, Y. Y.; Tao, Y. K.; Meng, R. L.; Hor, P. H. *Phys. Rev. B: Condens. Matter* **1993**, *47*, 10873.
(503) Pevzner, B.; Hebard, A. F.; Dresselhaus, M. S. *Phys. Rev. B: Condens. Matter* **1997**, *55*, 16439.
(504) Hänsel, H.; Zettl, H.; Krausch, G.; Schmitz, C.; Kisselev, R.; Thelakkat, M.; Schmidt, H. W. *Appl. Phys. Lett.* **2002**, *81*, 2106.
(505) Kawano, K.; Pacios, R.; Poplavskyy, D.; Nelson, J.; Bradley, D. D. C.; Durrant, J. R. *Sol. Energy Mater. Sol. Cells* **2006**, *90*, 3520.
(506) Huang, J.; Miller, P. F.; Wilson, J. S.; de Mello, A. J.; de Mello, J. C.; Bradley, D. D. C. *Adv. Funct. Mater.* **2005**, *15*, 290.
(507) Jeong, S. M.; Koo, W. H.; Choi, S. H.; Jo, S. J.; Baik, H. K.; Lee, S.-J.; Song, K. M. *Appl. Phys. Lett.* **2004**, *85*, 1051.
(508) Franke, R.; Maennig, B.; Petrich, A.; Pfeiffer, M. *Sol. Energy Mater. Sol. Cells* **2008**, *92*, 732.

CR9002984